

Durham E-Theses

Funny Bones: Ecomorphology of the Bovid Distal Humerus and its Paleontological Implications

ANDERSON, SOPHIA,CHRISTINA

How to cite:

ANDERSON, SOPHIA,CHRISTINA (2022) *Funny Bones: Ecomorphology of the Bovid Distal Humerus and its Paleontological Implications*, Durham theses, Durham University. Available at Durham E-Theses Online: <http://etheses.dur.ac.uk/14477/>

Use policy

The full-text may be used and/or reproduced, and given to third parties in any format or medium, without prior permission or charge, for personal research or study, educational, or not-for-profit purposes provided that:

- a full bibliographic reference is made to the original source
- a [link](#) is made to the metadata record in Durham E-Theses
- the full-text is not changed in any way

The full-text must not be sold in any format or medium without the formal permission of the copyright holders.

Please consult the [full Durham E-Theses policy](#) for further details.

Funny Bones: Ecomorphology of the Bovid Distal Humerus and its Paleontological Implications

Sophia C. Anderson

Supervised by Dr Kris (Fire) Kovarovic and Prof. Sarah Elton, in
collaboration with Dr W. Andrew Barr

Word count: 20780

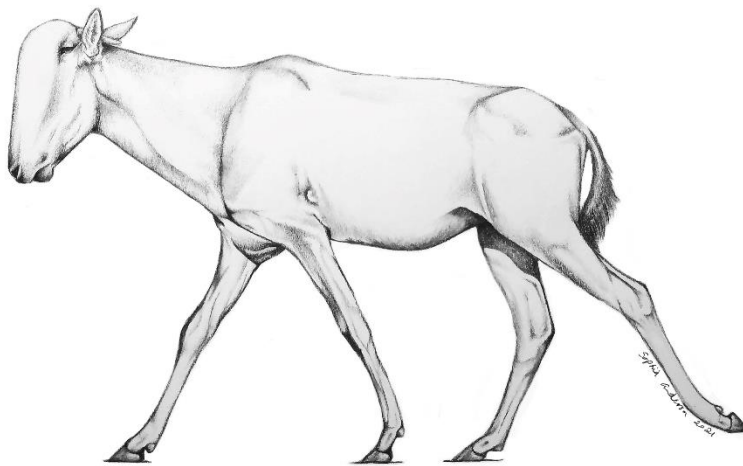
January 2022

Submitted for the degree of Master of Science by Research
in Biological Anthropology
University of Durham
Department of Anthropology



“If bone is the answer, then what is the question?”

~ Robert Huiskes, 2000



Reconstruction of *Rusingoryx atopocranion*, Sophia Anderson 2021

Table of Contents

List of Tables	iii
List of Illustrations	iv
List of Abbreviations	vi
Anatomical terms	vi
Institutional Abbreviations.....	vii
Programs and Software Used.....	vii
Statement of Copyright.....	vii
Acknowledgements.....	viii
Abstract.....	1
Chapter 1: Introduction.....	2
Geometric Morphometrics and its Application in Functional Morphology.....	3
The Mammal Humerus	5
The Bovidae: Phylogeny & Evolution.....	5
The Evolution of Unguligrady	6
Anatomy of the Distal Humerus in Bovids.....	12
<i>Rusingoryx atopocranion</i>	16
<i>Rusingoryx</i> Humerus.....	17
Cranial Dome	18
Distribution	20
Rusinga Island.....	21
<i>Rusingoryx</i> Assemblage at Bovid Hill	22
Rationale	23
Aims.....	23
Hypotheses.....	24
Chapter 2: Materials & Methods.....	25
Scan Acquisition	26
3D Landmarking	35
Generalized Procrustes Analysis.....	38
Multivariate Analyses	38
Categorical Variable Classification	38
Linear Regression	42
Analysis of Variance (ANOVA).....	42
Principal Components Analysis (PCA).....	43
Canonical Variate Analysis (CVA).....	44

Phylogenetic Analysis via PGLS.....	45
Chapter 3: Results.....	46
Tribe Affinity.....	46
Habitat Preference	49
Body Mass	52
Principal Components Analysis.....	55
Allometric Shape Variation	58
Interaction of Body Mass and Habitat Preference	60
Influence of Phylogeny.....	62
Summary.....	67
Chapter 4: A Palaeontological Application: <i>Rusingoryx atopocranion</i>	68
Results	68
Tribe Affinity.....	70
Habitat Preference	72
Body Mass	74
Summary.....	81
Chapter 5: Discussion.....	82
Extant Bovids	82
<i>Rusingoryx atopocranion</i>	87
Critical Assessment of the Study.....	92
Future Work.....	94
Chapter 6: Conclusions.....	95
References	96
Appendix I: Preliminary 2D Analyses.....	104
Results	107
Canonical Variate Analysis: Tribe.....	109
Canonical Variate Analysis: Habitat Preference	111
Canonical Variate Analysis: Body Mass	113
Conclusions & Discussion.....	115
Appendix II – Hoof Area and Pressure Analysis.....	116
Appendix III - 3D Landmarking Repeatability Testing	118
Trial 1	118
Trial 2	125
Trial 3	129
Trial 4	131
Trial 5	133
Appendix IV: R Code.....	138

Formatting 3D landmarks data from Avizo	138
Canonical Variate Analysis (CVA).....	138
Principal Components Analysis (PCA).....	139
Phylogenetic Generalized Least Squares (PGLS).....	140
Linear regression.....	142
ANOVA	142
Appendix V: Phylogenetic Tree.....	143

List of Tables

Table 1: Important statistical terms.....	24
Table 2: Specimen details.....	26-32
Table 3: 30 landmark schema used for 3D landmarking.....	35
Table 4: Categorical variables used in the study.....	37-39
Table 5: Results for the relationship between tribe and distal humerus morphology.....	46
Table 6: Summarization of Canonical Variate Analysis (CVA) on 3D Procrustes coordinates by habitat preference.....	49
Table 7: Summarization of Canonical Variate Analysis (CVA) on 3D Procrustes coordinates by body mass category.....	52
Table 8: Summarization of Principal Components Analysis (PCA) on 3D Procrustes coordinates.....	55
Table 9: Interaction of body mass and habitat preference.....	58
Table 10: Effect of interaction between body mass and habitat preference on shape analysis.....	59
Table 11: PGLS results on PCA data.....	62
Table 12: PGLS results on CVA data.....	64
Table 13: Procrustes distances between tribe groups including <i>Rusingoryx</i>	69
Table 14: Procrustes distances between habitat preference groups including <i>Rusingoryx</i>	71
Table 15: Procrustes distances between body mass groups including <i>Rusingoryx</i>	73
Table 16: Details of bovids closest to <i>Rusingoryx</i> in the PC2 vs PC1 morphospace.....	76

Table I: 19 landmark schema used for 2D landmarking.....	106
Table II: Significance of relationships between PCA axes and categorical variables in the extant bovid analysis.....	108
Table III: Coefficients of variation of landmarks in Trial 1.....	120
Table IV: Coefficients of variation of landmarks in Trial 2.....	126
Table V: Coefficients of variation of landmarks in Trial 4.....	133
Table VI: Coefficients of variation of landmarks in Trial 5.....	136-137

List of Illustrations

Figure 1: Bovid phylogeny and relationship to the wider Artiodactyla.....	9
Figure 2: Molecular bovid phylogenies.....	11
Figure 3: Diagrammatic representation of the distal humerus anatomy in bovids.....	14
Figure 4: Left distal humerus of <i>Rusingoryx atopocranion</i>	16
Figure 5: <i>Rusingoryx atopocranion</i> cranial material.....	18
Figure 6: <i>Rusingoryx</i> material distribution.....	19
Figure 7: Final 30 landmark schema used for 3D landmarking.....	34
Figure 8: Visualization of Canonical Variate Analysis (CVA) on 3D Procrustes coordinates by tribe affinity.....	45
Figure 9: Visualization of Canonical Variate Analysis (CVA) on 3D Procrustes coordinates by habitat preference.....	48
Figure 10: Visualization of Canonical Variate Analysis (CVA) on 3D Procrustes coordinates by body mass category.....	51
Figure 11: Visualization of Principal Components Analysis (PCA) on 3D Procrustes coordinates.....	54
Figure 12: The relationships between shape variation, centroid size and body mass in extant bovids.....	57
Figure 13: Interaction of body mass and habitat preference.....	58
Figure 14: Pruned bovid phylogeny.....	61
Figure 15: Visualization of Principal Components Analysis (PCA) on 3D Procrustes coordinates.....	62
Figure 16: <i>Rusingoryx</i> distal humerus shape as compared to mean extant bovid shape....	67

Figure 17: Visualization of Canonical Variate Analysis (CVA) on 3D Procrustes coordinates by tribe affinity, including <i>Rusingoryx</i>	68
Figure 18: Visualization of Canonical Variate Analysis (CVA) on 3D Procrustes coordinates by habitat preference, including <i>Rusingoryx</i>	70
Figure 19: Visualization of Canonical Variate Analysis (CVA) on 3D Procrustes coordinates by body mass category, including <i>Rusingoryx</i>	72
Figure 20: Visualization of Principal Components Analysis (PCA) on 3D Procrustes coordinates, including <i>Rusingoryx</i> – PC1 and PC2.....	75
Figure 21: Visualization of Principal Components Analysis (PCA) on 3D Procrustes coordinates, including <i>Rusingoryx</i> – PC2 and PC3.....	77
Figure 22: Notable characteristics of categories within the analysis.....	81-82
Figure 23: Penning elbow in a possible North Ronaldsay sheep.....	87
Figure I: 19 landmark schema used for 2D landmarking.....	105
Figure II: Visualization of Principal Components Analysis (PCA) on 2D Procrustes coordinates.....	108
Figure III: Visualization of Canonical Variate Analysis (CVA) on 2D Procrustes coordinates by tribe affinity.....	110
Figure IV: Visualization of Canonical Variate Analysis (CVA) on 2D Procrustes coordinates by habitat preference.....	112
Figure V: Visualization of Canonical Variate Analysis (CVA) on 2D Procrustes coordinates by body mass category.....	114
Figure VI: 36 landmark schema used in Trial 1 and Trial 3.....	119
Figure VII: Principal Components Analysis (PCA) visualization of Trial 1 data.....	121
Figure VIII: Principal Components Analysis (PCA) visualization of Trial 1 data following adjustment.....	122
Figure IX: Results relating to human error in landmarking.....	123
Figure X: Variation between successive landmarking attempts.....	124
Figure XI: 28 landmark schema used in Trial 2.....	125
Figure XII: Principal Components Analysis (PCA) visualization of Trial 2 data.....	127
Figure XIII: Results relating to human error in landmarking.....	128
Figure XIV: Principal Components Analysis (PCA) visualization of Trial 3 data.....	129
Figure XV: Principal Components Analysis (PCA) visualization of Trial 3 data following adjustment.....	130

Figure XVI: 31 landmark schema used in Trial 4.....	132
Figure XVII: 30 landmark schema used in Trial 5.....	134
Figure XVIII: Relationship between coefficient of variation and scan centroid size.....	135
Figure XIX: Linear Discriminant Analysis (LDA) and Principal Components Analysis (PCA) visualization of Trial 5 results.....	138

List of Abbreviations

CVA – Canonical Variate Analysis (CV – Canonical Variate)
F – Forest
GMM – Geometric Morphometrics
GT – Grassland/treeless
HWB – Heavy woodland/bushland
LWB – Light woodland/bushland
M – Montane
MSA – Middle Stone Age
Mya – million years ago
PGLS – Phylogenetic Generalized Least Squares
PCA – Principal Components Analysis (PC – Principal Component)
WBG – Wooded bushland/grassland

Anatomical terms

Ca – capitulum
Of – olecranon fossa
Gc – groove of capitulum
Gt – groove of trochlea
Lbc – lateral border of capitulum
Lclf – Lateral collateral ligament fossa
Le – lateral epicondyle
Lec – lateral epicondylar crest
Let – lateral epicondylar tubercle
Lrt – lateral ridge of trochlea
m. – musculus (muscle)
Mbt – medial border of trochlea

Me – medial epicondyle

Mrt – medial ridge of trochlea

Tr – trochlea

Institutional Abbreviations

AMNH – American Museum of Natural History

BERLIN - Berlin Museum für Naturkunde

KNM – National Museums of Kenya

NHM – Natural History Museum

NMNH – Smithsonian National Museum of Natural History

MNHN - Muséum National d'Histoire Naturelle

Programs and Software Used

- Avizo ver. 7.1.0 (Konrad-Zuse-Zentrum Berlin 2012)
- MorphoJ ver. 1.07a (Klingenberg 2011)
- R software ver. 4.0.3 (The R Foundation for Statistical Computing 2020)
 - *Arothron* package (Profico et al. 2021)
 - *caper* package (Orme et al. 2018)
 - *car* package (Fox et al. 2021)
 - *ggplot2* package (Wickham et al. 2021)
 - *MASS* package (Ripley et al. 2021)
 - *Morpho* package (Schlager et al. 2021)
 - *phytools* package (Revell 2021)
- tpsDig232 ver. 2.31 (Rohlf 2017)
- tpsUtil32 ver. 1.78 (Rohlf 2019)

Statement of Copyright

“The copyright of this thesis rests with the author. No quotation from it should be published without the author's prior written consent and information derived from it should be acknowledged.”

If approved for the degree, I am willing for this work to be deposited in the University Library and made available via an online repository immediately.

Acknowledgements

First, I owe immense thanks to my primary supervisor, Fire, for being such a wonderful mentor and friend. She has poured so much into helping me develop and carry out this project, as well as always being a compassionate source of support. The quality of this project, as well as the quality of my experience in this course, would not be what they are without her.

Of course, thanks also go to the rest of my support network at Durham – Sarah Elton, Russell Hill, the SSCC, the EARG and the whole Department of Anthropology. Completing a degree entirely within a year dominated by a global pandemic is a strange and unprecedented situation to be in, and the department has, without fail, striven to make sure the experience was as smooth as possible and help me feel integrated even though I have never met a single member of the department face to face, nor been inside the department building.

I am immensely grateful to fellow researchers who provided support, advice, and scans of bovid humeri – Cyril Etienne, Sabrina Curran, Frances Forrest, Tyler Faith, Phillip Cox, Eloy Galvez-Lopez – and particularly to W. Andrew Barr for going above and beyond to help and advise me, especially in the realm of phylogenetic correction.

Thanks also to my friends and family, many of whom I have not seen face to face throughout this degree; and especially to my parents for listening to the minute details of *Rusingoryx*, geometric morphometrics and strange bone tubercles while I stayed with them for five months.

This is my second master's by research degree and I cannot help but compare it to my first. Without a shadow of a doubt, this experience has been far better, and it is thanks entirely to the people who have supported me this year. Thank you all.

Abstract

When seeking to understand early human evolution, it is fundamental to understand the ecology of the environment in which those early humans lived. This is an important overlap between the fields of anthropology and palaeontology, and here I take an ecomorphological approach involving the study of variation in bone morphology as a proxy for ecology in bovids. The family Bovidae (Mammalia: Artiodactyla) dominated ecosystems at the time of early human (*Homo sapiens*) evolution, and continue to in many areas today, as well as frequently having been domesticated throughout human history. For these reasons, bovids provide an excellent study group for this research. The main aim of this project is to develop the bovid distal humerus as an ecological proxy using 3D geometric morphometrics on 116 scans of extant bovid species, representing 11 of the approximately 16 extant bovid tribes, and 40% of known extant species. The humerus is particularly informative due to its extensive roles in weight-bearing and forelimb use. This study focuses on the distal humerus (the elbow articulation) as this section of bone is dense and frequently preserved in the bovid fossil record, and additionally a great many attachment and origin sites for muscles involved in lower forelimb movement are concentrated at the distal humerus. I find evidence that aspects of distal humerus morphology have evolved convergently across bovids, relating to body mass and habitat preference, and that distal humerus morphology can be a proxy to infer such information in bovids. This information can be utilized to understand the ecology of extinct bovids, and in the final part of this project I apply this to the case of the unusual Pleistocene bovid *Rusingoryx atopocranion*, which is known to have been hunted by early humans. The results indicate that the unusual distal humerus morphology observed in *Rusingoryx* is directly related to the animal being highly adapted for cursoriality on the hard, flat terrain of the Kenyan shores of Lake Victoria in the Pleistocene.

Chapter 1: Introduction

The question of the relationship between shape and function – functional morphology – in vertebrate skeletons has long been discussed. In his book, ‘On Growth and Form’ (1961), D’Arcy Wentworth Thompson describes a situation in which:

“...adaptation in the strictest sense is obviously present, in the clearly demonstrable form of mechanical fitness for the exercise of some particular function or action which has become inseparable from the life and well-being of the organism.”

He suggests that bone is a simple example of this situation, such that studying the functional morphology of bone may be one of the clearest ways to study naturally-occurring functional morphology. Certainly, the study of the functional morphology of the skeleton is a vital field in support of the wider study of vertebrate palaeontology, given that extinct vertebrates are known almost entirely from skeletal remains alone.

Vertebrate palaeontology relies upon understanding the skeletons of extant animals and relating this to the fossil remains of those which have become extinct. In palaeontology, skeletal morphology is utilized in two, almost contradictory, ways. Systematics and phylogenetics rely on the assumption that morphology can be used to predict phylogenetic affinity (that morphology is primarily related to phylogenetic relationships), while functional morphology relies on the assumption that morphology can be used to reconstruct ecology and behaviour (that morphology is primarily related to function). While the two are not *necessarily* mutually exclusive (animals within a phylogenetic group may all share broadly the same ecology), convergent evolution of skeletal morphologies amongst disparate taxa is well documented (for instance, postorbital closure has evolved independently at least 11 times in mammals (Heesy 2005)), and vestigial morphologies may be retained in an entire taxon (the human tailbone, for example). A similar hypothetical situation is discussed eloquently by Raup and Stanley in their book, ‘Principles of Paleontology’ (1978):

“It is theoretically possible for morphologic features to evolve which are fundamentally neutral – features that do not benefit the organism. The present consensus among evolutionary biologists and paleontologists is that it is extremely rare for such “neutral” features to evolve in the form of important skeletal parts – rare if it occurs at all.”

Even if we are to assume that the morphology of a skeletal structure/feature is directly linked to function, there are multiple-effect factors to consider. For example, the

structure/feature may perform more than one function, or the genetic basis for the development of the morphology may influence the morphology of other features, or be influenced by genes predominantly related to other features (pleiotropy).

This must all be considered when studying functional morphology, and can never be omitted from interpretation of morphological data. In fact, there are methods to account for the effect of phylogenetic relatedness in this context, which will be discussed later in this dissertation. Currently, the most common way to collect said data on morphological variation is via geometric morphometrics.

Geometric Morphometrics and its Application in Functional Morphology

Geometric morphometrics (GMM) is a technique for assessing shape variation. Specifically, this technique assesses variation in the *form* of an object, which is defined in this context by Lele and Richtsmeier (2001) as “the characteristic that remains invariant under any translation, rotation or reflection of the object”. Bookstein (1991) lays out clearly the four principles foundational to GMM:

1. Landmark locations archive biological form. Loci on the object are selected for anatomical/morphological significance and homology across all specimens included in the study, and these landmarks are identified by names and Cartesian coordinates
2. The landmark coordinates for each specimen in the study are processed according to needs of the proceeding analyses
3. Multivariate analyses are performed on the resulting variables to address hypotheses/questions of the study
4. Results are interpreted according to the hypotheses/questions, and presented accordingly

A key part of standard GMM is Procrustes superimposition, which falls within the second principle, and seeks to mathematically fulfill the definition of form above. When a shape has been landmarked, the resulting simplified landmark-only visual representation of the shape is known as a configuration or constellation, and the aim of GMM is to compare multiple configurations. However, the raw configurations may be at entirely different scales, rotations and Cartesian positions based on the image used to landmark. These configurations cannot be compared without these ‘nuisance parameters’ obfuscating true

shape variation. Though there are alternative methods for eliminating these nuisance parameters (e.g. Lele and Richtsmeier, 2001), the most common method is an application of Generalized Procrustes Analysis (Gower 1975). This method mathematically aligns all the configurations at their centroids (the gravitational centre of the shape, or the point equidistant between all corners – which, in this case are the landmarks), as well as scaling and rotating the configurations to minimize variation between configurations at each landmark – this is Procrustes superimposition. The resulting variation between configurations should represent variation due only to form.

Thus, multivariate analyses on the output coordinates from the Procrustes superimposition (the Procrustes coordinates) allow aspects of an animal's ecology to be inferred from aspects of morphology, which is of great interest in palaeontology when seeking to reconstruct an animal from only fossil remains. However, this information can be taken a step further in order to better understand entire ecosystems. The ecologies of an individual species inferred from morphology inform our knowledge of the environment in which it must have lived – for example, highly cursorially-adapted fossil animals likely lived in an open, flat habitat because animals in such an environment gain the greatest advantage from being adapted to move efficiently over large flat areas. This use of the relationship between morphology and ecology is known as 'ecomorphology'.

Many elements of the postcranial skeleton can be and have been used to investigate functional morphology and ecomorphology across mammals. For example, the scapula has been shown to distinguish locomotor mode in carnivorans (Galvez Lopez 2014), mustelids (Holmes 1980), and xenarthans (Monteiro and Abe 1999). In bovids, morphology of both the calcaneus (Barr 2020) and astragalus (Barr 2014) have been shown to be related to habitat preference, and Etienne et al. found significant relationships between morphology and mass across all long limb bones and relationships between morphology and habitat preference in all but the tibia (Etienne et al. 2020). Cranial morphology has recently been found to distinguish European and American mink, which have only subtly differing ecologies (Gálvez-López et al. 2021).

The mammalian humerus was chosen for this study as it provides an ideal candidate for skeletal functional morphology analyses, for several reasons outlined below.

The Mammal Humerus

The limb bones are of great interest for functional and biomechanical study in general, offering the potential for insight into the evolution of limb and locomotor specialisations. Ungulates are one such case of extreme specialisation, having evolved unguligrady from pentadactyl digitigrade animals – a transition which took place at least three times independently in artiodactyls (even-toed ungulates) alone (Clifford 2010).

The humerus is a highly informative part of the mammalian skeleton, and the vertebrate skeleton more broadly. It is one of the three long bones of the forelimb, constituting the stylopod (most proximal element) of the forelimb. It attaches proximally to the shoulder girdle at the scapula and distally to the radius and ulna at the elbow joint.

The bone is comprised of a (generally) cylindrical diaphysis (shaft), with an epiphysis at each end. The humerus is a weight-bearing bone which has been shown repeatedly to be an accurate tool for estimating body mass across tetrapods (Anyonge 1993; Figueirido et al. 2011; Campione and Evans 2012), as well as providing a large number of muscle attachment and origin sites for muscles crucial to forelimb and manus movement. Across tetrapods and within mammals, the humerus, while retaining its general form, is highly morphologically plastic and varies greatly amongst taxonomic groups and locomotor modes (Flower 1876). This makes it an excellent candidate for functional morphology research, and specifically in the case of this study, for studying the highly specialised ungulates.

The family Bovidae within the Artiodactyla provide an ideal study group for this research because Bovidae represents a large taxonomic group with a dramatic size range (approximately 2.4 kg – 1200 kg) and varying ecologies and social dynamics (including solitary, highly gregarious, montane, forest dwelling, and those which live in vast open plains).

The Bovidae: Phylogeny & Evolution

The class Mammalia is subdivided into three extant groupings: Monotremata, Marsupialia and Placentalia. Placentalia (a.k.a. placentals), consists of mammals which carry their foetuses within the womb throughout a large part of development - longer than in

Marsupialia, who can only carry the foetus for one oestrus cycle. Molecular studies which used analysis of retroposons (DNA elements which are randomly integrated into genomes, the presence/absence of which can be tested for) have recovered four major subdivisions of placentals: Afrotheria, Xenarthra, Laurasiatheria and Euarchontoglires (the latter two are often grouped together as the Boreoeutheria) (Kriegs et al. 2006; Prasad et al. 2008; Nishihara et al. 2009), the divergence time of which are still being investigated. The Afrotheria contains groups of placentals which originated in Africa or currently live in Africa (elephant shrews, golden moles, otter shrews, tenrecs, armadillos, hyraxes, elephants, dugongs and manatees); the Xenarthra contains anteaters, sloths and armadillos; the Euarchontoglires contains lagomorphs, rodents, colugos, primates and treeshrews; and the Laurasiatheria contains placentals which originated on the supercontinent of Laurasia (terrestrial ungulates, whales, bats, shrews, pangolins, carnivorans etc.).

The Euungulata (the ungulates) is a very diverse group within the Laurasiatheria which is comprised of terrestrial mammals with hooves (the Perissodactyla and terrestrial Artiodactyla) and the aquatic Cetacea. It is, of course, the Artiodactyla (cetaceans and artiodactyls, previously referred to as Cetartiodactyla) which are of interest for this dissertation. Zurano et al. (2019) found evidence (using mitochondrial DNA) for divergence of the Perissodactyla (odd-toed ungulates) and Artiodactyla (even-toed ungulates) in the late Cretaceous, around 68 mya, with the Cetacea and terrestrial Artiodactyla diverging during the Palaeocene approximately 60 mya. The actual phylogeny of the ungulates is somewhat controversial, as Euungulata may not be monophyletic, as was once thought. Perissodactyla has been reconstructed with a variety of differing phylogenetic relationships via molecular analyses (Nery et al. 2012 and references therein), but evidence increasingly supports a position for the Artiodactyla as sister to Chiroptera (with Perissodactyla sister to Carnivora) (Hallström and Janke 2008; Hallström and Janke 2010; Nery et al. 2012), thereby indicating a non-monophyletic Euungulata.

The Evolution of Unguligrady

The key defining characteristic of terrestrial ungulates is their highly derived unguligrade limb posture. The term ‘unguligrade’ refers to an animal which bears its weight on only the most distal portion of the digits, the distal phalanx. The key features of unguligrade limbs are elongation of distal limb segments, hinge-like joints, musculature concentrated proximally, and a ligamentous interosseous system (a complex system of ligaments around

the distal elements of the limb) (Clifford 2010). The evolution of unguligrady has long been thought to be driven by a transition towards increased cursoriality – the elongated limb allowing greater stride length for faster movement, and the hinge-like joints increasing efficiency for this type of motion. However, it has been suggested that this may not have been the driver of unguligrade evolution, and it may have instead evolved to increase passive stance maintenance efficiency (Clifford 2010). Though it is true that many ungulates are fast cursorial runners, this type of locomotion is actually more metabolically costly for unguligrade animals as compared to digitigrade or plantigrade animals (this has been demonstrated in horses (Reilly et al. 2007)), and suids (pigs) are unguligrade without being otherwise adapted for fast running. In fact, distal limb segment elongation (often cited as a key fast movement adaptation in unguligrade animals) has been shown not to correlate with increased speed – when cursorial carnivorans (digitigrade) and ungulates were compared, the ungulates were not found to be faster (Garland and Janis 1993). Key to understanding this is the preponderance of interosseous ligament structures in the limbs. Ligaments cannot actively contract and, thus have no value in aiding fine motor control at high speeds, but they are low-cost structures which provide stability in low-force and passive stance contexts (Clifford 2010). Additionally, the hinge-like joints required lower muscle activity to maintain stability than non-hinge-like joints. The elongated distal limb in ungulates, rather than functioning to increase speed through increased stride length, may function to decrease stride frequency and, thereby, increase movement efficiency even at slow speeds (Clifford 2010). Rather than unguligrady evolving in order to facilitate fast movement, it appears that the energetic costs of fast movement are increased as a trade-off for more efficient slow movement.

As mentioned previously, bovids are an excellent study group for researching functional morphology in animals which have evolved unguligrady. The Bovidae are a ruminant family within the order Artiodactyla (Figure 1), the largest family within the order, in fact, containing 137 extant species (Hernández Fernández and Vrba 2005). Bovids are characterized by the presence of non-deciduous, unbranched horns which are present in all males, and may also be present in females (where they are generally less complex, and thinner at the base (Huffman 2020)). All bovids have one pair of unbranched horns, with the exception of the chousingha (*Tetracerus quadricornis*), which has two pairs (Grzimek et al. 2003). Bovids vary considerably in appearance, ranging from the smallest, the royal antelope (*Neotragus pygmaeus*), weighing on average just 2.4 kg (Kingdon 2013), to the

largest, the water buffalo (*Bubalus bubalis*), which can weigh as much as 1200 kg (Grzimek et al. 2003), and with coats varying in colour from near white, through browns and oranges, to black. The characteristic horns, themselves, also vary considerably in size and shape (Grzimek et al. 2003). As ungulates, bovids are unguligrade with keratinous paraxonic hooves bearing weight on digits III and IV. Digits II and V are reduced, forming lateral hooves (a.k.a. dewclaws), or may be absent entirely.

Bovids, being ruminants, are obligate herbivores (either grazers, browsers, or mixed grazer-browsers), and they are found in a wide variety of habitats. In fact, members of the family can be found in almost every major terrestrial ecosystem, from the arctic tundra to tropical forests (Grzimek et al. 2003). Bovids are only native to Africa, North America, Europe and Asia, but now have a worldwide distribution, thanks to human introductions. Several species have been domesticated (e.g. cattle, *Bos taurus*, and sheep, *Ovis aries*), and many exist only in protected sites due to an extensive history of human hunting. Some bovids are solitary (e.g. dik diks, *Madoqua*), while others live in huge herds of several thousand (e.g. wildebeest, *Connochaetes*), and many make seasonal migrations according to food availability etc.

The family Bovidae is further subdivided into 8 subfamilies (Novak 1991) and commonly into 16 tribes (Huffman (2020), and references therein) (Figure 1), though number of tribes varies amongst sources. The earliest identified bovid in the fossil record is *Eotragus*, which was discovered in Miocene deposits from Pakistan, dating to 18 mya (Pilgrim 1939), and which has been assigned to the subfamily Boselaphinae (Simpson 1945). Thus, the boselaphines are the first tribe to appear in the fossil record, being recovered from the mid-Miocene of Africa, Europe and Pakistan, and the late Miocene of China. The most recent molecular-based fossil-calibrated phylogeny of extant bovids produced the tree shown in Figure 2 (Bibi 2013). This study utilized molecular data from 127 ruminant species, while an earlier study from Hernández Fernández and Vrba (2005) utilized molecular data from 197 ruminant species (represented in Figure 2). Broadly, the two studies agree, and can both be considered valid reconstructions of bovid phylogeny based on differing taxa selection.

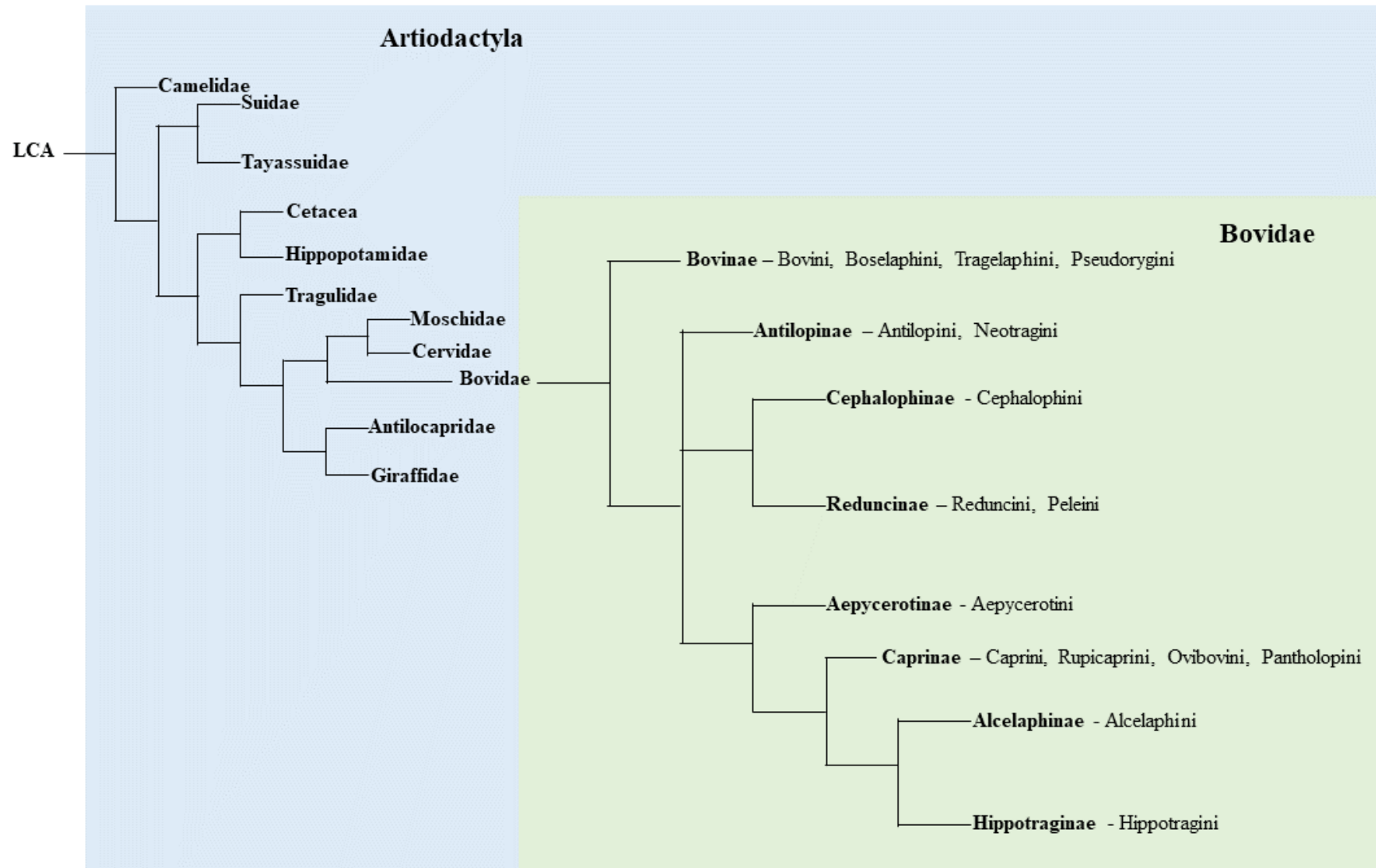


Figure 1: Bovid phylogeny and relationship to the wider Artiodactyla

Showing the placement of the family Bovidae within the Artiodactyla, as well as the interfamilial relationships of the bovids, and tribes contained within the families. Follows Huffman (2020), and references therein.

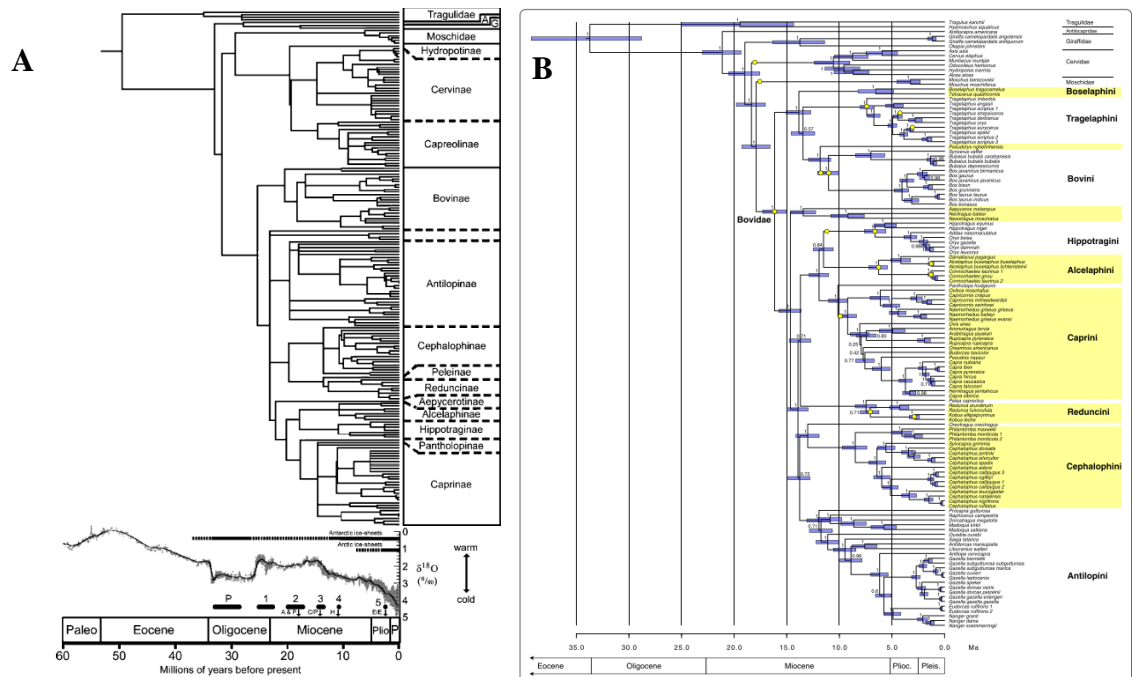


Figure 2: Molecular bovid phylogenies

Showing combined molecular and fossil based phylogenies from A) Hernández Fernández and Vrba (2005), and B) Bibi (2013). A) Consensus tree which utilized molecular data from 197 ruminant species and was fossil-calibrated; B) Bayesian tree which utilized molecular data from 127 ruminant species and was fossil-calibrated.

Based on all that has now been discussed, it is clear that the humerus is a valuable skeletal element when it comes to studying functional morphology, and that the family Bovidae represents an excellent study group for this research. However, there is another reason that the humeral morphology in bovids is of interest – the existence of a Pleistocene bovid called *Rusingoryx atopocranion* with unusual distal humerus morphology. The distal humerus is a dense area of bone and, as a result, is preserved well and often in the fossil record – there are multiple individual distal humerus specimens from *Rusingoryx*. Thus, understanding the morphology of the distal humerus is particularly valuable in a paleontological context.

Anatomy of the Distal Humerus in Bovids

The ungulate humerus (Figure 3) is generally stout and short relative to the other forelimb segments. The medial side of the distal humerus is flat and straight, meaning the medial epicondyle is reduced compared to other mammals. The lateral epicondyle, meanwhile, is more prominent, as is the lateral epicondylar ridge. A supracondylar foramen is never present (Flower 1876).

In bovids, the articular portion of the distal humerus forms a cylinder-like shape, being flat at the lateral and medial ends with a curved barrel between that appears as a variably proportioned 4-sided polygon in anterior view. In alcelaphines, for example, the shape is approximately rectangular, while in bovines the medial edge is longer than the lateral edge, resulting in a more trapezoidal shape. Directly proximal to this shape the bone is very antero-posteriorly thin where the radial fossa on the anterior side and olecranon fossa on the posterior side are aligned – in some individuals of some tribes (e.g. some *Eudorcas thomsonii* and some *Tragelaphus spekii*) the bone is so thin that a foramen has appeared, known as the supratrochlear foramen. On the lateral edge, above the articular shape is a tubercle of varying sizes – in some species it is a barely visible protrusion, while in others (and most prominently in *Rusingoryx*) it is a larger protrusion extending laterally. From the vicinity of this tubercle, the lateral epicondylar crest extends proximally to meet the diaphysis. The prominence of this ridge varies amongst species.

The articular area itself is made up of a series of ridges and troughs which align closely with corresponding topology on the radioulna (the radius and ulna are fused into one bone in bovids and other ungulates). The lateral portion is known as the capitulum and the larger

medial portion is known as the trochlea. The capitulum is comprised of the most lateral ridge border and the groove of the capitulum medial to this. Bordering the groove of the capitulum on the medial side is the slim lateral ridge of the trochlea, followed medially by the groove of the trochlea at approximately the medio-lateral centre of the articular shape. The last and most medial section of the shape is the medial trochlear ridge, which is broad and flat. The morphology of the ridges and grooves making up this morphology extends around the cylindrical shape of the articulation from the proximal edge to the most distal end of the bone, allowing a full range of motion at the elbow joint in the singular plane of motion of the hinge joint – pronation and supination are not possible in ungulates.

On the posterior side, the most dominant feature of the distal humerus is the deep olecranon fossa. On either side of this, the medial and lateral epicondyles, respectively, project posteriorly, with the medial epicondyle generally projecting further than the lateral as well as projecting slightly distally.

Looking at the humerus laterally, the lateral epicondylar crest can be seen extending from the diaphysis to meet the lateral epicondylar protrusion. The protrusion itself also extends in a ridge disto-posteriorly, forming the proximal border of a circular/oval fossa which dominates the lateral epicondyle. In medial view, the medial epicondyle can be seen to be relatively featureless, but it does provide the origin sites of the forearm flexors.

Results obtained by studying the distal humerus of extant bovids can be used to investigate the functional morphology and ecology of fossil bovids, and *Rusingoryx* provides an ideal example, as it is already known to have had unique adaptations which have been strongly associated with its ecology and the environment in which it lived (O'Brien et al. 2016; Kovarovic et al. 2021). Additionally, there is a substantial quantity of *Rusingoryx* material available, specifically with multiple examples of the unusual distal humerus.

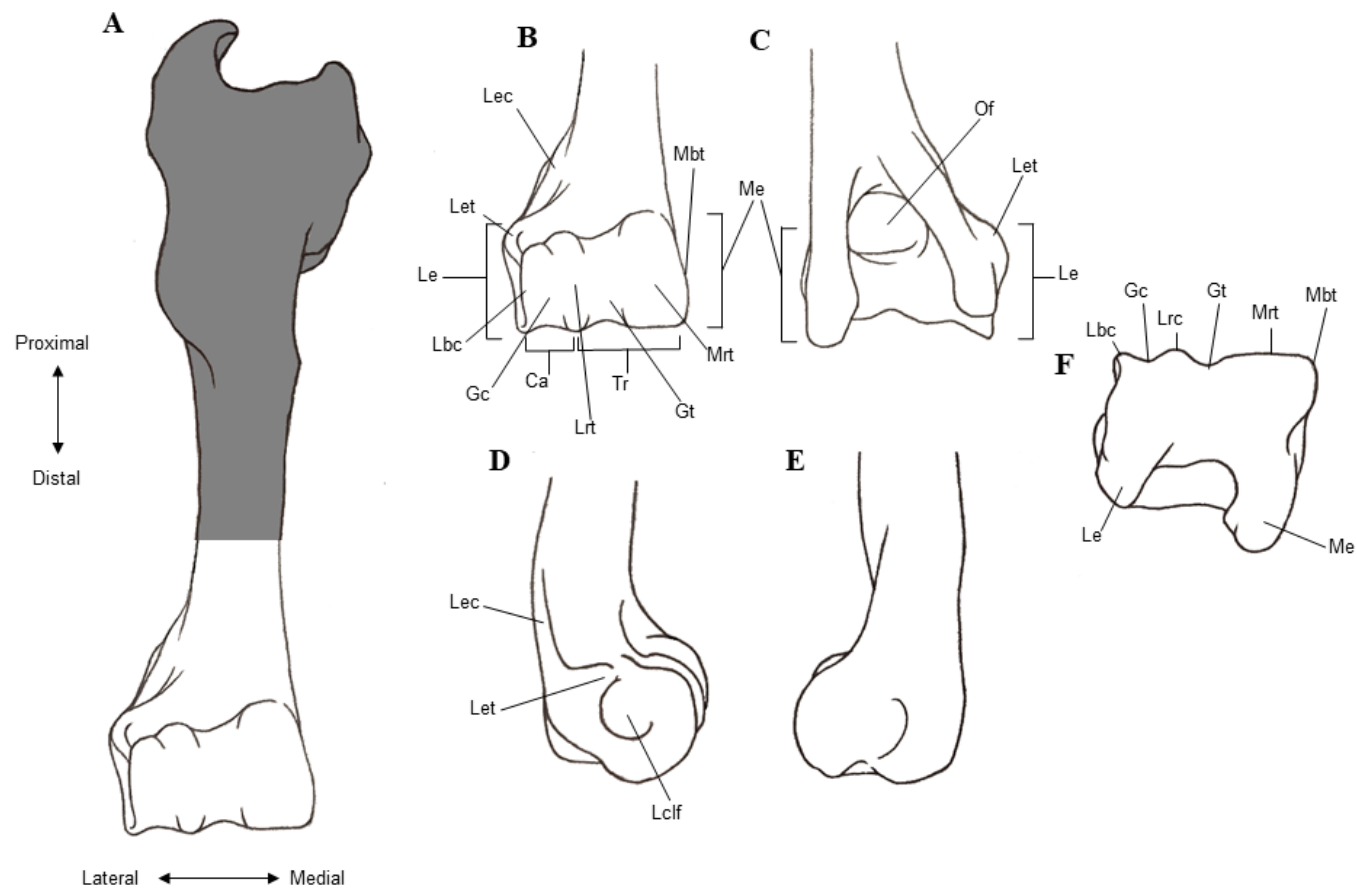


Figure 3: Diagrammatic representation of the distal humerus anatomy in bovids

Diagrammatic representation of the left distal humerus of *Connochaetes gnou* (black wildebeest) as an exemplar bovid. A) Cranial view of complete humerus with relevant distal portion in white, and the more proximal regions in grey; B) distal humerus in cranial view; C) distal humerus in caudal view; D) distal humerus in lateral view; E) distal humerus in medial view; F) distal humerus in distal view. Abbreviations: Ca, capitulum; Of, olecranon fossa; Gc, groove of capitulum; Gt, groove of trochlea; Lbc, lateral border of capitulum; Lclf, lateral collateral ligament fossa; Le, lateral epicondyle; Lec, lateral epicondylar crest; Let, lateral epicondylar tubercle; Lrt, lateral ridge of trochlea; Mbt, medial border of trochlea; Me, medial epicondyle; Mrt, medial ridge of trochlea; Tr, trochlea. Not to scale. Illustration by Sophia Anderson, 2020.

Rusingoryx atopocranion

MAMMALIA (Linnaeus 1758)

EUTHERIA (Gill 1872)

ARTIODACTYLA (Owen 1848)

BOVIDAE (Gray 1821)

ALCELAPHINI (Brooke in Wallace 1876)

Rusingoryx (Pickford and Thomas 1984)

Type species: *Rusingoryx atopocranion* (Pickford and Thomas 1984)

Holotype: KNM RU 10553A, skull with two horn cores, lacking the rostral portion of the face, the maxilla, the upper teeth, the zygomatic arch, and the tip of the left horn core.

Type locality: Wakondu, Rusinga Island, Lake Victoria, Kenya

Type horizon: Wasiriya Beds

Age: Late Pleistocene to Early Holocene

Rusingoryx atopocranion is the only species of its genus within the bovid tribe Alcelaphini, the tribe containing modern wildebeest (among others). *Rusingoryx* was first described in 1984 by Pickford & Thomas from a partial cranium uncovered at the Pleistocene Wasiriya Beds on Rusinga Island in Lake Victoria, Kenya. Since its original description, *Rusingoryx atopocranion* has been taxonomically reassigned multiple times, first being included in the genus *Megalotragus* by Harris (1991) – a placement supported by Vrba's 1997 phylogenetic analysis, which also agrees with Gentry et al.'s synonymization of *Rhynotragus* and *Megalotragus* into *Megalotragus* (1995). Since then, *Rusingoryx* was regarded as a junior synonym of *Megalotragus* (Geraads et al. 2004; Brink 2005) until Faith et al.'s 2011 reassessment of its taxonomic status via morphological comparison and phylogenetic analysis, which indicated that *Rusingoryx* represents a separate genus sharing a common ancestor with *Megalotragus* (Faith et al. 2011). For the rest of this dissertation, *Rusingoryx* will be considered a valid genus separate from *Megalotragus*.

Though no formal quantitative estimate has been produced for the body mass of *Rusingoryx*, it has been presumed to have had approximately similar body mass to its close living relative, the blue wildebeest (*Connochaetes taurinus*), based on the size of the skeletal elements found (O'Brien et al. 2016). This would give *Rusingoryx* a mean

estimated body mass of approximately 215 kg (Etienne et al. 2020), potentially ranging from 140-290 kg (Kingdon 2013).

***Rusingoryx* Humerus**

The distal humerus of *Rusingoryx atopocranion* conforms to the expected anatomy of a bovid and is overall visually similar to that of other alcelaphines. The capitulum/trochlea is approximately rectangular in anterior view, but with the medial trochlea being proximo-distally taller than the capitulum. This is most similar to its fellow alcelaphines, and similar also to the hippotragines. The supracondylar ridge is much reduced, giving the distal diaphysis a gracile appearance.

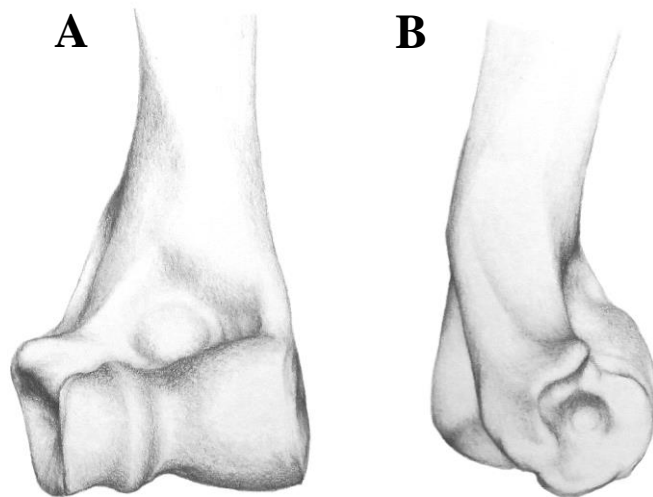


Figure 4: Left distal humerus of *Rusingoryx atopocranion*

Illustrated reconstruction of the distal humerus based on specimens BH-EX-1077, RU06-74, RU06-75/85, RU06-84 and RU06-86 in A) cranial view and B) lateral view. Illustration by Sophia Anderson, 2021.

The most notable aspect of the distal humerus morphology is a prominent tubercle extending from the lateral epicondyle. The protrusion follows directly from the distal end of the lateral epicondylar crest, forming a ridge across the top of the lateral epicondyle concavity and extending to an extremity antero-laterally at the level of the radial fossa. While some other ungulates exhibit a small protuberance in this region (for example, the closest living relatives of *Rusingoryx*, the wildebeests), the shape and extent of the tubercle in *Rusingoryx* is unlike the morphology of other known ungulates.

This is not, however, the only aspect of *Rusingoryx* morphology which has raised questions.

Cranial Dome

Perhaps the most striking aspect of *Rusingoryx* anatomy is its cranial morphology. The type specimen described by Pickford & Thomas in 1984 represents a partial cranium, including the horns, and it presented a surprising challenge when it came to orientation. The skull was originally oriented as shown in Figure 5A but, in 1991, Harris presented an orientation based on the occiput orientation found in *Megalotragus*, which results in the horns being directed downwards and what is present of the face projecting upwards abnormally (Figure 5B).

In 2016, O'Brien et al. described six new (and more complete) cranial specimens of *Rusingoryx* from the type locality (the Wasiriya Beds). They identified that the strange upward projection of the facial region in front of the horns was, in fact, the rising portion of a large nasal dome (Figure 5C). No analogous structure is known in extant vertebrates, and it is considered the first mammal ever discovered to possess hollow nasal crests (Figure 5D), but this structure is actually believed to be convergent with some hadrosaur dinosaurs,

functioning to allow the production of low-pitched resonant vocalisations which were, potentially, below the audible range of predators (O'Brien et al. 2016).

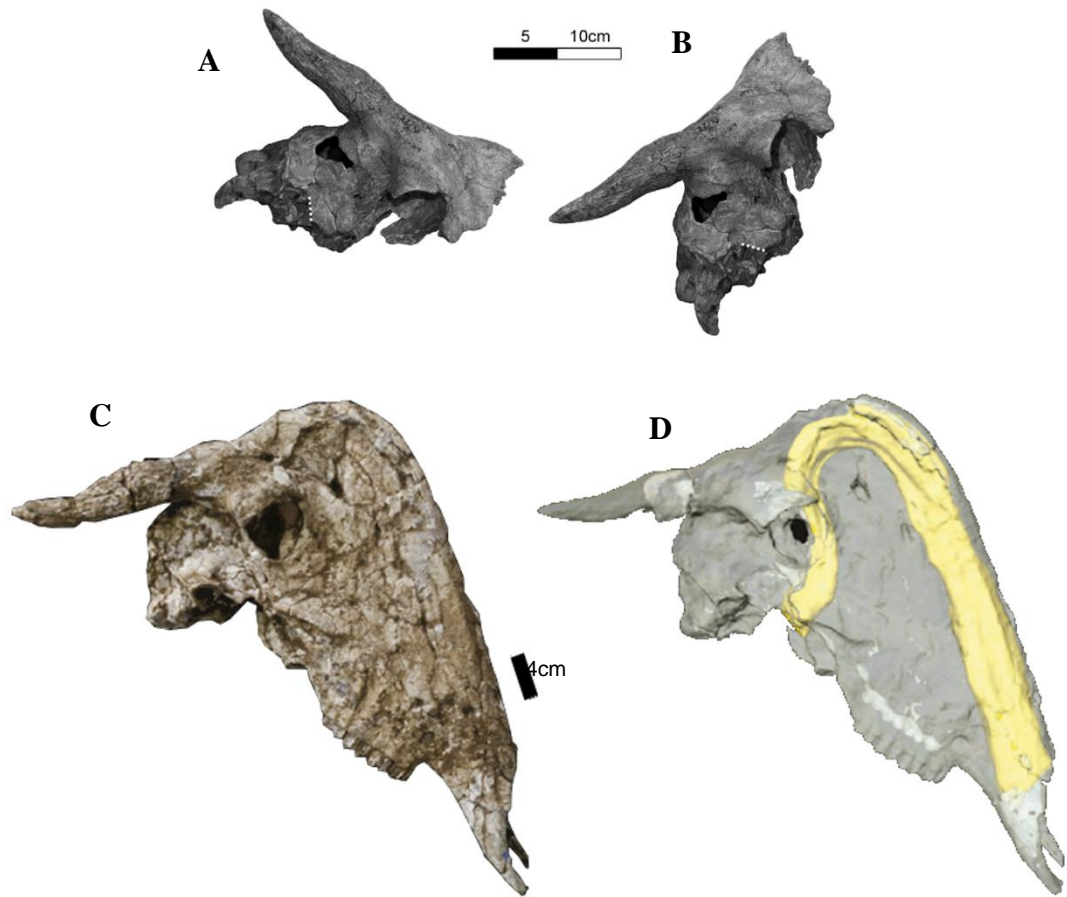


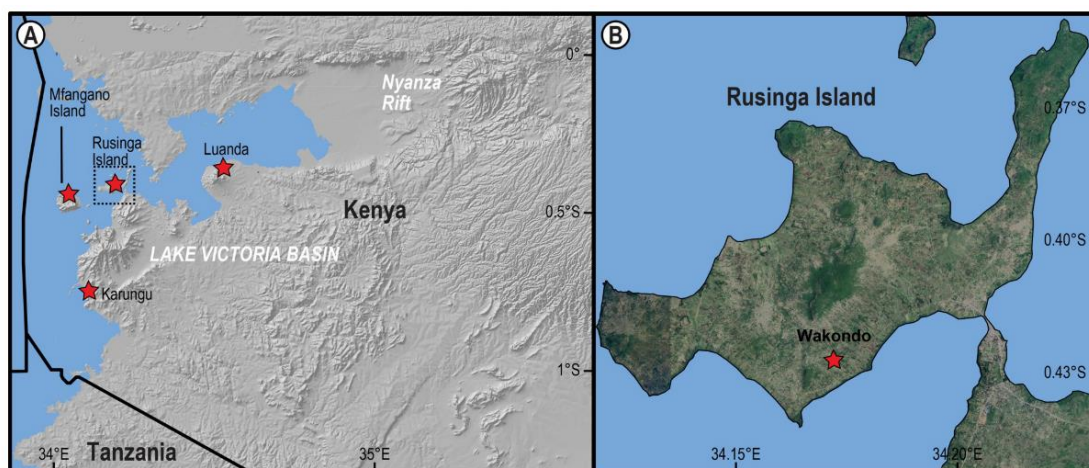
Figure 5: *Rusingoryx atopocranion* cranial material

A & B) Type specimen (KNM-RU-10553A) in lateral view, modified from Faith et al. 2011. A) Shows the orientation of the material as proposed by Pickford & Thomas (1984). B) Shows the orientation proposed by Harris (1991) to be analogous to the skull orientation of *Megalotragus*. In both, the line of the occiput is shown as a dotted white line.

C & D) KNM-RU-52571 in lateral view, modified from O'Brien et al. 2016. C) Shows a photograph of the specimen. D) Shows the specimen following CT segmentation to visualize the hollow nasal crest (yellow).

Distribution

Rusingoryx is not only known from Rusinga Island. Material has also been found on the nearby island of Mfangano (Tryon et al. 2016), and on the mainland around the eastern shores of Lake Victoria (Tryon et al. 2016; O'Brien et al. 2016) (Figure 6A). However, as shown in the table within Figure 6, the vast majority of known *Rusingoryx* material has been recovered from Rusinga Island.



Location	Number of identified pieces of material	Reference
Rusinga Island	329	Tryon et al. (2016)
Mfangano Island	12	Tryon et al. (2016)
Luanda	1	O'Brien et al. (2016)
Karungu	69	Tryon et al. (2016)

Figure 6: *Rusingoryx* material distribution

A) Showing a topographic map of the Kenyan Lake Victoria area with fossil localities denoted by red stars; B) showing Rusinga Island with the Wakondo Bovid Hill fossil locality (part of the Wasiriya Beds) denoted with a red star. Modified from Kovarovic et al. 2021.

Table provides details of the quantities of *Rusingoryx* material found at each locality.

Rusinga Island

Rusinga Island (Figure 6B) is an approximately 40 km² island in the Kenyan portion of Lake Victoria, Africa, which bears a rich Pleistocene deposit, as does the neighboring Mfangano Island (Tryon et al. 2014). The Pleistocene deposits of Rusinga are known as the Wasiriya Beds, and radiocarbon dating of fossil gastropods combined with archaeological analysis of stone artifacts from the beds has placed their age in the middle to late Pleistocene (285,000 to 28,000 years ago) (Tryon et al. 2010; Tryon and McBrearty 2006; Morgan and Renne 2008). The deposits are fluvial, arranged in a complex array of stratigraphic layers alternating between sandstone, siltstone, mudstone, tephra (pyroclastic ash) and conglomerates (Tryon et al. 2012).

Vertebrate material recovered from the Wasiriya Beds is predominantly comprised of alcelaphine bovids, with *Rusingoryx atopocranion* being the most abundant in the record so far. This is suggestive of an open grassland environment, and the presence of species such as the gemsbok (*Oryx gazella*) and Grevy's zebra (*Equus grevyi*) indicates that the area was arid. This, of course, appears contradictory to the fluvial nature of the sediment deposits, but taken together these pieces of evidence suggests that the Wasiriya Beds represent a time when Rusinga was connected to mainland Kenya (Faith et al. 2011). Today, Rusinga is only separated from mainland Kenya by a passage approximately 350 m wide and 5 m deep, and the level of Lake Victoria in the last 200 years has been recorded to fluctuate by around 4 m due to variation in precipitation (Nicholson 1998). Given this evidence, we cannot consider the Wasiriya Bed fauna to have been isolated from the mainland for long enough periods to allow speciation and endemism, and we may consider the Rusinga fauna as one with the mainland fauna (Faith et al. 2011). The presence of reduncine bovids and a hippopotamus in the faunal assemblage suggests seasonally available water, and this is supported by chemical analysis which indicates the Wasiriya Beds representing a wetter environment within a broader open grassland (Tryon et al. 2012). Taphonomically speaking, it is likely that the conditions of the Wasiriya Beds offered the best preservation conditions, but the wider area was equally diverse and species-rich at the time.

***Rusingoryx* Assemblage at Bovid Hill**

The richest deposit of *Rusingoryx* so far known was found at a site of the Wasiriya Beds at Wakondo, Rusinga Island. Three partial bovid skeletons were uncovered in 2007, and the sub-locality became known as ‘Bovid Hill’. Cut marks found on the bones led to focused, systematic surface collection at Bovid Hill in 2009 and 2010 and eventually a full 19m² excavation in 2011 (Jenkins et al. 2017). Though teeth and occasionally partial mandibles of other ungulate species were found at the site, the material recovered from Bovid Hill is dominated by *Rusingoryx*, including multiple skulls and associated postcrania, representing a minimum number of 16 individuals (Jenkins et al. 2017). The assemblage includes individuals of all ages, but is dominated by adults considered to be at ‘prime-age’ for hunting by humans. Surface marks on the bones are interpreted as evidence of anthropogenic disarticulation and butchery, particularly chop marks on the radio-ulna and tibia, and scrape marks on the radio-ulna. Breakages of the long bones are also consistent with fresh/green breaks, indicative of disarticulation of a freshly deceased animal. This all leads to the conclusion that Middle Stone Age (MSA) humans were present at the death assemblage, and utilizing at least parts of the deceased *Rusingoryx* material (Jenkins et al. 2017). Jenkins et al.’s analyses support the assemblage representing a single catastrophic event rather than an accumulation of remains over long periods of time, due to the relative monospecificity of the assemblage and the consistency of weathering on the bones. This leaves the question, were these animals killed by the MSA humans, or simply scavenged by them after a natural catastrophe? There is a notable lack of any evidence of projectile damage to the bones, which appears to counter-indicate hunting, but what is clear is that MSA humans likely had primary/early access to the carcasses, as evidenced by a lack of apparent carnivore damage, the surface cut marks on the bone, and the substantial number of lithic artefacts at the site which can be directly associated with the production of such marks. While mass drowning events are often responsible for large death assemblages of ungulates, this is not likely to have been the case at Bovid Hill, as the topography of the region and the placement of the stream means that the water was not likely to have become particularly deep at any point, or to have had a fast enough current to become dangerous. Taking all of this into account, Jenkins et al. (2016) favour the idea that the Bovid Hill assemblage represents an incidence of tactical hunting. They suggest that the MSA humans actively drove the *Rusingoryx* herd into a particularly treacherous part of the stream during the wet season, leaving the animals in danger from the water itself, and unable to escape the hunters, or that *Rusingoryx* which came to drink from the stream were targeted while

vulnerable. This type of tactical hunting, utilizing the landscape, has been documented many times around the world in modern human groups, including the Murle of South Sudan who hunt kob near Pibor Post (at the confluence of the Kengen and Pibor Rivers) during the migration season (Jenkins et al. (2016) and references therein). Undoubtedly, this site shows the importance of *Rusingoryx* to the MSA humans of the area, exemplifying the important relationship between these humans and the surrounding ecosystem.

Rationale

Deposits and materials from the Middle Stone Age (MSA) provide an important insight into a key point in human evolution, and understanding the environment in which these early anatomically modern humans existed is a key part of understanding this evolution as a whole. This period of human history is of great significance as the MSA was dominated by not only anatomically archaic humans (*Homo helmei*), but also anatomically modern humans (*Homo sapiens*) (Herries 2011), and it is during the MSA that modern human behaviour is believed to have begun developing (McBrearty and Brooks 2000). Studying the ecosystems and individual species known to have been present alongside the MSA humans is one of the best ways to gain insight into the early human world, particularly when it comes to studying animals which the MSA humans are known to have interacted with. *Rusingoryx* is one such animal, and since it has been shown to have been highly adapted to a very specific environment, it is a particularly ecomorphologically informative species. By studying the functional morphology of extant bovids, not only will it be possible to better understand *Rusingoryx*, but more data can be added to the broader understanding of bovid functional morphology and ecomorphology. The distal humerus provides an ideal skeletal element to use for such a study, being a robust and frequently preserved region which is highly functionally relevant. This is the rationale which leads into the rest of this project.

Aims

To better understand the relationship between morphology of the distal humerus and ecology in bovids, thus establishing shape changes in this region as ecological proxies. Secondly, to utilize this ecomorphology data in modern bovids to understand the unusual distal humerus morphology of the extinct alcelaphine *Rusingoryx atopocranion*.

Hypotheses

H₀ – Shape variation in the distal humerus of bovids is not related to phylogenetic affinity, habitat preference or body mass.

H₁ - Shape variation in the distal humerus of bovids is related to phylogeny (tribe).

H₂ - Shape variation in the distal humerus of bovids is related to preferred habitat of the animal.

H₃ - Shape variation in the distal humerus of bovids is related to body mass.

Chapter 2: Materials & Methods

Table 1: Important statistical terms

Statistical term	Meaning
Pagel's lambda value (λ)	Used in phylogenetic generalized least squares (PGLS) analysis. Lambda is a measure of the phylogenetic signal contained in the residuals of the regression of x on y. This value relates explicitly to the effect of phylogeny on the relationship between the dependent and independent variable(s), and ranges from 0 to 1. Lambda equals 1 when the residual covariance between individuals is directly proportional to phylogenetic distance. Thus, in simple interpretation, lambda of 0 implies that phylogeny has no bearing on the observed relationship, and 1 implies that the observed relationship is entirely due to the effect of phylogeny.
Regression coefficient	A value representing the relationship between an independent variable and the dependent variable in a regression. In a linear relationship of the form $y = mx + c$, the regression coefficient is equal to m (the gradient of the line of best fit).
r-squared (r^2)	An indicator of the goodness of fit of a linear model. Strictly, the proportion of variance in the dependent variable which can be explained/predicted from the independent variable or variables. An r^2 value of 0 would indicate very poor fit of the model (none of the variance in the dependent variable can be explained by the independent variable(s)), while a value of 1 would indicate a perfect fit (100% of the variance in the dependent variable may be explained by the independent variables(s)). The term 'adjusted r^2 ' refers to an r^2 value which has been mathematically adjusted to account for the number of independent variables in the model. This value is always \leq the value of the r^2 for the same analysis, and may be negative.
t-statistic	Used in hypothesis testing as part of the process of determining whether there is a significant difference between the means of two groups, this represents the ratio. High values of the t-statistic indicate a large difference between the two group means in question.

Providing some key statistical terms which will be used throughout this dissertation.

Geometric Morphometrics (GMM) – the principles of which are discussed above – was utilized to address the hypotheses and aims of the study. In order to conduct GMM analyses, 3D scans of specimens were acquired from which the raw data could be obtained.

Scan Acquisition

All 3D scans of bovid humeri used in this study were acquired from supervisors, collaborators and online repositories, as in-person scanning was not possible due to Covid-19. The scans were produced via surface scanning for the most part (a method in which light is directed at the specimen and details of its reflection off the specimen are recorded and translated into a scanned image), with some provided by Cyril Etienne being produced via photogrammetry (a technique which involves photographing a subject from multiple angles and combining these images digitally to gain a 3D representation). For surface scanning, Etienne et al. used the Artec Eva and for photogrammetry they used a Nikon D550 & Agisoft Photoscan v1.4.0. Both Andrew Barr and Frances Forrest used the EinScan for surface scanning, and Kris Kovarovic used NextEngine. Details of each specimen are provided in Table 2A, and scanning methods are given in Table 2B.

A

Table 2: Specimen details

Tribe	Genus	Species	Specimen accession number	Scan source
Alcelaphini	<i>Alceplaphus</i>	<i>buselaphus</i>	MNHN 1899-238	Cyril Etienne
Alcelaphini	<i>Alceplaphus</i>	<i>buselaphus</i>	BERLIN 71862	Cyril Etienne
Alcelaphini	<i>Connochaetes</i>	<i>gnou</i>	NHM 1850.11.22.70.645	Fire Kovarovic
Alcelaphini	<i>Connochaetes</i>	<i>gnou</i>	MNHN 1976-344	Cyril Etienne
Alcelaphini	<i>Connochaetes</i>	<i>gnou</i>	MNHN 2013-26	Cyril Etienne
Alcelaphini	<i>Connochaetes</i>	<i>taurus</i>	NMNH 161976	Cyril Etienne
Alcelaphini	<i>Connochaetes</i>	<i>taurus</i>	NMNH 163012	Andrew Barr
Alcelaphini	<i>Connochaetes</i>	<i>taurus</i>	NHM 1936.3.30.15	Fire Kovarovic
Alcelaphini	<i>Damaliscus</i>	<i>lunatus</i>	NMNH 163170	Andrew Barr
Alcelaphini	<i>Damaliscus</i>	<i>lunatus</i>	NMNH 163172	Andrew Barr
Alcelaphini	<i>Damaliscus</i>	<i>pygargus</i>	BERLIN 70722	Cyril Etienne
Alcelaphini	<i>Damaliscus</i>	<i>pygargus</i>	BERLIN 7165	Cyril Etienne
Antilopini	<i>Antidorcas</i>	<i>marsupialis</i>	MNHN 1971-89	Cyril Etienne
Antilopini	<i>Antidorcas</i>	<i>marsupialis</i>	MNHN 1993-1670	Cyril Etienne
Antilopini	<i>Antilope</i>	<i>cervicapra</i>	MNHN 1901-174	Cyril Etienne
Antilopini	<i>Antilope</i>	<i>cervicapra</i>	MNHN 1992-618	Cyril Etienne

Antilopini	<i>Eudorcas</i>	<i>rufifrons</i>	NMNH 252685	Andrew Barr
Antilopini	<i>Eudorcas</i>	<i>thomsonii</i>	NMNH 163048	Andrew Barr
Antilopini	<i>Eudorcas</i>	<i>thomsonii</i>	NMNH 162007	Andrew Barr
Antilopini	<i>Eudorcas</i>	<i>thomsonii</i>	NMNH 163055	Andrew Barr
Antilopini	<i>Gazella</i>	<i>dorcas</i>	NMNH 329355	Andrew Barr
Antilopini	<i>Gazella</i>	<i>dorcas</i>	NMNH 328577	Andrew Barr
Antilopini	<i>Gazella</i>	<i>dorcas</i>	NMNH 328578	Andrew Barr
Antilopini	<i>Litocranius</i>	<i>walleri</i>	NMNH 163033	Andrew Barr
Antilopini	<i>Litocranius</i>	<i>walleri</i>	NMNH 163034	Andrew Barr
Antilopini	<i>Litocranius</i>	<i>walleri</i>	NMNH 164035	Andrew Barr
Antilopini	<i>Nanger</i>	<i>dama</i>	BERLIN 68971	Cyril Etienne
Antilopini	<i>Nanger</i>	<i>dama</i>	BERLIN 83430	Cyril Etienne
Antilopini	<i>Nanger</i>	<i>granti</i>	NMNH 163070	Cyril Etienne
Antilopini	<i>Nanger</i>	<i>granti</i>	NMNH 163080	Andrew Barr
Antilopini	<i>Nanger</i>	<i>granti</i>	NMNH 163083	Andrew Barr
Antilopini	<i>Saiga</i>	<i>tatarica</i>	MNHN 1959-177	Cyril Etienne
Antilopini	<i>Saiga</i>	<i>tatarica</i>	MNHN 1964-313	Cyril Etienne
Boselaphini	<i>Boselaphus</i>	<i>tragocamelus</i>	MNHN 1864-103	Cyril Etienne
Boselaphini	<i>Boselaphus</i>	<i>tragocamelus</i>	MNHN 1907-146	Cyril Etienne

Boselaphini	<i>Tetracerus</i>	<i>quadricornis</i>	MNHN 1988-223	Cyril Etienne
Boselaphini	<i>Tetracerus</i>	<i>quadricornis</i>	MNHN 1993-4627	Cyril Etienne
Bovini	<i>Bison</i>	<i>bison</i>	MNHN 1885-339	Cyril Etienne
Bovini	<i>Bison</i>	<i>bison</i>	MNHN 1902-316	Cyril Etienne
Bovini	<i>Bos</i>	<i>frontalis</i>	MNHN 1965-120	Cyril Etienne
Bovini	<i>Bos</i>	<i>frontalis</i>	MNHN 1970-280	Cyril Etienne
Bovini	<i>Bos</i>	<i>grunniens</i>	MNHN 1886-300	Cyril Etienne
Bovini	<i>Bos</i>	<i>grunniens</i>	MNHN 2008-107	Cyril Etienne
Bovini	<i>Bos</i>	<i>javanicus</i>	MNHN 1994-101	Cyril Etienne
Bovini	<i>Bos</i>	<i>javanicus</i>	MNHN 1967-1689	Cyril Etienne
Bovini	<i>Bos</i>	<i>taurus</i>	MNHN 1926-302	Cyril Etienne
Bovini	<i>Bos</i>	<i>taurus</i>	MNHN A10916	Cyril Etienne
Bovini	<i>Bubalus</i>	<i>bubalis</i>	MNHN 1857-19	Cyril Etienne
Bovini	<i>Bubalus</i>	<i>bubalis</i>	MNHN 1863-65	Cyril Etienne
Bovini	<i>Bubalus</i>	<i>depressicornis</i>	MNHN 2009-421	Cyril Etienne
Bovini	<i>Bubalus</i>	<i>depressicornis</i>	MNHN SSN	Cyril Etienne
Bovini	<i>Syncerus</i>	<i>caffer</i>	NMNH 161945	Andrew Barr
Bovini	<i>Syncerus</i>	<i>caffer</i>	NMNH 163336	Andrew Barr
Bovini	<i>Syncerus</i>	<i>caffer</i>	NMNH 164768	Andrew Barr

Caprini	<i>Ammotragus</i>	<i>lervia</i>	MNHN 1896-439	Cyril Etienne
Caprini	<i>Ammotragus</i>	<i>lervia</i>	MNHN 2010-643	Cyril Etienne
Caprini	<i>Capra</i>	<i>hircus</i>	MNHN 2007-1349	Cyril Etienne
Caprini	<i>Capra</i>	<i>hircus</i>	MNHN SSN	Cyril Etienne
Caprini	<i>Capricornis</i>	<i>milneedwardsii</i>	MNHN 1874-283	Cyril Etienne
Caprini	<i>Hemitragus</i>	<i>jemlahicus</i>	MNHN 1971-68	Cyril Etienne
Caprini	<i>Hemitragus</i>	<i>jemlahicus</i>	MNHN 1972-133	Cyril Etienne
Caprini	<i>Naemorhedus</i>	<i>goral</i>	MNHN 1963-320	Cyril Etienne
Caprini	<i>Oreamnos</i>	<i>americanus</i>	BERLIN 67805	Cyril Etienne
Caprini	<i>Oreamnos</i>	<i>americanus</i>	MNHN 2009-253	Cyril Etienne
Caprini	<i>Pseudois</i>	<i>nayaur</i>	MNHN 1972-92	Cyril Etienne
Caprini	<i>Pseudois</i>	<i>nayaur</i>	MNHN 1966-136	Cyril Etienne
Caprini	<i>Rupicapra</i>	<i>rupicapra</i>	MNHN 1995-183	Cyril Etienne
Caprini	<i>Rupicapra</i>	<i>rupicapra</i>	MNHN 1923-2326	Cyril Etienne
Cephalophini	<i>Cephalophus</i>	<i>monticola</i>	AMNH M-52725	Frances Forrest
Cephalophini	<i>Cephalophus</i>	<i>monticola</i>	AMNH M-52726	Frances Forrest
Cephalophini	<i>Cephalophus</i>	<i>monticola</i>	AMNH M-52753	Frances Forrest
Cephalophini	<i>Cephalophus</i>	<i>silvicultor</i>	MNHN 1981-1023	Cyril Etienne
Cephalophini	<i>Sylvicapra</i>	<i>grimmia</i>	AMNH M-187810	Frances Forrest

Cephalophini	<i>Sylvicapra</i>	<i>grimmia</i>	AMNH M-80563	Frances Forrest
Hippotragini	<i>Addax</i>	<i>nasomaculatus</i>	MNHN 1970-277	Cyril Etienne
Hippotragini	<i>Hippotragus</i>	<i>equinus</i>	MNHN 1969-167	Cyril Etienne
Hippotragini	<i>Hippotragus</i>	<i>equinus</i>	MNHN 1995-147	Cyril Etienne
Hippotragini	<i>Hippotragus</i>	<i>niger</i>	BERLIN SSN	Cyril Etienne
Hippotragini	<i>Oryx</i>	<i>dammah</i>	MNHN 1972-106	Cyril Etienne
Hippotragini	<i>Oryx</i>	<i>dammah</i>	MNHN 1905-227	Cyril Etienne
Hippotragini	<i>Oryx</i>	<i>gazella</i>	MNHN 1994-009	Cyril Etienne
Hippotragini	<i>Oryx</i>	<i>gazella</i>	MNHN 1997-009	Cyril Etienne
Hippotragini	<i>Oryx</i>	<i>leucoryx</i>	MNHN 1996-2100	Cyril Etienne
Hippotragini	<i>Oryx</i>	<i>leucoryx</i>	MNHN 1996-2101	Cyril Etienne
Neotragini	<i>Madoqua</i>	<i>kirkii</i>	BERLIN 77194	Cyril Etienne
Neotragini	<i>Madoqua</i>	<i>kirkii</i>	AMNH M-35956	Frances Forrest
Neotragini	<i>Madoqua</i>	<i>kirkii</i>	AMNH M-36352	Frances Forrest
Neotragini	<i>Oreotragus</i>	<i>oreotragus</i>	MNHN 2007-1388	Cyril Etienne
Neotragini	<i>Oreotragus</i>	<i>oreotragus</i>	MNHN SSN	Cyril Etienne
Neotragini	<i>Ourebia</i>	<i>ourebi</i>	BERLIN 77195	Cyril Etienne
Neotragini	<i>Ourebia</i>	<i>ourebi</i>	MNHN 1972-93	Cyril Etienne
Ovibovini	<i>Ovibos</i>	<i>moschatus</i>	MNHN 1997-39	Cyril Etienne

Redunicini	<i>Kobus</i>	<i>ellipsiprymnus</i>	NMNH 161989	Andrew Barr
Redunicini	<i>Kobus</i>	<i>ellipsiprymnus</i>	NMNH 164689	Andrew Barr
Redunicini	<i>Kobus</i>	<i>ellipsiprymnus</i>	NMNH 164737	Andrew Barr
Redunicini	<i>Kobus</i>	<i>kob</i>	NMNH 163193	Andrew Barr
Redunicini	<i>Kobus</i>	<i>kob</i>	NMNH 163195	Andrew Barr
Redunicini	<i>Kobus</i>	<i>kob</i>	NMNH 164499	Andrew Barr
Redunicini	<i>Kobus</i>	<i>vardonii</i>	NMNH 334255	Andrew Barr
Redunicini	<i>Redunca</i>	<i>arundinum</i>	NMNH 469909	Andrew Barr
Redunicini	<i>Redunca</i>	<i>fulvorufula</i>	NMNH 161992	Andrew Barr
Redunicini	<i>Redunca</i>	<i>fulvorufula</i>	NMNH 161994	Andrew Barr
Redunicini	<i>Redunca</i>	<i>redunca</i>	MNHN 1881-1147	Cyril Etienne
Redunicini	<i>Redunca</i>	<i>redunca</i>	NMNH 163188	Andrew Barr
Redunicini	<i>Redunca</i>	<i>redunca</i>	NMNH 163190	Andrew Barr
Rusingoryx	<i>Rusingoryx</i>	<i>atopocranion</i>	KNM-BH-EX-1077	Fire Kovarovic
Rusingoryx	<i>Rusingoryx</i>	<i>atopocranion</i>	KNM-RU06-74	Fire Kovarovic
Rusingoryx	<i>Rusingoryx</i>	<i>atopocranion</i>	KNM-RU06-75,85	Fire Kovarovic
Tragelaphini	<i>Taurotragus</i>	<i>derbianus</i>	NMNH 164646	Andrew Barr
Tragelaphini	<i>Taurotragus</i>	<i>derbianus</i>	NMNH 164647	Andrew Barr
Tragelaphini	<i>Taurotragus</i>	<i>oryx</i>	MNHN AGA-7983	Cyril Etienne

Tragelaphini	<i>Taurotragus</i>	<i>oryx</i>	NMNH 1633308	Andrew Barr
Tragelaphini	<i>Tragelaphus</i>	<i>eurycerus</i>	NMNH 163226	Andrew Barr
Tragelaphini	<i>Tragelaphus</i>	<i>scriptus</i>	NMNH 164500	Andrew Barr
Tragelaphini	<i>Tragelaphus</i>	<i>scriptus</i>	NMNH 164560	Andrew Barr
Tragelaphini	<i>Tragelaphus</i>	<i>scriptus</i>	NMNH 164741	Andrew Barr
Tragelaphini	<i>Tragelaphus</i>	<i>spekii</i>	NMNH 164558	Andrew Barr
Tragelaphini	<i>Tragelaphus</i>	<i>spekii</i>	MNHN 1980-7	Cyril Etienne
Tragelaphini	<i>Tragelaphus</i>	<i>strepsiceros</i>	BERLIN SSN	Cyril Etienne
Tragelaphini	<i>Tragelaphus</i>	<i>strepsiceros</i>	NMNH 21655	Andrew Barr

B

Source	Scan type	Equipment used
Etienne et al.	Surface scanning	Artec Eva
	Photogrammetry	Nikon D550 & Agisoft Photoscan v1.4.0
Kris Kovarovic	Surface scanning	NextEngine 3D Desktop scanner
Andrew Barr	Surface scanning	EinScan
Frances Forrest	Surface scanning	EinScan

A) For each specimen, details are provided on taxonomy, acquisition number, and source. Specimens in grey were not included in the final 3D analysis, but were included in preliminary 2D analyses (Appendix I).

B) For each scan source, details of the scan type and equipment used are provided.

Quantitative shape data are then acquired via landmarking these 3D scans.

3D Landmarking

Landmarks are points on the shape which are homologous across all specimens. There are four main classifications of landmark type within geometric morphometrics (Zelditch et al. 2004):

- Type 1 – A point at the juxtaposition of tissues, or the intersection of boundary lines
- Type 2 – A point of maximum curvature of a surface
- Type 3 – An extreme point (e.g. the most distal point on a structure)
- Other – A point defined by surrounding arrangements (e.g. the point 50% the distance between two other points)

Before the final landmarking to collect data for the study could be completed, a landmark schema had to be decided upon. An initial landmark schema was devised based on anatomical significance of each locus and ability to represent the shape as a whole. A series of repeatability tests were conducted (the results of which can be found in Appendix III) to ascertain the reliability of the proposed landmark schema and modify it to maximise repeatability. The final landmarking schema used is shown in Figure 7, with each landmark locus defined in Table 3. The scans were landmarked in Avizo ver. 7.1.0 (Konrad-Zuse-Zentrum Berlin 2012), then the coordinate data of the landmarks (saved as an ascii file) was brought into R ver. 4.0.3 (The R Foundation for Statistical Computing 2020) where it was converted into a file readable by MorphoJ ver. 1.07a (Klingenberg 2011) (the code utilised is given in Appendix IV). It should be noted that only three of the five available *Rusingoryx* scans (KNM-BH-EX-1077, KNM-RU06-74, and KNM-RU06-75,85) could be included in the 3D analysis as the remaining two did not include enough of the diaphysis to landmark using the finalised schema. It was decided that it was, on balance, more important to capture the diaphysis landmarks than to change the schema in order to include all of the *Rusingoryx* specimens.

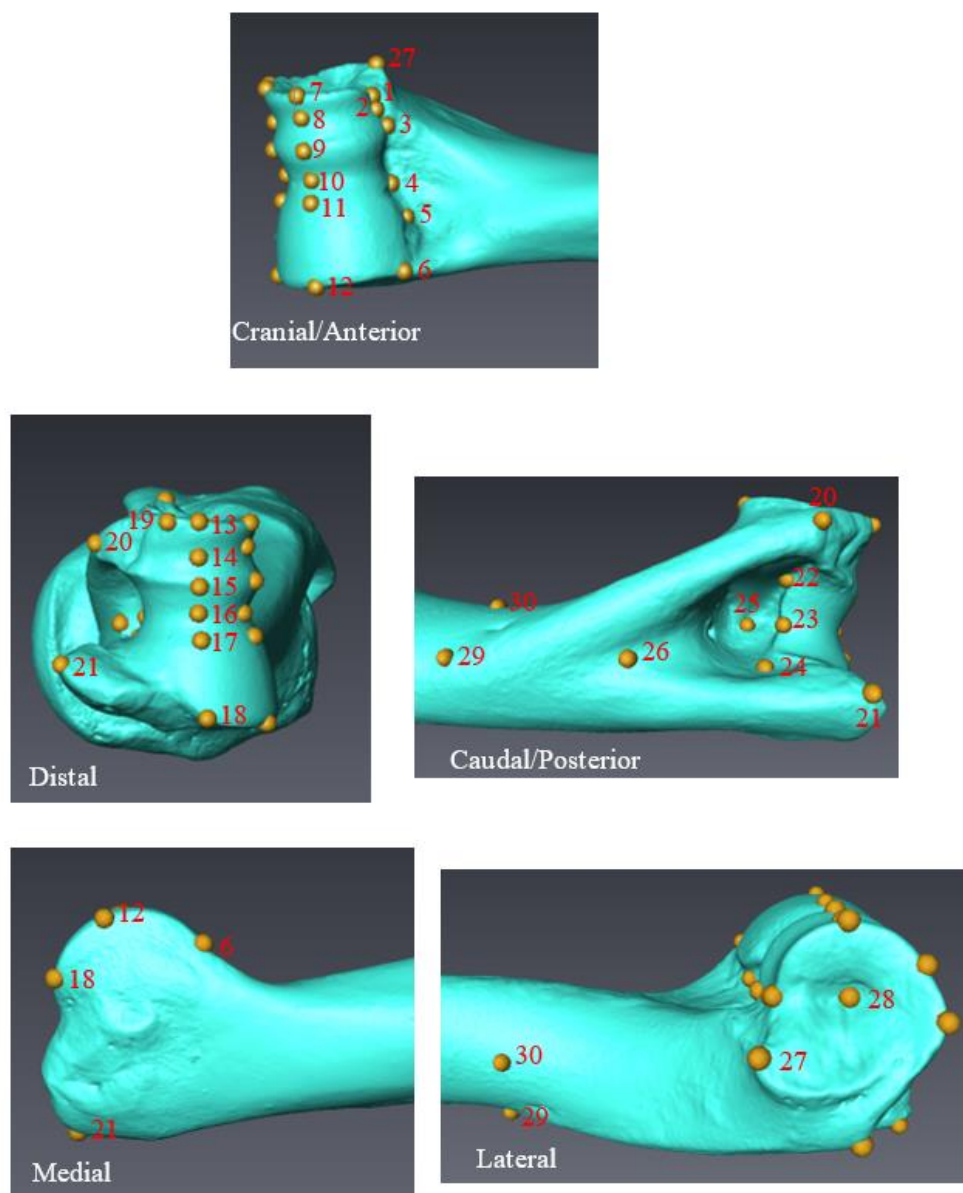


Figure 7: Final 30 landmark schema used for 3D landmarking

Screenshots of *Damaliscus lunatus* (NMNH 163170) landmarked in Avizo following a 30 landmark schema. Landmarks are numbered in red according to the order in which the locus was landmarked. Full descriptions of the landmark locus are given in Table 3.

Table 3: 30 landmark schema used for 3D landmarking

Landmark number	Landmark type	Description
1	1	Point where proximal end of the lateral border of the capitulum meets the diaphysis
2	1	Point where proximal end of the groove of the capitulum meets the diaphysis
3	1	Point where proximal end of the lateral trochlear ridge meets the diaphysis
4	1	Point where proximal end of the groove of the trochlea meets the diaphysis
5	1	Point where proximo-lateral corner of the medial trochlear ridge meets the diaphysis
6	1	Point where proximo-medial corner of the medial trochlear ridge meets the diaphysis
7	other	Point at 50% height of the lateral border of the capitulum in cranial view
8	other	Point at 50% height of the groove of the capitulum in cranial view
9	other	Point at 50% height of the lateral trochlear ridge in cranial view
10	other	Point at 50% height of the groove of the trochlea in cranial view
11	other	Point at 50% height of the lateral edge of the medial trochlear ridge in cranial view
12	other	Point at 50% height of the medial edge of the medial trochlear ridge in cranial view
13	other	Point at 50% depth of lateral border of the capitulum in distal view
14	other	Point at 50% depth of the groove of the capitulum in distal view
15	other	Point at 50% depth of the lateral trochlear ridge in distal view
16	other	Point at 50% depth of the groove of the trochlea in distal view
17	other	Point at 50% depth of the lateral edge of the medial trochlear ridge in distal view
18	other	Point at 50% depth of the medial edge of the medial trochlear ridge in distal view
19	3	Most distal extension of the lateral epicondyle
20	3	Most caudo-distal extension of the lateral epicondyle
21	3	Most caudo-distal extension of the medial epicondyle
22	2	Lateral interior corner of olecranon fossa
23	other	Point on the distal border of the olecranon fossa equidistant between landmarks 22 & 24
24	2	Medial interior corner of olecranon fossa
25	3	Cranio-caudally deepest point of olecranon fossa
26	2	Most proximal point of olecranon fossa
27	3	Most lateral extent of protuberance on lateral epicondyle
28	2	Deepest point of fossa for lateral collateral ligament
29	3	Most proximal point of lateral epicondylar crest
30	other	Point at 50% cranio-caudal width of diaphysis in line with landmark 29 in medial view

Providing anatomical placement and type for each landmark used in the full 3D analysis.

Generalized Procrustes Analysis

The coordinates of all 30 landmarks for each of the 118 specimens were saved as ascii files within Avizo, then converted into .txt files using R ver. 4.0.3 in order to be easily read into MorphoJ. Within MorphoJ, a Procrustes superimposition was carried out (with all specimens aligned to the first specimen), such that all the configurations of landmarks were translated, scaled and rotated to minimize variation between specimens at each landmark. The output Procrustes coordinates were then used in the subsequent multivariate analyses, much of which was also carried out in MorphJ, with additional analyses in R.

Multivariate Analyses

Categorical Variable Classification

In order to uncover functional and ecological relationships with form in the bovid distal humerus, three categorical variables were used.

Tribe classification at eleven levels follows ultimateungulate.com (Huffman 2020) and references therein.

A six-level habitat preference classification system was used: Grassland/treeless (GT), Wooded bushland/grassland (WBG), Light woodland/bushland (LWB), Heavy woodland/bushland (HWB), Forest (F), and Montane (M). These classification data were compiled from Barr (2020), Etienne et al. (2020), and Kovarovic et al. (2021).

A seven-level biologically-derived body mass classification system was used following Andrews et al. (1979) and Kovarovic et al. (2002): 1-10 kg, 10-45 kg, 45-90 kg, 90-180 kg, 180-360 kg, 360-575 kg, >575 kg. These category delineations are based on the exponential decay relationship between increasing size and weight-bearing functional adaptations, in which there is little functional variation at the large body mass end of the scale. These classification data were compiled from Barr (2020), Etienne et al. (2020), and Kovarovic et al. (2021). A list of these categorical variables for each species in the dataset is given in Table 4.

Table 4: Categorical variables used in the study

Tribe	Genus	Species	Habitat preference category	Mean body mass	Body mass category
Alcelaphini	<i>Alceplaphus</i>	<i>buselaphus</i>	WBG ¹	169 ³	90-180kg
Alcelaphini	<i>Connochaetes</i>	<i>gnou</i>	GT ¹	145 ³	90-180kg
Alcelaphini	<i>Connochaetes</i>	<i>taurus</i>	GT ¹	215 ⁴	180-360kg
Alcelaphini	<i>Damaliscus</i>	<i>pygargus</i>	GT ¹	71 ³	45-90kg
Alcelaphini	<i>Damaliscus</i>	<i>lunatus</i>	GT ²	117.5 ⁴	90-180kg
Antilopini	<i>Antidorcas</i>	<i>marsupialis</i>	WBG ¹	29 ³	10-45kg
Antilopini	<i>Antilope</i>	<i>cervicapra</i>	WBG ³	37.5 ³	10-45kg
Antilopini	<i>Eudorcas</i>	<i>rufifrons</i>	WBG ¹	25 ⁴	10-45kg
Antilopini	<i>Eudorcas</i>	<i>thomsonii</i>	WBG ¹	19 ³	10-45kg
Antilopini	<i>Gazella</i>	<i>dorcas</i>	GT ¹	19 ³	10-45kg
Antilopini	<i>Litocranius</i>	<i>walleri</i>	LWB ¹	40 ³	10-45kg
Antilopini	<i>Nanger</i>	<i>dama</i>	WBG ¹	57.5 ³	45-90kg
Antilopini	<i>Nanger</i>	<i>granti</i>	WBG ²	59.75 ⁴	45-90kg
Antilopini	<i>Saiga</i>	<i>tatarica</i>	GT ³	36 ³	10-45kg
Boselaphini	<i>Boselaphus</i>	<i>tragocamelus</i>	WBG ³	205 ³	180-360kg
Boselaphini	<i>Tetracerus</i>	<i>quadricornis</i>	F ³	20 ³	10-45kg
Bovini	<i>Bison</i>	<i>bison</i>	GT ³	679 ³	>575kg
Bovini	<i>Bos</i>	<i>frontalis</i>	Domestic ³	455 ³	360-575kg
Bovini	<i>Bos</i>	<i>grunniens</i>	F ³	395 ³	360-575kg
Bovini	<i>Bos</i>	<i>javanicus</i>	F ³	600 ³	>575kg
Bovini	<i>Bos</i>	<i>taurus</i>	Domestic ³	725 ³	>575kg
Bovini	<i>Bubalus</i>	<i>bubalis</i>	F ³	700 ³	>57kg
Bovini	<i>Bubalus</i>	<i>depressicornis</i>	F ³	225 ³	180-360kg

Bovini	<i>Syncerus</i>	<i>caffer</i>	LWB ³	625 ³	>575kg
Caprini	<i>Ammotragus</i>	<i>lervia</i>	M ³	87.5 ³	45-90kg
Caprini	<i>Capra</i>	<i>hircus</i>	Domestic ³	66.5 ³	45-90kg
Caprini	<i>Capricornis</i>	<i>milneedwardsii</i>	M ³	112.5 ³	90-180kg
Caprini	<i>Hemitragus</i>	<i>jemlahicus</i>	M ³	85 ³	45-90kg
Caprini	<i>Naemorhedus</i>	<i>goral</i>	M ³	38.5 ³	10-45kg
Caprini	<i>Oreamnos</i>	<i>americanus</i>	M ³	95 ³	90-180kg
Caprini	<i>Pseudois</i>	<i>nayaur</i>	M ³	53.5 ³	45-90kg
Caprini	<i>Rupicapra</i>	<i>rupicapra</i>	M ³	38 ³	10-45kg
Cephalophini	<i>Cephalophus</i>	<i>silvicultor</i>	F ¹	62.5 ³	45-90kg
Cephalophini	<i>Cephalophus</i>	<i>monticola</i>	F ¹	6.25 ⁴	1-10kg
Cephalophini	<i>Sylvicapra</i>	<i>grimmia</i>	LWB ¹	18 ³	10-45kg
Hippotragini	<i>Addax</i>	<i>nasomaculatus</i>	GT ¹	92.5 ³	90-180kg
Hippotragini	<i>Hippotragus</i>	<i>equinus</i>	WBG ¹	257.5 ³	180-360kg
Hippotragini	<i>Hippotragus</i>	<i>niger</i>	LWB ¹	205 ³	180-360kg
Hippotragini	<i>Oryx</i>	<i>dammah</i>	WBG ³	150.5 ³	90-180kg
Hippotragini	<i>Oryx</i>	<i>gazella</i>	WBG ¹	227.5 ³	180-360kg
Hippotragini	<i>Oryx</i>	<i>leucoryx</i>	GT ³	64.5 ³	45-90kg
Neotragini	<i>Madoqua</i>	<i>kirkii</i>	HWB ¹	4.6 ³	1-10kg
Neotragini	<i>Oreotragus</i>	<i>oreotragus</i>	WBG ¹	13.5 ³	10-45kg
Neotragini	<i>Ourebia</i>	<i>ourebi</i>	WBG ¹	12.5 ³	10-45kg
Ovibovini	<i>Ovibos</i>	<i>moschatus</i>	GT	295 ³	180-360kg
Redunicini	<i>Kobus</i>	<i>ellipsiprymnus</i>	HWB ¹	217.5 ³	180-360kg
Redunicini	<i>Kobus</i>	<i>kob</i>	LWB ¹	90.5 ⁴	90-180kg
Redunicini	<i>Kobus</i>	<i>vardonii</i>	LWB ¹	69.5 ⁴	45-90kg
Redunicini	<i>Redunca</i>	<i>arundinum</i>	LWB ¹	72.5 ⁴	45-90kg

Redunicini	<i>Redunca</i>	<i>fulvorufula</i>	LWB ¹	28.5 ⁴	10-45kg
Redunicini	<i>Redunca</i>	<i>redunca</i>	LWB ¹	50 ³	45-90kg
Tragelaphini	<i>Taurotragus</i>	<i>derbianus</i>	HWB ²	675 ⁴	>575kg
Tragelaphini	<i>Taurotragus</i>	<i>oryx</i>	HWB ²	575 ³	360-575 kg
Tragelaphini	<i>Tragelaphus</i>	<i>eurycerus</i>	HWB ¹	293.5 ⁴	180-360kg
Tragelaphini	<i>Tragelaphus</i>	<i>scriptus</i>	HWB ¹	39 ⁴	10-45kg
Tragelaphini	<i>Tragelaphus</i>	<i>spekii</i>	HWB ¹	87.5 ³	45-90kg
Tragelaphini	<i>Tragelaphus</i>	<i>strepsiceros</i>	HWB ¹	217.5 ³	180-360kg

Providing details of the categorical variables assigned to each species in the study.
References: ¹ Kovarovic et al. (2021); ² Barr (2020); ³ Etienne et al. (2020); ⁴ Kingdon (2013).

Linear Regression

Linear regression analyses test for the presence and nature of a relationship between two or more variables, (in which at least the dependent variable must be continuous). Here, the general linear model function in R was used, which models the independent variable(s) to predict the dependent variable by fitting linear functions which minimize the sum of squared residuals. For example, in this project, a general linear model is used to test for a relationship between body mass (a continuous dependent variable) and habitat preference (an independent categorical variable). The output from the analysis in R reports regression coefficients, error, t values, p-values for each variable (or each level of a categorical variable and/or interaction term), as well as an overall p-value and adjusted r^2 value for the model. This analysis is parametric and, as such, requires the assumptions of normality and homoscedasticity in the residuals, and independence in the observations.

This was carried out using R ver. 4.0.3 (The R Foundation for Statistical Computing 2020).

Analysis of Variance (ANOVA)

An analysis of variance is an aspect of regression analysis developed in the 1920s (Fisher 1921) which is primarily used to test the *nature* of relationships in which there is more than one categorical independent variable. In essence, the analysis tests whether the population means of a selection of independent variables are equal, generalizing a t-test to greater than two means. Using an ANOVA, it is possible to identify the variance accounted for by each variable, as well as the effect of interactions between the independent variables. For example, in this project, an ANOVA is used to test for the effect of body mass (a continuous independent variable), habitat preference (a categorical independent variable), and the interaction of body mass and habitat preference on shape variation at the distal humerus (the continuous dependent variable). This analysis is parametric and, as such, requires the assumptions of normality and homoscedasticity in the residuals, and independence in the observations.

This was carried out using R ver. 4.0.3 (The R Foundation for Statistical Computing 2020).

Principal Components Analysis (PCA)

Principal Components Analysis (PCA) was developed and named in the 1933 by Harold Hotelling, but the concept had already been developed by Karl Pearson in 1901. PCA is used to analyse data in which there are many continuous variables recorded for each observation (specimen, in this case). Where a dataset containing two continuous variables could be represented in 2D space on an x and y axis, datasets containing a potentially infinite number of continuous variables could be represented in multidimensional space. PCA does just this with dimensions equal to continuous variables in the data, then mathematically determines 'slices' through this multidimensional space which represent the greatest variation in the data. These 'slices' are known as principal components (PCs) and are numbered numerically in order of decreasing percentage variance accounted for (i.e. PC1 accounts for the greatest variation in the dataset). Each PC is the result of all the continuous variables in the dataset to varying extents, and as part of the output each variable in each PC is given a loading value which represents its relative importance in determining an individual observation's position on that axis. An observation's position on an axis is determined by multiplying that observation's raw data values by the loading values of the axis, the final value being the coordinate value for that observation on that axis. It is important that the raw data inputted into the PCA are standardised, otherwise numerically high values will appear to account for far higher proportions of variation. For example, in a dataset including a measurement of height and head width in a human sample, measurements of height will be numerically far larger than measurements of head width, though the two variables may be equally important in representing variation in the sample. Dividing each observation's value by the standard deviation of the sample for that variable would be one way to standardise these data. In geometric morphometrics, the input data are coordinate values for the landmarks after Procrustes superimposition (the Procrustes coordinates) and do not require further standardisation.

By reading the outputted loading values for each axis, it is possible to determine which variables in the dataset are responsible for the greatest variation. The PCA can also be visualised as a scatter plot which, in biology, is known as a morphospace (a graphical representation of organismal phenotypic forms). In this morphospace, observations will lie close to observations which have similar values for the most dominant variables on the axes shown. Observations can then be colour-coded according to a categorical variable, allowing a visual representation of the relationship between variation in the data and real-life

groupings of the observations. Here, the PCA is colour-coded by tribe affinity, habitat preference, and body mass category. This is used to investigate if categories of specimens are visually separated into individual clusters based on overall morphological variation in the dataset, and to determine which of the variables this is due to, in turn providing a potential suite of morphological characters which can be used to distinguish and describe categories.

This was carried out using MorphoJ ver. 1.07a (Klingenberg 2011).

Canonical Variate Analysis (CVA)

A Canonical Variate Analysis (CVA) is, in some ways, similar to a PCA, and was also first presented by Hotelling (Hotelling 1936). They are both performed on the same type of dataset, and both provide information on axes representing greatest variation in multidimensional space. However, CVA relies on prior knowledge of a categorical variable at the outset. The analysis uses the information to ‘learn’ the values of the other variables which place an observation within a specific category in the dataset. As a result, the loading values outputted indicate which variables are most important in distinguishing categories on each axis. The analysis can be used to predict the category in which an unspecified observation is likely to fall, with a given percentage accuracy of the analysis. Clear visual separation and high percentage accuracy indicate that the variables identified in the analysis are strongly related to distinguishing the category into which an observation falls.

Part of the output of a CVA in GMM are Procrustes distances. These are values which indicate the distance in Euclidean multidimensional space between each category within the analysis and each other category, for example, providing the distances between each habitat preference group and each other habitat preference group. The values are relative to other Procrustes distance values in the output, and a relatively low Procrustes distance between two groups indicates morphological similarity between the two categories.

This was carried out using MorphoJ ver. 1.07a (Klingenberg 2011).

An important consideration for these analyses is phylogeny. It is possible that any apparent trends in the data are, in fact, due to phylogenetic relatedness of the animals and not due to

true convergent evolution as a consequence of ecological and functional adaptation. In order to address this, Phylogenetic Generalized Least Squares was employed.

Phylogenetic Analysis via PGLS

Generalized Least Squares (GLS) is a statistical method for estimating unknown parameters within a linear regression model, specifically when there is correlation between residuals (that is, when the data regarding one observation are likely to be related to data regarding another observation in an unspecified way)(Aitken 1936). In this case, there is correlation between the residuals in the model due to the likelihood of similarity between species which are closely phylogenetically related. The unknown parameter which this method seeks to account for is usually given the symbol Ω within GLS. In a Phylogenetic Least Squares (PGLS) analysis, the unknown parameter, Ω , is considered to be phylogeny, the effect of which upon the model is unclear. Information regarding phylogeny is introduced into the model by providing a phylogenetic tree which includes data regarding branch lengths/divergence times of the taxa. The resulting output gives evidence as to the true relationship between a categorical variable and shape variation in the dataset when phylogeny is considered.

For this study, PGLS was conducted on the first four principal components (PCs) of the PCA with respect to habitat, and separately with respect to mass. PGLS was also conducted on the first four canonical variates (CVs) of the CVA by habitat, and the first four CVs of the CVA by mass. This was conducted in R using the *caper* package version 1.0.1 and the code used can be found in Appendix IV. This effectively corrects the relationship between shape variation and mass or habitat for any influence of phylogenetic relatedness. The output of the PGLS analysis provides a p-value for significance of the overall relationship between the categorical variable, as well as p-values for each level of the categorical variable. In addition, the output differs from a linear model output in providing a lambda (λ) value, as defined in Table 1.

This analysis requires the assumptions of normality and homoscedasticity in the residuals, and independence in the observations which is theoretically accounted for by phylogeny.

This was carried out in R ver. 4.0.3 (The R Foundation for Statistical Computing 2020).

Chapter 3: Results

Tribe Affinity

A Canonical Variate Analysis (CVA) with tribe affinity as the categorical variable reveals a strong predictive relationship between distal humerus morphology and tribe affinity in extant bovids. In fact, the results show 100% prediction accuracy for this CVA –it suggests that, based on the Procrustes coordinates of the landmarks, it is possible to predict the tribe affinity of the specimen correctly 100% of the time. CV1 represents 43.4% of variation in the dataset, and CV2 represents 18.4%, so cumulatively the first two canonical variates account for 61.8% of variation in the dataset.

Bovini and Cephalophini are diametrically opposed on the CV1 axis (Figure 8), with the majority of other tribes lying closer to the Bovini at the high end of the axis. In the Bovini at the high end of CV1, the medial trochlear ridge is medio-laterally wider, the lateral epicondylar crest is shorter (landmark 29), the medial epicondyle extends further caudally (landmark 21), and the olecranon fossa is deeper (landmark 25). CV2 separates the Neotragini at the high end very clearly from the other bovids, while Antilopini, Caprini and Bovini all lie at the low end. In the Neotragini, the olecranon fossa is shallow (landmark 25), the lateral epicondylar protuberance is short (landmark 27), the medial epicondyle is more medially directed (landmark 21), and the trochlea/capitulum is cranio-caudally deeper (landmarks 4 & 5 are highly caudally positioned).

Interestingly, the Procrustes distances (Table 5) do not reflect relative phylogenetic relatedness – tribes which are closely phylogenetically related do not necessarily have the lowest Procrustes distances between them. For example, according to the phylogeny of bovids presented in the Introduction above, Caprini would be expected to be closest to Hippotragini and Alcelaphini, but in the Procrustes distance output, Caprini is, in fact, closest to Reduncini and Tragelaphini. This is suggestive of some level of convergent morphological evolution based on ecology within extant bovids.

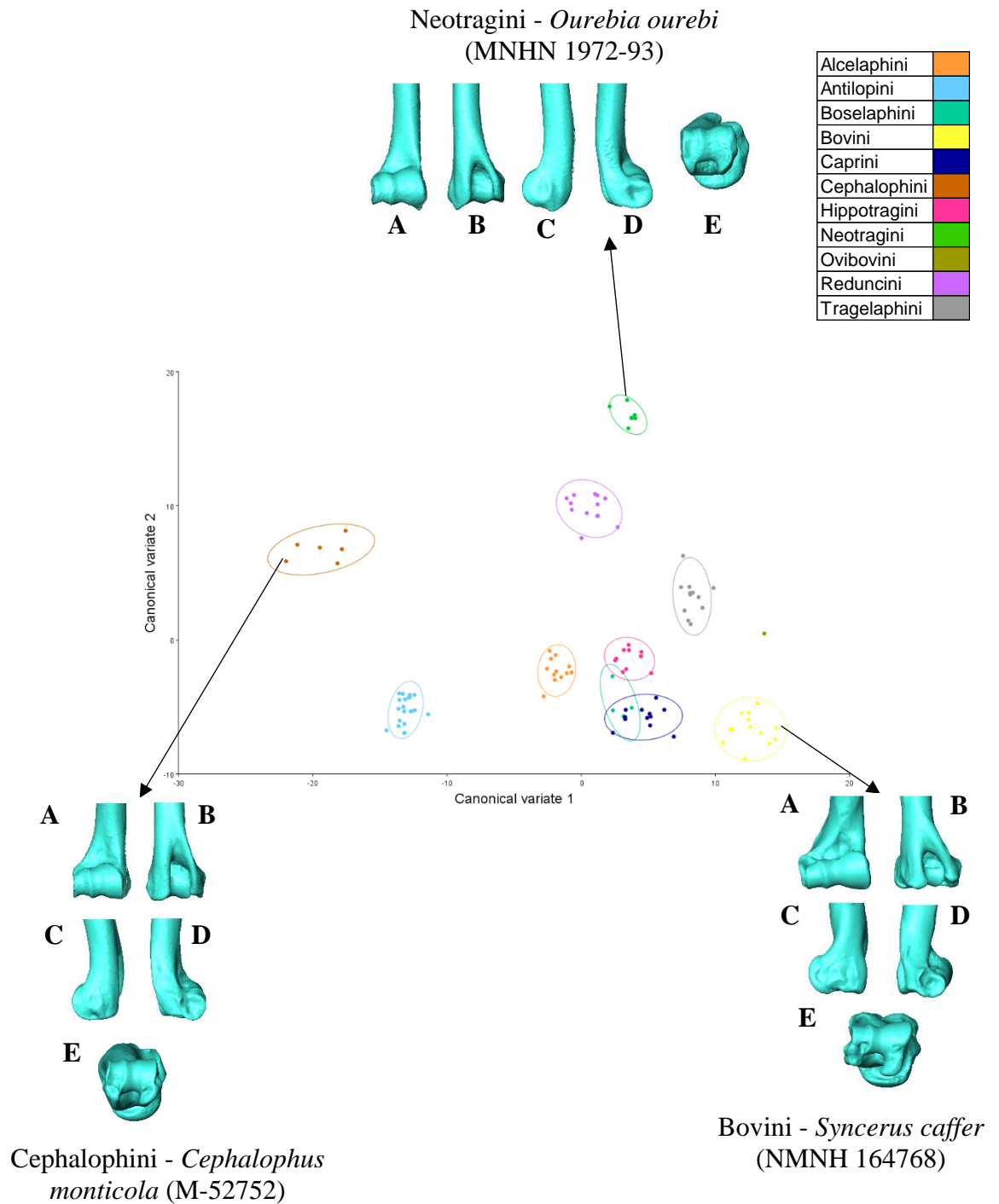


Figure 8: Visualization of Canonical Variate Analysis (CVA) on 3D Procrustes coordinates by tribe affinity

Showing the first two canonical variate axes with specimen points colour-coded by tribe affinity. Individuals representing extremes of the axes are indicated and images of the specimen are provided in A) cranial; B) caudal; C) medial; D) lateral; E) distal view. Ellipses represent 90% confidence interval.

Table 5: Results for the relationship between tribe and distal humerus morphology

A

	Alc	Ant	Bos	Bov	Cap	Cep	Hip	Neo	Ovi	Red
Alc	0.1347									
Ant	0.1057	0.0814								
Bos	0.0941	0.1698	0.1283							
Bov	0.1383	0.1145	0.1014	0.126						
Cap	0.1436	0.1287	0.1156	0.149	0.1042					
Cep	0.1006	0.0817	0.0849	0.1192	0.1009	0.1247				
Hip	0.1302	0.1415	0.11	0.1514	0.121	0.1117	0.1469			
Neo	0.191	0.1391	0.1549	0.1792	0.1381	0.1717	0.1176	0.2132		
Ovi	0.1147	0.0937	0.0855	0.1257	0.082	0.0721	0.0929	0.0982	0.1551	
Red	0.1148	0.1042	0.0829	0.1112	0.0795	0.0926	0.0824	0.1299	0.1334	0.064

B

Axis	Percentage variation	Morphological change
CV1	37.518	The trochlea/capitulum is medio-laterally wider. The most proximal point of the lateral epicondylar crest (landmark 29) is more distal (the crest is shorter). The medial epicondyle extends further caudally (landmark 21). The olecranon fossa is deeper (landmark 25).
CV2	18.662	The deepest point of the olecranon fossa (landmark 25) is more medial and shallower. The most caudal extent of the medial epicondyle is more medial (landmark 21).
CV3	12.499	The trochlear groove is more medial at the proximal edge (landmarks 3 & 4). The olecranon fossa is more laterally positioned. The epicondyles (landmarks 20 & 21) extend further caudally and distally. The medial trochlear ridge is cranio-caudally wider
CV4	9.247	The most proximal point of the lateral epicondylar crest (landmark 29) is more caudally positioned. The trochlear groove is medio-laterally wider along the proximal edge (landmarks 3 & 4). The origin of the lateral collateral ligament (landmark 28) is more medial (deeper)

A) Showing Procrustes distance between tribe affinity pairs in the dataset. Abbreviations: Alc = Alcelaphini; Ant = Antilopini; Bos = Boselaphini; Bov = Bovini; Cap = Caprini; Cep = Cephalophini; Hip = Hippotragini; Neo = Neotragini; Ovi = Ovibovini; Red = Reduncini; Tra = Tragelaphini. N.B. Procrustes distance indicates morphological similarity, with a relatively small value indicating that two groups are highly similar.

B) Showing results for the first four CVs in a CVA with tribe as the canonical variable, providing the percentage of total variance represented and a summary of shape change from low to high for each axis.

Habitat Preference

A CVA by habitat preference reveals a strong relationship between distal humerus morphology and habitat preference, but not with high visual differentiation of some morphospaces on the first two axes (CV1 accounts for 55.3% of variation in the data, and CV2 accounts for 23.9%). While the montane cluster separates clearly from all other clusters on the CV1 axis (Figure 9), the two most open habitat categories (grassland/treeless and wooded bushland/grassland) are poorly separated from one another on either axis, and the same can be said for the remaining three categories (light woodland/bushland, heavy woodland/bushland and forest). Thus, despite the poor visual separation of some morphospaces on the first two axes, they do serve to separate montane species, open-living species, and species preferring some level of cover. This CVA has a prediction accuracy of 100%.

The montane bovids are the most morphologically distinct on the CV1 axis. The proximal edge of the capitulum and the proximal edge of the lateral trochlear ridge (landmarks 1-3) are more lateral in montane bovids, resulting in a more acute angle between the medio-lateral axis of the distal humerus and the ridges and grooves of the lateral half of the area in cranial view. Additionally, the medial trochlear ridge is less cranially protruding in montane bovids, being reduced in size cranio-caudally. The epicondyles (landmarks 20 & 21) do not extend as far caudally in montane bovids as they do in other bovids, and the lateral epicondyle (landmark 20) is more medially directed at its caudal extremity. The medial epicondyle also does not extend so far distally in montane bovids (landmark 21). The lateral epicondylar protuberance (landmark 27) does not extend as far proximo-laterally in montane bovids. The deepest point of the olecranon fossa (landmark 25) is more medially positioned in montane bovids, as is the outline of the olecranon fossa itself (landmarks 22-24 & 26) on the caudal side of the humerus.

CV2 separates the most open-living species at the high end from the species preferring some degree of cover at the lower end. In more open-living bovids, the proximal edge of the distal humerus (landmarks 1-6) is wider in cranial view, being approximately equal in width to the distal edge. In the bovids preferring cover, the proximo-medial corner of the medial trochlear ridge (landmark 6) is far more laterally positioned, and the proximal edge of the capitulum is more laterally positioned (similarly to the highly montane bovids). In the open-living bovids, the olecranon fossa is slightly deeper (landmark 25) and the outline

on the caudal side of the humerus is medio-laterally wider (landmark 22 more lateral). The deepest point of the lateral epicondyle (landmark 28, where the lateral collateral ligament originates) is more caudally positioned in the open-living bovids. The lateral epicondyle extends more distally (landmark 19) in open-living bovids, and the lateral epicondylar protuberance (landmark 27) extends further proximo-laterally in these animals.

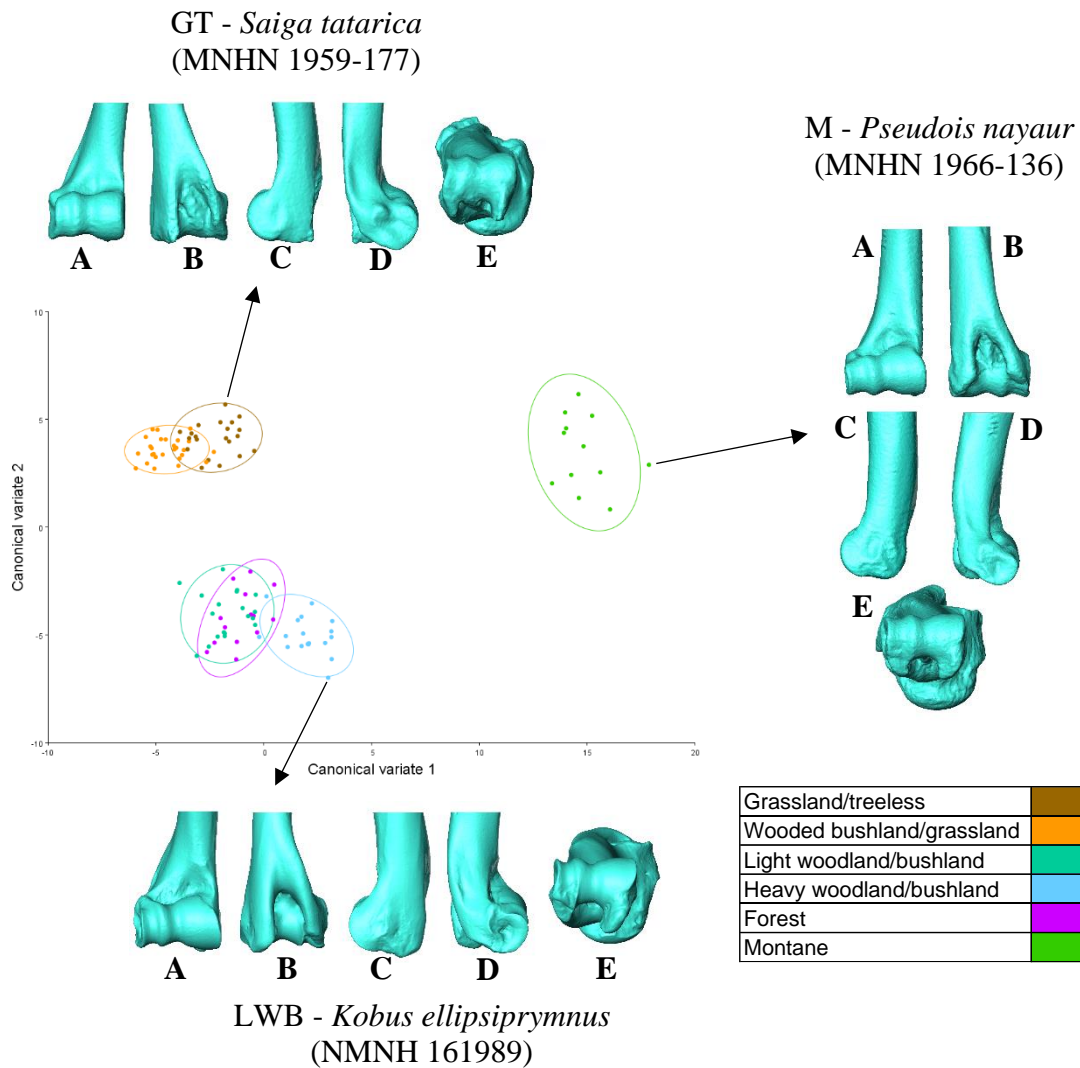


Figure 9: Visualization of Canonical Variate Analysis (CVA) on 3D Procrustes coordinates by habitat preference

Showing the first two canonical variate axes with specimen points colour-coded by habitat preference. Individuals representing extremes of the axes are indicated and images of the specimen are provided in A) cranial; B) caudal; C) medial; D) lateral; E) distal view. Ellipses represent 90% confidence interval.

Table 6: Summarization of Canonical Variate Analysis (CVA) on 3D Procrustes coordinates by habitat preference

	% variation	Morphological change
CV1	51.666	The proximal edge of the capitulum and the proximal edge of the lateral trochlear ridge (landmarks 1-3) are more lateral, resulting in a more acute angle between the medio-lateral axis of the distal humerus and the ridges and grooves of the lateral half of the area in cranial view. Additionally, the medial trochlear ridge is less cranially protruding in montane bovids, being reduced in size cranio-caudally. The epicondyles (landmarks 20 & 21) do not extend as far caudally, and the lateral epicondyle (landmark 20) is more medially directed at its caudal extremity. The medial epicondyle also does not extend so far distally (landmark 21). The lateral epicondylar protuberance (landmark 27) does not extend as far proximo-laterally. The deepest point of the olecranon fossa (landmark 25) is more medially positioned, as is the outline of the olecranon fossa itself (landmarks 22-24 & 26) on the caudal side of the humerus.
CV2	27.965	The proximal edge of the distal humerus (landmarks 1-6) is wider in cranial view, being approximately equal in width to the distal edge. The olecranon fossa is slightly deeper (landmark 25) and the outline on the caudal side of the humerus is medio-laterally wider (landmark 22 more lateral). The deepest point of the lateral epicondyle (landmark 28, where the lateral collateral ligament originates) is more caudally positioned. The lateral epicondyle extends more distally (landmark 19), and the lateral epicondylar protuberance (landmark 27) extends further proximo-laterally.
CV3	11.325	The lateral epicondyle does not extend so far caudally, the olecranon fossa is deeper, the caudal extent of the medial epicondyle is more laterally directed, the lateral epicondylar protuberance is slightly enlarged.
CV4	5.187	The medial trochlear ridge is proximo-distally compressed and medio-laterally enlarged, the most proximal end of the lateral epicondylar ridge is more distally and caudally located, the olecranon fossa is proximo-distally taller and deeper, the lateral epicondyle extends further caudally, the lateral epicondylar protuberance is enlarged.

Showing results for the first four CVs in a CVA with habitat preference as the canonical variable, providing the percentage of total variance represented and a summary of shape change from low to high for each axis.

Body Mass

A CVA by body mass category reveals a strong relationship between distal humerus morphology and body mass, with some areas of poor visual resolution in the first two CV axes (CV1 accounts for 64.6% of variation in the data, and CV2 accounts for 16.4%). The smallest mass category (1-10 kg) separates entirely from the other categories on the CV1 axis (Figure 10), while categories ranging from 10-360 kg cluster closely together and successive mass categories show considerable overlap with one another, and finally the highest two categories (360-575 kg and >575 kg) cluster closely with some overlap. Broadly, mass increases along the CV1 axis. However, the category 360-575 kg lies highest on the axis, slightly beyond (with considerable overlap) the highest category, >575 kg.

CV1 fully separates out the lowest body mass bovids (1-10 kg) at the low end and the highest body mass bovids (360+ kg) at the highest end, with all other body masses clustering centrally. In the heaviest bovids, the medial trochlear ridge is wider at the distal end than it is in lighter bovids, extending further medially at the distal corner (landmark 18) than at the proximal corner (landmark 6) in cranial view. The lateral epicondylar protuberance (landmark 27) extends further proximo-laterally in heavier bovids, and the most proximal end of the lateral epicondylar crest (landmark 29) is located more caudally. The olecranon fossa is also deeper (landmark 25) in the heavier bovids, and its outline on the caudal side of the bone is medio-laterally wide. The lateral epicondyle extends more caudally, and is more laterally directed at its caudal extremity in heavier bovids. The medial epicondyle also extends more caudally in heavier bovids.

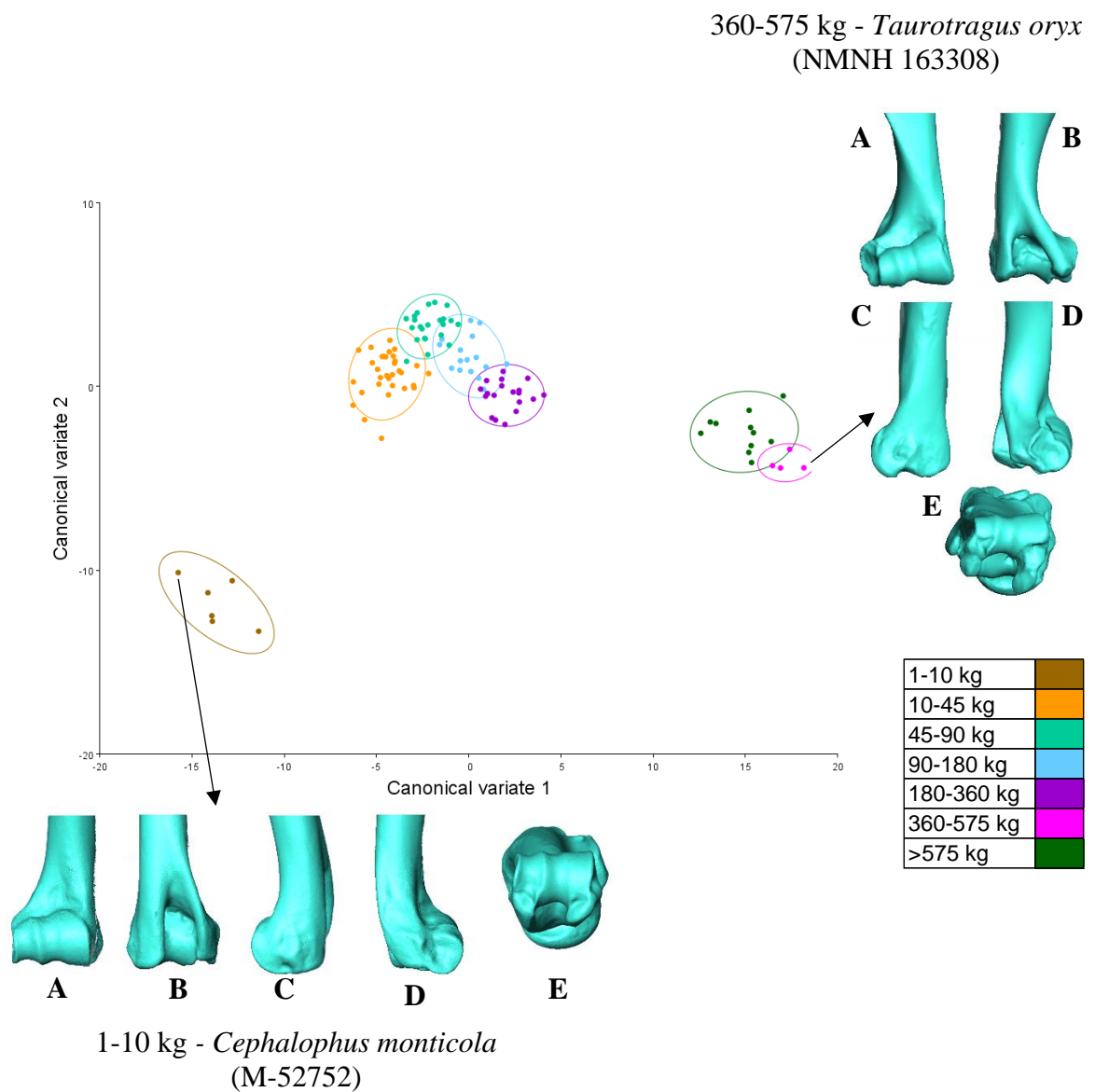


Figure 10: Visualization of Canonical Variate Analysis (CVA) on 3D Procrustes coordinates by body mass category

Showing the first two canonical variate axes with specimen points colour-coded by body mass category. Individuals representing extremes of the axes are indicated and images of the specimen are provided in A) cranial; B) caudal; C) medial; D) lateral; E) distal view. Ellipses represent 90% confidence interval.

Table 7: Summarization of Canonical Variate Analysis (CVA) on 3D Procrustes coordinates by body mass category

	% variation	Morphological change
CV1	63.814	The medial trochlear ridge is wider at the distal end than it is in lighter bovids, extending further medially at the distal corner (landmark 18) than at the proximal corner (landmark 6) in cranial view. The lateral epicondylar protuberance (landmark 27) extends further proximo-laterally, and the most proximal end of the lateral epicondylar crest (landmark 29) is located more caudally. The olecranon fossa is also deeper (landmark 25), and its outline on the caudal side of the bone is medio-laterally wide. The lateral epicondyle extends more caudally, and is more laterally directed at its caudal extremity. The medial epicondyle also extends more caudally.
CV2	16.769	The medial trochlear ridge is more medially directed at the proximal corner, the most proximal end of the lateral epicondylar crest is more proximally located, the olecranon fossa is proximo-distally shorter and slightly shallower, the insertion of the lateral collateral ligament is deeper.
CV3	8.505	The medial trochlear ridge is proximo-distally taller, the olecranon fossa is medio-laterally reduced and shallower, the caudal extent of the medial epicondyle is more proximal and medially directed.
CV4	4.843	The trochlea/capitulum is proximo-distally compressed with the trochlear groove particularly reduced in height, the most proximal point of the lateral epicondylar crest is more caudally positioned, the most caudal extent of the medial epicondyle is more proximally located, the olecranon fossa is shallower.

Showing results for the first four CVs in a CVA with body mass as the canonical variable, providing the percentage of total variance represented and a summary of shape change from low to high for each axis.

Principal Components Analysis

In a Principal Components Analysis (PCA) of the 3D Procrustes coordinates from extant bovids, there is no visual separation on any of the first four PCs of any tribe/habitat preference/body mass categories (Figure 11). However, despite this lack of visual clustering, all of the first four PCs have a significant relationship with tribe (PC1 $p = 0.02851$; PC2 $p = 7.18 \times 10^{-8}$; PC3 $p = 3.71 \times 10^{-13}$; PC4 $p = 2.02 \times 10^{-5}$). PC2 and PC4 are also significantly related to habitat preference (PC2 $p = 1.94 \times 10^{-7}$; PC4 $p = 0.0002$), but PC1 and PC3 are not (PC1 $p = 0.7909$; PC3 $p = 0.08652$). Lastly, only PC3 is significantly related to body mass category ($p = 1.27 \times 10^{-9}$). While there are significant relationships between shape variation and the categorical ecological variables, the PCA is difficult to interpret with reference to only one of the variables, (as was also observed to be the case in the 2D preliminary analysis shown in Appendix I). It appears that the shape variation detected by the analysis is related to the mosaic interactions of phylogenetic affinity, habitat preference and body mass, as well as other factors not considered here.

The shape changes along each axis represent the areas of the morphology which are most variable across the sample, regardless of specimen categorisations. This reveals that, on the PC1 axis (which accounts for 33.447% of variation), the most variable aspect of the distal humerus is the proximo-distal position of the proximal end of the lateral epicondylar crest (landmark 29), i.e. the relative length of the lateral epicondylar crest. The position of the most proximal extent of the olecranon fossa (landmark 26), which is more distal when the lateral epicondylar crest is longer. Lastly, the extent of the epicondyles caudally is also relatively variable (landmarks 20 & 21), as is the depth of the origin of the lateral collateral ligament (landmark 28).

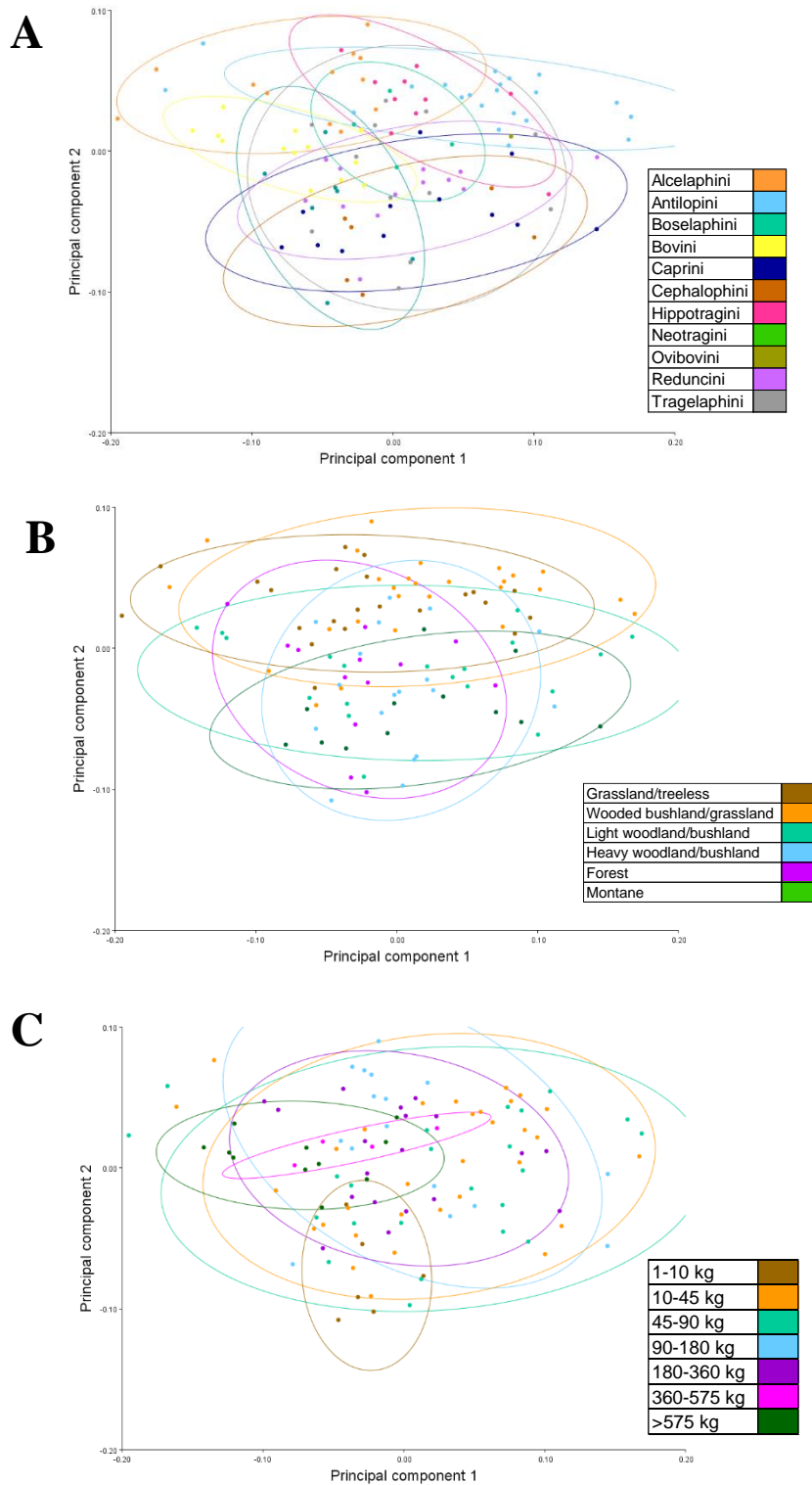


Figure 11: Visualization of Principal Components Analysis (PCA) on 3D Procrustes coordinates

Showing the first two principal component axes, points colour-coded by A) tribe affinity; B) habitat preference; C) body mass category. Ellipses represent 90% confidence interval.

Table 8: Summarization of Principal Components Analysis (PCA) on 3D Procrustes coordinates

	% variation	Morphological change
PC1	33.447	The most variable aspect of the distal humerus is the proximo-distal position of the proximal end of the lateral epicondylar crest (landmark 29), i.e. the relative length of the lateral epicondylar crest. Additionally, the position of the most proximal extent of the olecranon fossa (landmark 26), which is more distal when the lateral epicondylar crest is longer. The extent of the epicondyles caudally is also relatively variable (landmarks 20 & 21), as is the depth of the origin of the lateral collateral ligament (landmark 28).
PC2	12.301	The proximo-medial corner of the trochlea is medially enlarged, the lateral epicondyle is enlarged distally and caudally, the lateral epicondyle is more laterally directed at its caudal extent, the olecranon fossa is more laterally located, the lateral epicondylar protuberance is larger.
PC3	11.257	The trochlea/capitulum is proximo-distally compressed, the capitulum is cranio-caudally compressed, the proximal end of the lateral epicondylar protuberance is more caudally located, the medial epicondyle extends further caudally and is more laterally directed, the olecranon fossa is deeper.
PC4	5.091	The capitulum is medio-laterally compressed, the olecranon fossa is proximo-distally taller and shallower and more laterally located, the most caudal extent of the medial epicondyle is highly distally located, the lateral epicondylar protuberance is enlarged.

Showing results for the first four PCs, providing the percentage of total variance represented and a summary of shape change from low to high for each axis.

Allometric Shape Variation

An important question which can be asked of the data is, do large bovids exhibit more or less morphological variation in the distal humerus than small bovids? This can be assessed using outputs from the MorphoJ analysis – centroid size (the raw size of the landmark configuration prior to scaling correction in the Procrustes superimposition), and shape variation (a variable generated by MorphoJ to represent the morphometric data on a single axis).

As can be seen in Figure 12A, there is evidence of a significant positive correlation ($p < 2.2 \times 10^{-16}$) between shape variation and centroid size (and indication that the heavier body mass categories have larger centroids and greater shape variation) in extant bovids. Figure 12B shows that shape variation generally increases with increasingly large body mass, seeming to plateau from the 360-575 kg category. These results indicate that the bovids with the larger distal humerus (which are also the heavier bovids), exhibit greater shape variation at the distal humerus.

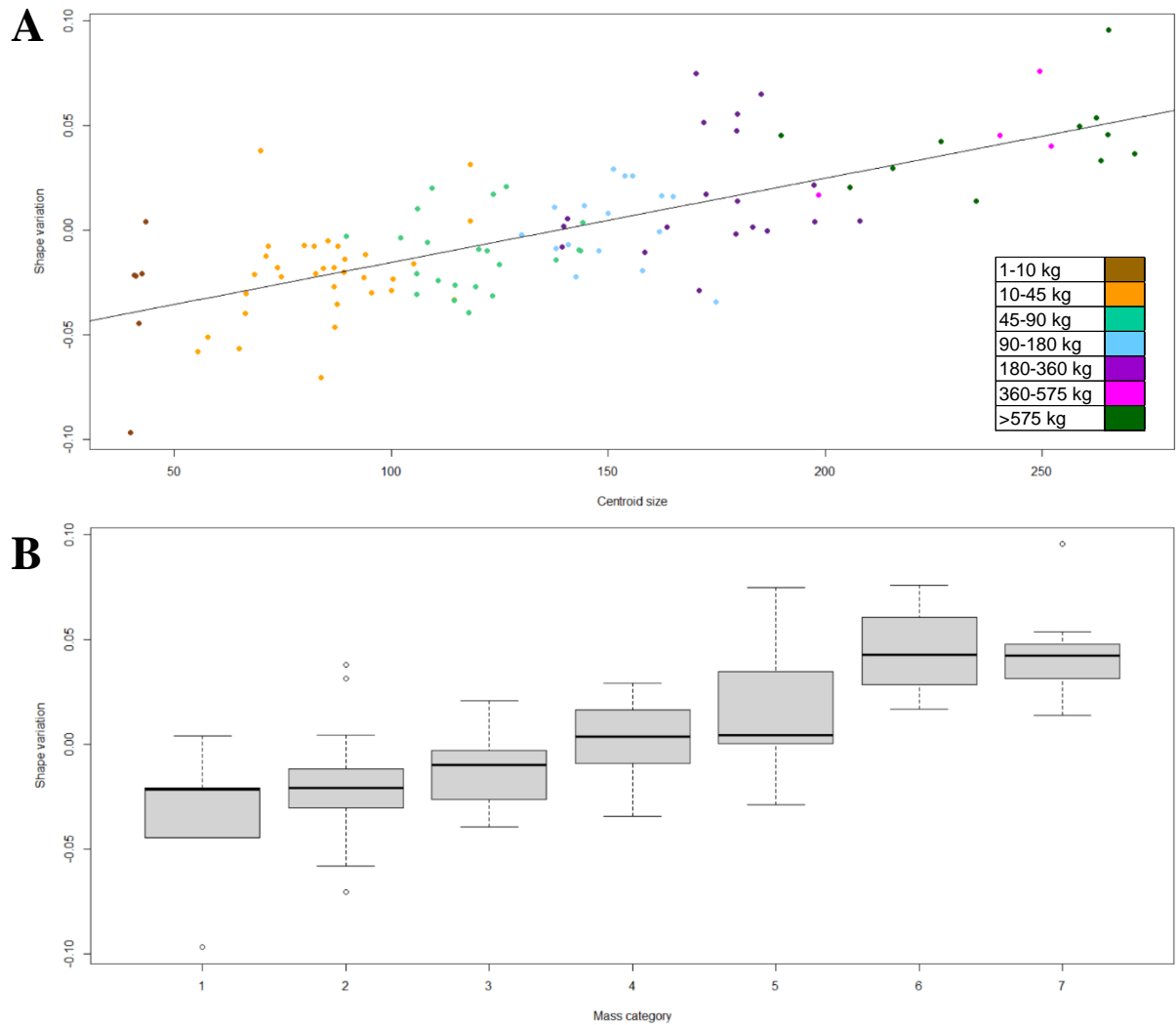


Figure 12: The relationships between shape variation, centroid size and body mass in extant bovids

A) Scatter plot of shape variation against centroid size, colour-coded by body mass category. Shape variation = $(4.023 \times 10^{-4}) \times \text{Centroid size} + (-5.562 \times 10^{-2})$, $p < 2.2 \times 10^{-16}$, adjusted $r^2 = 0.532$; B) Boxplot of shape variation in each body mass category, $p = 2.086 \times 10^{-14}$.

(N.B. The scans were obtained from multiple sources and the scale used when scanning influences centroid size in the analysis by factors of 10 (the differences in scale relating to measurements in millimetres vs centimetres etc.). The majority of scans were taken at the same scale, but scans from Etienne et al. were a factor of 10 smaller. This does not affect the shape analysis in any way, as Procrustes superimposition accounts for scaling, but for allometry analysis, the centroid sizes of these Etienne et al. scans were multiplied by 10 for the analysis).

Interaction of Body Mass and Habitat Preference

It is important to consider that body mass may influence habitat preference in a species, and vice versa. According to a general linear model (Table 9), body mass and habitat preference are significantly related overall ($p = 0.01632$), with the forest category (F) being very highly significantly related ($p = 1.35 \times 10^{-7}$), followed by wooded bushland/grassland (WBG, $p = 0.00299$) and montane (M, $p = 0.00513$). Montane body masses appear to be the most constrained, with a mean of 72.4 kg and a standard deviation of 25.2 kg. Meanwhile, forest body masses are the most variable, with a mean of 283.0 kg and a standard deviation of 266.9 kg, including the second smallest animal in the dataset (*Cephalophus monticola* at 6.3 kg) and the largest animal (*Bubalus bubalis* at 700 kg).

Table 9: Interaction of body mass and habitat preference

Habitat preference category	p value
GT	0.0702
WBG	0.0030
LWB	0.0469
HWB	0.4521
F	1.35E-07
M	0.0051
Overall	0.0163

Showing the significance of the relationship between body mass and each habitat preference category in the analysis.

N.B. Body mass is included here as a continuous variable with data for mean species masses as shown in Table 4, rather than as a categorical variable as in other analyses.

Abbreviations: GT = grassland/treeless; WBG = wooded bushland/grassland; LWB = light woodland/bushland; HWB = heavy woodland/bushland; F = forest; M = montane

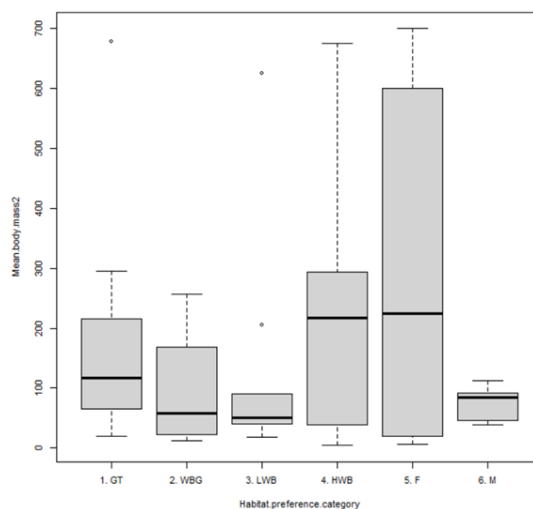


Figure 13: Interaction of body mass and habitat preference

Boxplot of mean body mass against habitat preference group in extant bovids.

N.B. Body mass is included here as a continuous variable with data for mean species masses as shown in Table 4, rather than as a categorical variable as in other analyses.

Abbreviations: GT = grassland/treeless; WBG = wooded bushland/grassland; LWB = light woodland/bushland; HWB = heavy woodland/bushland; F = forest; M = montane

However, the most important question at hand here is whether or not this relationship between body mass and habitat affects the previous morphology results. In order to assess this, another general linear model was produced for each of the first four CVs of the habitat preference CVA (as the independent variable) against habitat preference, body mass, and an interaction term for habitat preference and body mass (e.g. for CV1 the model can be represented in R as:

CV1 ~ Habitat_preference + Body_mass + Habitat_preference*Body_mass)

The interaction term significance results are shown in Table 10. It can be seen that none of the interaction terms for habitat preference and body mass are significant on any of the first four CVs, indicating that the morphological changes identified in the analysis along each of these axes can be said to be related to habitat preference only and not affected by the interaction of body mass and habitat preference.

An ANOVA was also performed on the habitat preference CVA data, and the interaction term was found not to be significant in any CV (CV1 $p = 0.8153$; CV2 $p = 0.692$; CV3 $p = 0.6701$; CV4 $p = 0.2545$), indicating that the relationship between habitat preference and body mass does not play a significant role in the variance observed in the shape data.

Table 10: Effect of interaction between body mass and habitat preference on shape analysis

	Interaction term					
	GT:BM	WBG:BM	LWB:BM	HWB:BM	F:BM	M:BM
CV1	0.5151	0.4857	0.3193	0.4349	0.3530	0.4237
CV2	0.5910	0.9910	0.6740	0.5840	0.5740	0.2540
CV3	0.9585	0.6699	0.6785	0.2702	0.9650	0.8164
CV4	0.1591	0.9418	0.7414	0.1908	0.0862	0.5851

Showing the significance of the interaction between body mass and each habitat preference category on the first four CVs of the habitat preference CVA.
 N.B. Body mass is included here as a continuous variable with data for mean species masses as shown in Table 4, rather than as a categorical variable as in other analyses.
 Abbreviations: BM = body mass; GT = grassland/treeless; WBG = wooded bushland/grassland; LWB = light woodland/bushland; HWB = heavy woodland/bushland; F = forest; M = montane

Influence of Phylogeny

Lastly, it is important to consider the role of phylogenetic relatedness in morphological similarity – in essence to test for evidence of convergent morphological evolution due to ecology, rather than to the inevitable variability brought about by speciation. The results of a Phylogenetic Generalized Least Squares (PGLS) analysis run on each of the four first principal components (PCs) of the PCA with respect to habitat can be seen in Table 11. The pruned phylogenetic tree used for this analysis is shown in Figure 14. Overall, the results imply that phylogeny is highly influential on the distribution of specimens on the first four PCs, and that the lack of distinct visual clustering in the PCA can be explained this way – a specimen's position in the PCA is influenced by a mosaic of phylogenetic, habitat preference and body mass effects, and their interactions. This indicates that the most variable landmarks in the dataset do not vary explicitly in relation to only one of the categorical variables and, therefore, cannot be used to predict the categorical variables. Instead, they represent variation due to the combined influence of phylogeny, habitat preference, and body mass (and potentially other variables not considered in this study).

Nevertheless, it can be seen that, even accounting for phylogenetic relatedness, habitat preference is significantly related to position on PC2 and PC4 (more so on PC2), and body mass is significantly related to position on PC2 and PC3. Consequently, the PC2 and PC3 axes can be considered the most informative of the PCs for assessing habitat preference and body mass. In a visualization of these two axes, the conditions represented by the most extreme corners of the four quadrants can be labelled (Figure 15), and this could potentially be informative for inferring phylogeny in extinct bovids, though with low differentiation.

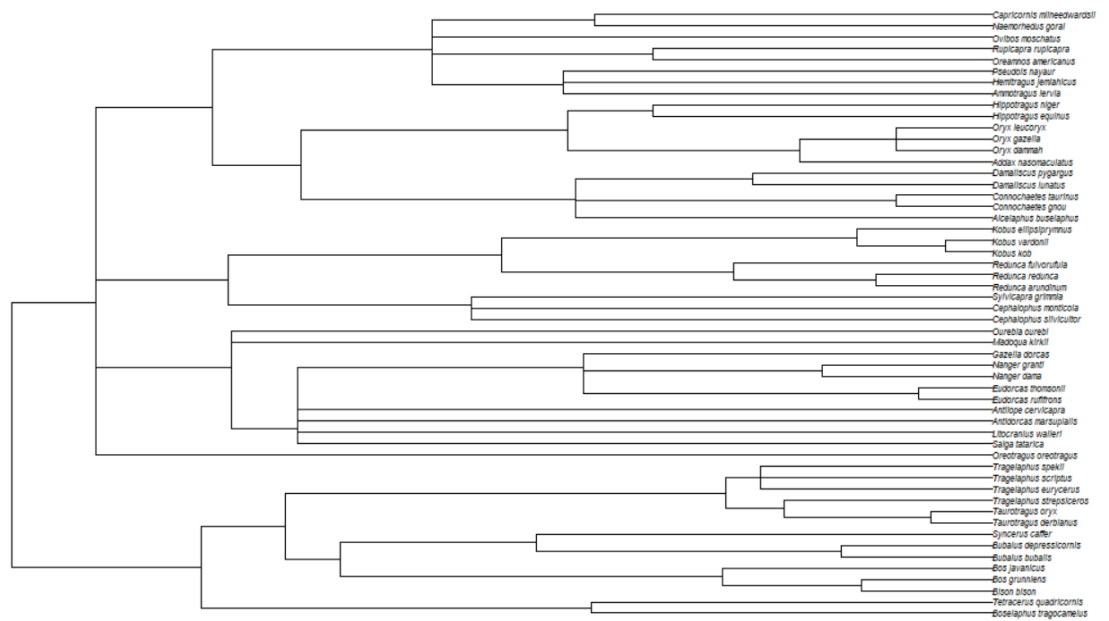


Figure 14: Pruned bovid phylogeny

Phylogeny used for PGLS in this study, based on Hernandez-Fernandez & Vrba (2005) and Bibi (2013), and pruned automatically by R according to species included in the dataset.

Table 11: PGLS results on PCA data

	Percentage variance	PGLS habitat preference		PGLS body mass	
		Lambda (λ)	p value	Lambda (λ)	p value
PC1	33.447	0.916	0.4605	0.91	0.7119
PC2	12.301	1.00	0.01512	1.00	0.04052
PC3	11.257	0.989	0.7906	0.941	0.000303
PC4	5.091	0.624	0.02375	0.876	0.5499

Showing the lambda value and p-value for the first four PCs with either habitat preference or body mass category as the categorical variable. Significant p-values in bold.

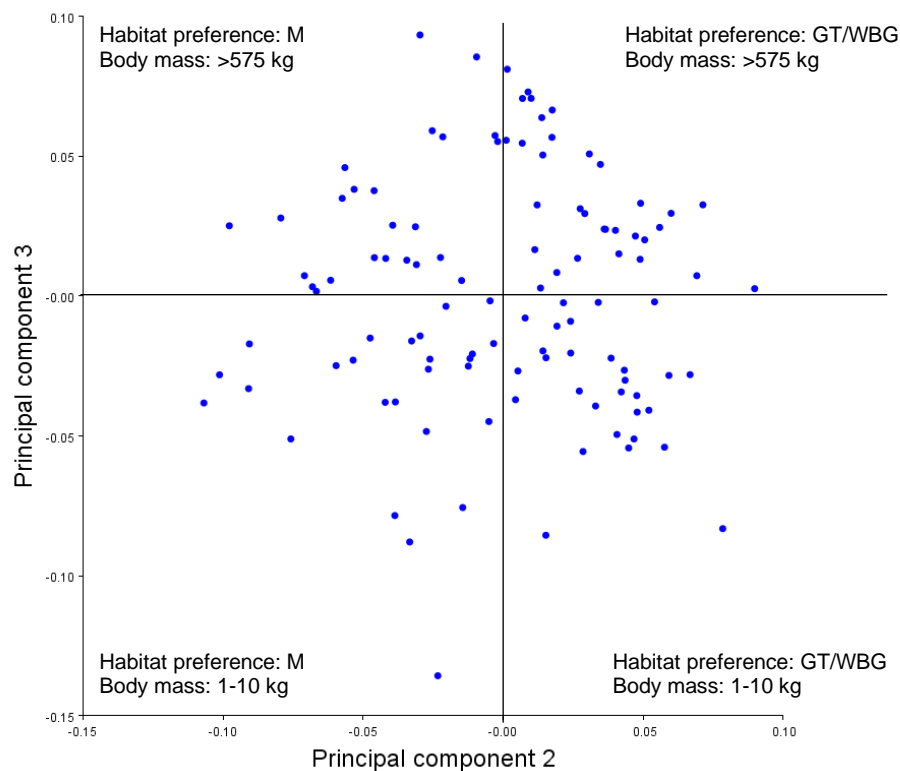


Figure 15: Visualization of Principal Components Analysis (PCA) on 3D Procrustes coordinates

Showing PC2 and PC3, and additionally divided into four visual quadrants with the statistically implied characteristics of the extremes of each quadrant given.

The results of the PGLS run on the first four CVs of the previous habitat preference CVA with habitat preference as the categorical variable are shown in Table 12A. It can be seen that all four CVs have a significant relationship with habitat preference even when phylogeny is accounted for. In fact, none of the lambda values were found to be significantly different from 0. This suggests that the shape variations being used to differentiate habitat preference groups in the CVA are representing variation in habitat preference only and that the observed clustering is not due to phylogenetic relatedness. Importantly, these results suggest that 3D shape variation of the distal humerus can be used as a predictor of habitat preference in bovids.

The results of the PGLS run on the first four CVs of the body mass CVA with body mass category as the categorical variable are shown in Table 12B. It can be seen that all four CVs have a significant relationship with body mass, even when phylogeny is accounted for, at the maximum level of significance which R can estimate. Additionally, all four CVs have a lambda value of 0.00 which indicates that phylogenetic relatedness has no bearing on the relationship between body mass and the shape variations dominant in the CVA. This suggests that 3D shape variation of the distal humerus can be used as a predictor of body mass category in bovids. It is important to note that these results do not imply that there is no relationship between body mass and phylogeny, but rather imply that the morphological variations most strongly identified in the analysis as related to body mass are not related to phylogenetic affinity, and the same is true for the habitat preference CVA results.

Table 12: PGLS results on CVA data

A

	Habitat preference category												Lambda value	Overall p value
	GT		WBG		LWB		HWB		F (intercept)		M			
	Coefficient	p value	Coefficient	p value	Coefficient	p value	Coefficient	p value	Coefficient	p value	Coefficient	p value		
CV1	-0.97452	0.1127	-3.10827	1.81E-06	-0.41261	0.4863	2.33605	0.00026	-1.21183	0.00986	16.11296	<2.2E-16	0.09	<2.2E-16
CV2	8.03899	9.42E-14	7.44113	9.39E-14	0.21514	0.7671	0.5366	0.4725	-4.17317	5.05E-09	7.65956	1.64E-11	0.264	<2.2E-16
CV3	-6.82031	4.93E-14	-3.72065	1.25E-07	-3.21894	3.50E-06	-7.67504	4.44E-16	4.33376	9.27E-12	-3.11541	1.25E-07	0.182	4.89E-16
CV4	0.43357	0.2185	-4.30016	<2.2E-16	-2.62756	1.33E-09	-3.0759	1.71E-11	2.16262	1.09E-10	-2.52608	1.52E-08	0	<2.2E-16

B

	Body mass category														Lambda value	Overall p value
	1-10 kg (intercept)		10-45 kg		45-90 kg		90-180 kg		180-360 kg		360-575 kg		>575 kg			
	Coefficient	p value	Coefficient	p value	Coefficient	p value	Coefficient	p value	Coefficient	p value	Coefficient	p value	Coefficient	p value		
CV1	13.73164	<2.2E-16	-9.35056	<2.2E-16	-11.60927	<2.2E-16	-13.95223	<2.2E-16	-15.97325	<2.2E-16	-29.47475	<2.2E-16	-28.99877	<2.2E-16	0	<2.2E-16
CV2	-11.76963	<2.2E-16	12.60382	<2.2E-16	15.82869	<2.2E-16	12.95792	<2.2E-16	10.06425	<2.2E-16	10.81573	2.22E-16	9.104	<2.2E-16	0	<2.2E-16
CV3	2.01424	4.39E-05	-1.06787	2.98E-02	-0.66671	1.72E-01	-4.84958	1.16E-12	-5.04513	1.77E-13	10.16197	<2.2E-16	-1.3142	1.63E-02	0	<2.2E-16
CV4	-2.1738	2.74E-05	4.59235	6.08E-12	0.49034	3.35E-01	0.44178	4.01E-01	1.91989	4.81E-04	-2.85464	9.43E-04	3.43682	1.38E-07	0	<2.2E-16

Showing the ANOVA coefficient and p-value for each category, as well as the lambda value and overall p-value for A) results of a PGLS analysis on habitat preference CVA data with habitat preference as the categorical variable; B) results of a PGLS analysis on body mass CVA data with body mass category as the categorical variable of the first four CVs of each analysis. Significant p-values in bold

Summary

- 3D morphology of the distal humerus in extant bovids can be used to predict tribe affinity, particularly relating to trochlea/capitulum width, caudal extent of the medial epicondyle, and depth of the olecranon fossa.
- 3D morphology of the distal humerus in extant bovids can be used to predict habitat preference, particularly the proportions of the capitulum/trochlea, the caudal extent of the epicondyles, the length of the lateral epicondylar crest, and the relative size of the lateral epicondylar protuberance.
- 3D morphology of the distal humerus in extant bovids can be used to predict body mass category, particularly the relative dimensions of the trochlea, the relative size of the lateral epicondylar protuberance, the depth of the olecranon fossa, and the caudal extent of the epicondyles.
- Shape variation at the distal humerus is greater in large bovids with high body mass than small bovids.
- Overall, the most extreme morphological variations in the distal humerus of extant bovids are the result of a complex interplay of ecological variables.

Chapter 4: A Palaeontological Application: *Rusingoryx atopocranion*

Results

When compared to the mean shape generated for extant bovids via the Procrustes superimposition process (Figure 16), there are several aspects of *Rusingoryx atopocranion*'s relative morphology which are notable. Firstly, of course, the lateral epicondylar protuberance (landmark 27) is much elongated in *Rusingoryx*, extending highly laterally (as opposed to more proximo-laterally, as is observed in other bovids). Overall, the trochlea/capitulum region is long medio-laterally in *Rusingoryx*, but not compressed proximo-distally. The proximo-lateral corner of the capitulum (landmark 1) is relatively high, almost horizontally in line with the proximo-medial corner of the trochlea (landmark 6), making the capitulum almost the same proximo-distal height as the trochlea. Additionally, the proximal edge of the trochlea/capitulum (landmarks 1-6) is approximately the same length as the distal edge (landmarks 13-18). The groove of the trochlea is particularly deep in *Rusingoryx* (landmark 10). The lateral epicondyle extends relatively far distally and caudally, as well as being directed laterally at its caudal extent (landmarks 19 & 20). The most caudo-distal point of the medial epicondyle is located relatively less distally and more caudally than in the mean bovid. The olecranon fossa is relatively shallow, with the deepest point being located highly laterally. The deepest point of the lateral epicondyle, where the lateral collateral ligament originates (landmark 28), is slightly caudally positioned in *Rusingoryx*. Lastly, the most proximal point of the lateral epicondylar ridge (landmark 29) is relatively distal (i.e., the lateral epicondylar crest is short), and caudal in *Rusingoryx*.

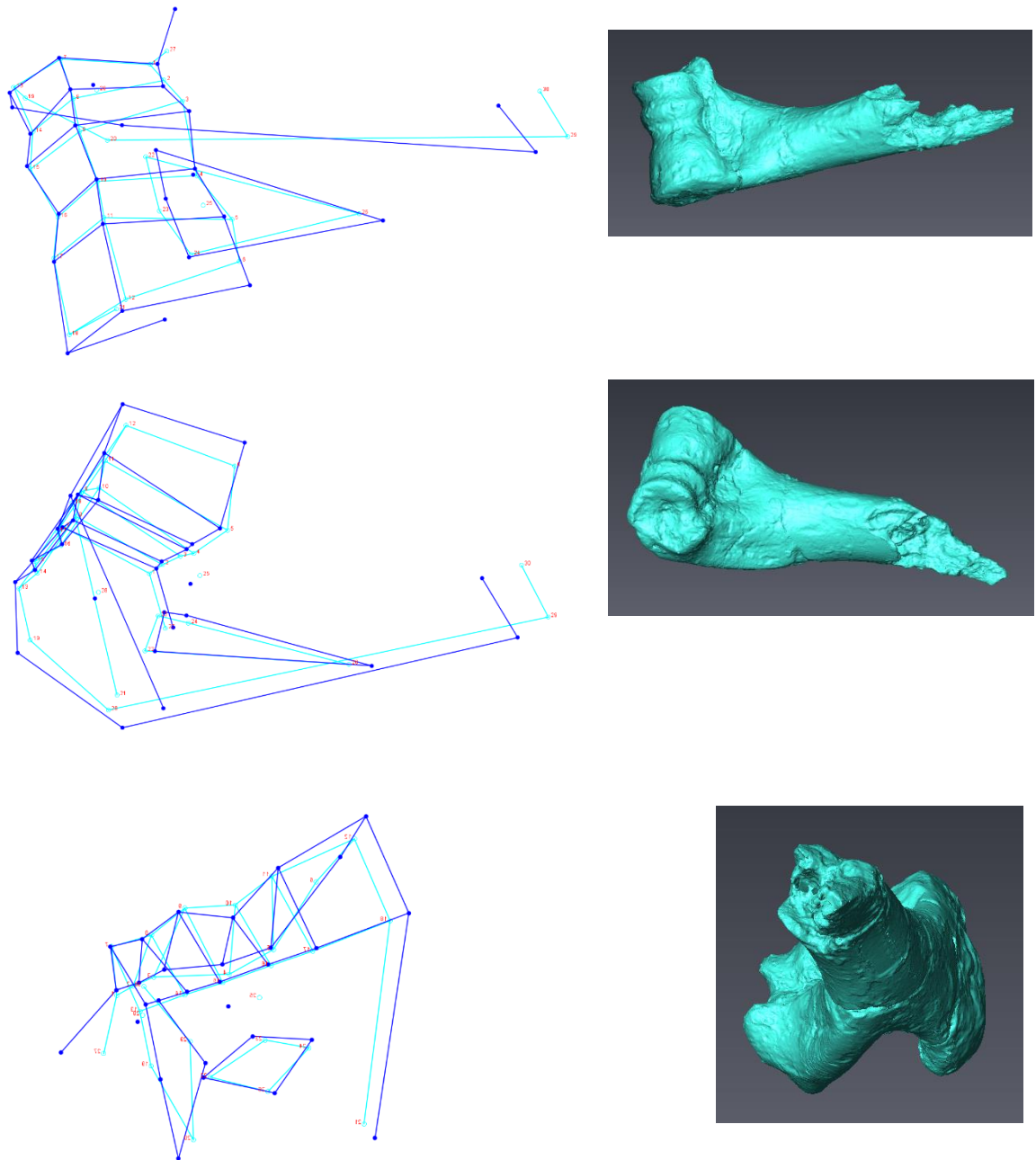


Figure 16: *Rusingoryx* distal humerus shape as compared to mean extant bovid shape

Showing visual outputs from MorphoJ in the form of wireframes (constructed by manually choosing landmarks to be connected to one another by lines), with pale blue representing the mean shape of the distal humerus in extant bovids, and the darker blue representing the shape of *Rusingoryx* (BH EX-1077) distal humerus. On the right are images of the specimen in the orientations represented by the wireframes, for reference.

Tribe Affinity

In a CVA including all the extant bovids and *Rusingoryx atopocranion* with tribe affinity as the categorical variable (Figure 17), *Rusingoryx* falls centrally on CV1 and low on CV2, overlapping with the morphospaces of Caprini, Boselaphini and Alcelaphini. Most informative though, according to the Procrustes distances (Table 13) *Rusingoryx* is closest by far to the Alcelaphini, supporting its historical assignment to this tribe (Pickford and Thomas 1984).

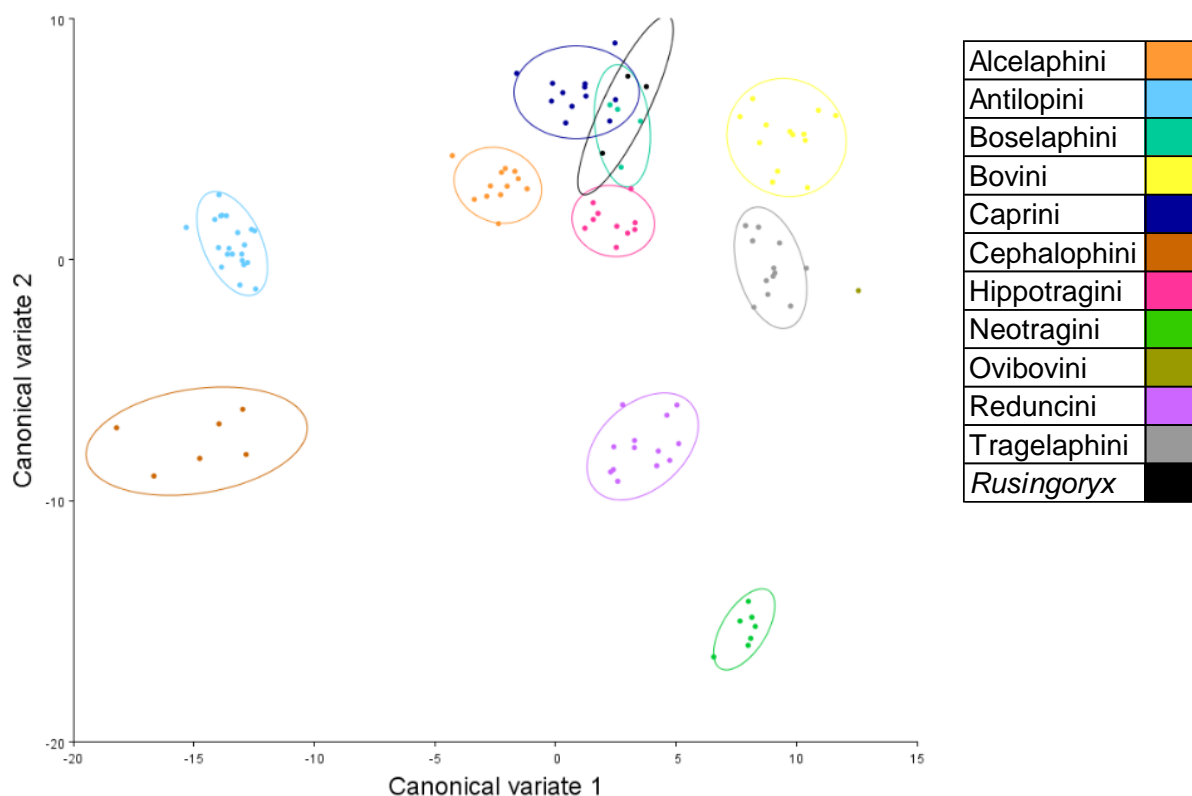


Figure 17: Visualization of Canonical Variate Analysis (CVA) on 3D Procrustes coordinates by tribe affinity, including *Rusingoryx*

Showing the first two canonical variate axes with specimen points colour-coded by tribe affinity, including *Rusingoryx* (BH EX-1077, RU06-74, and RU06-75,85) indicated in black.

Table 13: Procrustes distances between tribe groups including *Rusingoryx*

	Alcelaphini	Antilopini	Boselaphini	Bovini	Caprini	Cephalophini	Hippotragini	Neotragini	Ovibovini	Reduncini	Tragelaphini
Antilopini	0.1347										
Boselaphini	0.1058	0.0814									
Bovini	0.0941	0.1698	0.1283								
Caprini	0.1383	0.1145	0.1014	0.1260							
Cephalophini	0.1436	0.1286	0.1156	0.1490	0.1041						
Hippotragini	0.1006	0.0816	0.0849	0.1192	0.1009	0.1247					
Neotragini	0.1302	0.1414	0.1100	0.1514	0.1210	0.1117	0.1469				
Ovibovini	0.1910	0.1391	0.1548	0.1792	0.1380	0.1717	0.1176	0.2131			
Reduncini	0.1148	0.0937	0.0855	0.1258	0.0820	0.0721	0.0929	0.0982	0.1551		
Tragelaphini	0.1148	0.1042	0.0829	0.1112	0.0795	0.0926	0.0824	0.1299	0.1333	0.0640	
<i>Rusingoryx</i>	0.0717	0.1732	0.1419	0.1045	0.1571	0.1604	0.1331	0.1496	0.2147	0.1392	0.1357

Showing Procrustes distance between tribe affinity pairs in the dataset, including *Rusingoryx* as a distinct category (bottom row of the table, highlighted in green with the lowest distance in bold).

Habitat Preference

In a CVA including all the extant bovids and *Rusingoryx atopocranion* with habitat preference as the categorical variable (Figure 18), *Rusingoryx* appears to fall in a unique morphospace separated from all established habitat preference categories in the analysis on CV1 and CV2, being central on CV1 and low on CV2. However, the Procrustes distances (Table 14) are more enlightening, showing *Rusingoryx* being clearly closest to bovids preferring grassland/treeless (GT) habitats. This supports previous reconstructions of *Rusingoryx*'s habitat preference, and ecomorphological studies of this area of Pleistocene Africa (Faith et al. 2011; Tryon et al. 2012; Kovarovic et al. 2021).

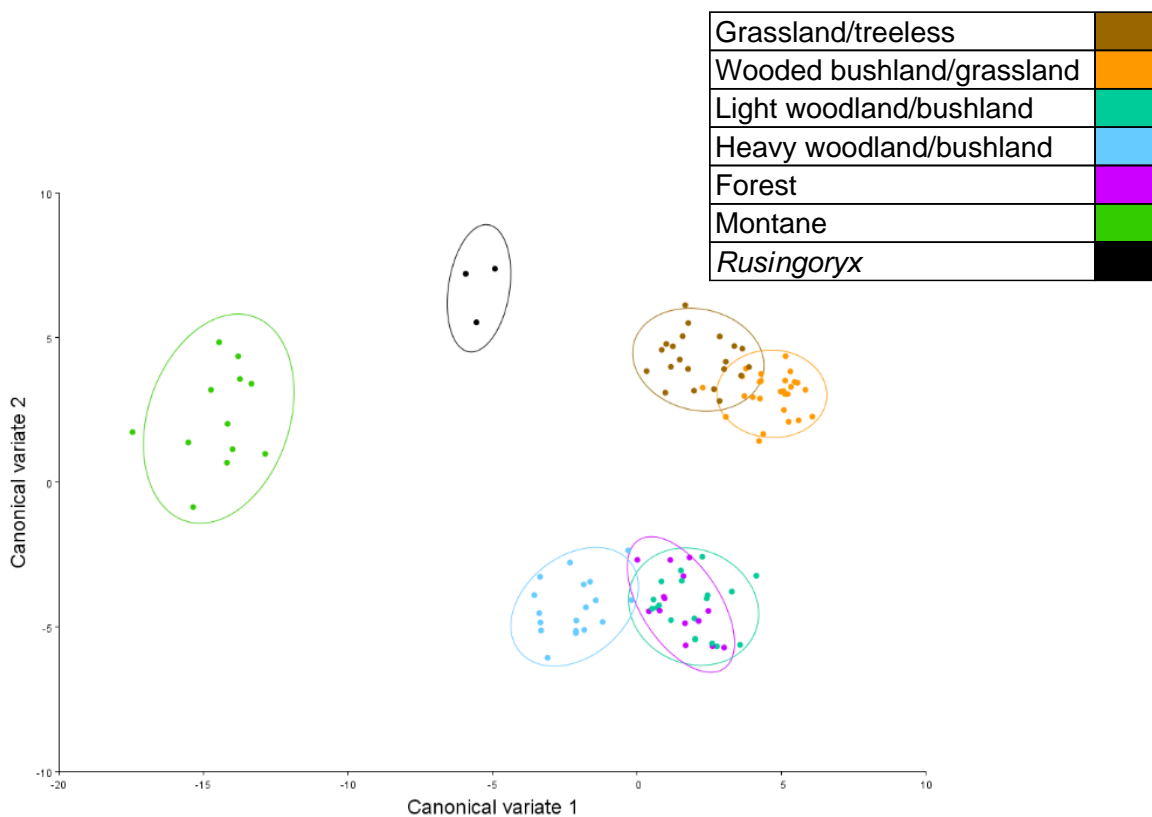


Figure 18: Visualization of Canonical Variate Analysis (CVA) on 3D Procrustes coordinates by habitat preference, including *Rusingoryx*

Showing the first two canonical variate axes with specimen points colour-coded by habitat preference group, including *Rusingoryx* (BH EX-1077, RU06-74, and RU06-75,85) indicated in black.

Table 14: Procrustes distances between habitat preference groups including *Rusingoryx*

	F	GT	HWB	LWB	M	WBG
GT	0.0657					
HWB	0.0557	0.0754				
LWB	0.0596	0.0716	0.0361			
M	0.0815	0.1035	0.0718	0.0732		
WBG	0.0881	0.0587	0.0818	0.0643	0.1009	
<i>Rus</i>	0.1166	0.0936	0.1305	0.1353	0.1571	0.134

Showing Procrustes distance between habitat preference pairs in the dataset, including *Rusingoryx* (*Rus*) as a distinct category (bottom row of the table, highlighted in green with the lowest distance in bold). Abbreviations: F= Forest; GT = Grassland/treeless; HWB = Heavy woodland/bushland; LWB = Light woodland/bushland; M = Montane; WBG = Wooded bushland/grassland

Given the importance of the lateral epicondylar protuberance area in distinguishing open living bovids from montane bovids and those preferring cover, it is prudent to consider the potential overwhelming influence of this feature in associating *Rusingoryx* with the GT category. However, when the protuberance (landmark 27) is removed from the analysis, the results remain consistent – in terms of Procrustes distances, *Rusingoryx* is still closest to the GT category.

Body Mass

In a CVA including all the extant bovids and *Rusingoryx atopocranion* with body mass category as the categorical variable (Figure 19), *Rusingoryx* lies centrally on the CV1 axis with the majority of the other bovids (except the greatest extremes of mass), and low on the CV2 axis closest to the 45-90 kg bovids. However, according to the Procrustes distances (Table 15), *Rusingoryx* is actually closest to the heaviest bovids – the >575 kg category. This is unexpected based on a previous estimate of *Rusingoryx* mass as being close to that of *Connochaetes taurinus* (O'Brien et al. 2016) which is assigned to the 180-360 kg category in this analysis (mean body mass 215 kg, (Etienne et al. 2020)).

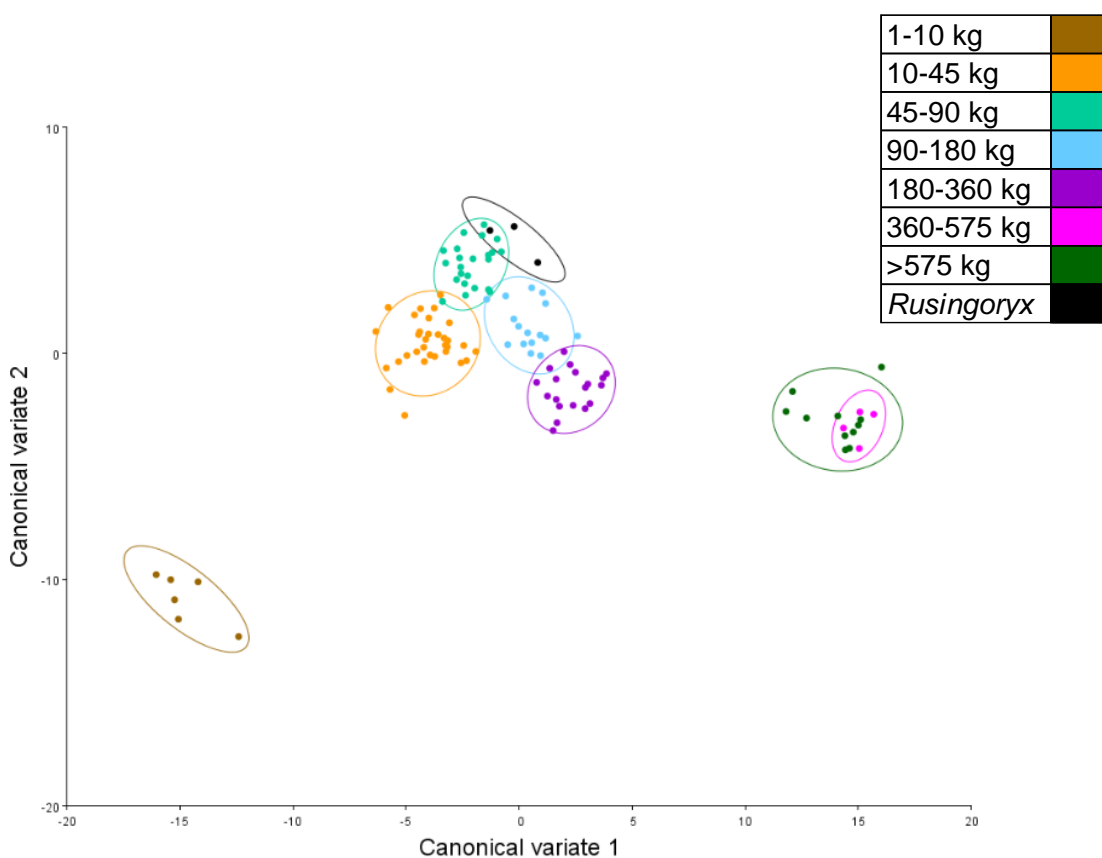


Figure 19: Visualization of Canonical Variate Analysis (CVA) on 3D Procrustes coordinates by body mass category, including *Rusingoryx*
Showing the first two canonical variate axes with specimen points colour-coded by body mass category, including *Rusingoryx* (BH EX-1077, RU06-74, and RU06-75,85) indicated in black.

Table 15: Procrustes distances between body mass groups including *Rusingoryx*

	1-10 kg	10-45 kg	45-90 kg	90-180 kg	180-360 kg	360-575 kg	>575 kg
10-45 kg	0.1029						
45-90 kg	0.1085	0.0395					
90-180 kg	0.1258	0.0543	0.0441				
180-360 kg	0.1221	0.0648	0.0504	0.0407			
360-575 kg	0.1599	0.1164	0.1023	0.0923	0.0802		
>575 kg	0.1613	0.1375	0.1223	0.1073	0.091	0.0759	
<i>Rus</i>	0.1601	0.1423	0.137	0.1188	0.1152	0.1121	0.1004

Showing Procrustes distance between body mass category pairs in the dataset, including *Rusingoryx* (*Rus*) as a distinct category (bottom row of the table, highlighted in green with the lowest distance in bold)

Again, given the importance of the lateral epicondylar protuberance area in distinguishing heavy from light bovids, it is prudent to consider the potentially overwhelming influence of this feature in associating *Rusingoryx* with the >575 kg category. However, when the protuberance (landmark 27) is removed from the analysis, the results remain consistent – in terms of Procrustes distances, *Rusingoryx* is still closest to the >575 kg category.

Principal Components Analysis

When *Rusingoryx atopocranion* is added to the PCA of extant bovids (Figure 11), the overall distribution of the points on the first two PCs is visually unchanged from the analysis excluding *Rusingoryx* (Figure 20), and *Rusingoryx* lies low on PC1 and high on PC2. The species which the *Rusingoryx* specimens are closest to in this morphospace are labelled in Figure 20, and more information on their categorical variable assignments is given in Table 16. On initial observation, there is little linking these animals – several tribes are represented, as well as several habitat preferences and body masses. However, what is notable is that all of these are bovids which experience strain on their forelimbs. They are all open-living and/or heavy species, the former experiencing strain related to fast movement on hard terrain, and the latter experiencing higher weight-bearing strain. This supports evidence previously found that there are morphological similarities in the long bones between open-living and high mass bovids, even when few animals fall into both categories (Etienne et al. 2020).

As previously established, PC2 and PC3 are most informative for assessing habitat preference and body mass category respectively when accounting for phylogeny. When *Rusingoryx* is added to the PCA and these axes are visualised (Figure 21), two of the three specimens lie clearly in the top right quadrant (representing open-living, heavy bovids), and the other specimen lies lower on PC3, falling in the upper extent of the bottom right quadrant with lighter bovids. This position almost on the centre line of PC3 suggests an average body mass between the lightest bovids and the heaviest (which is in line with the previous estimate (O'Brien et al. 2016)). However, it is important to bear in mind that, even though PC2 is significantly related to habitat preference and PC3 is significantly related to body mass category, there is still a significant influence of phylogeny on a bovid's position on these axes.

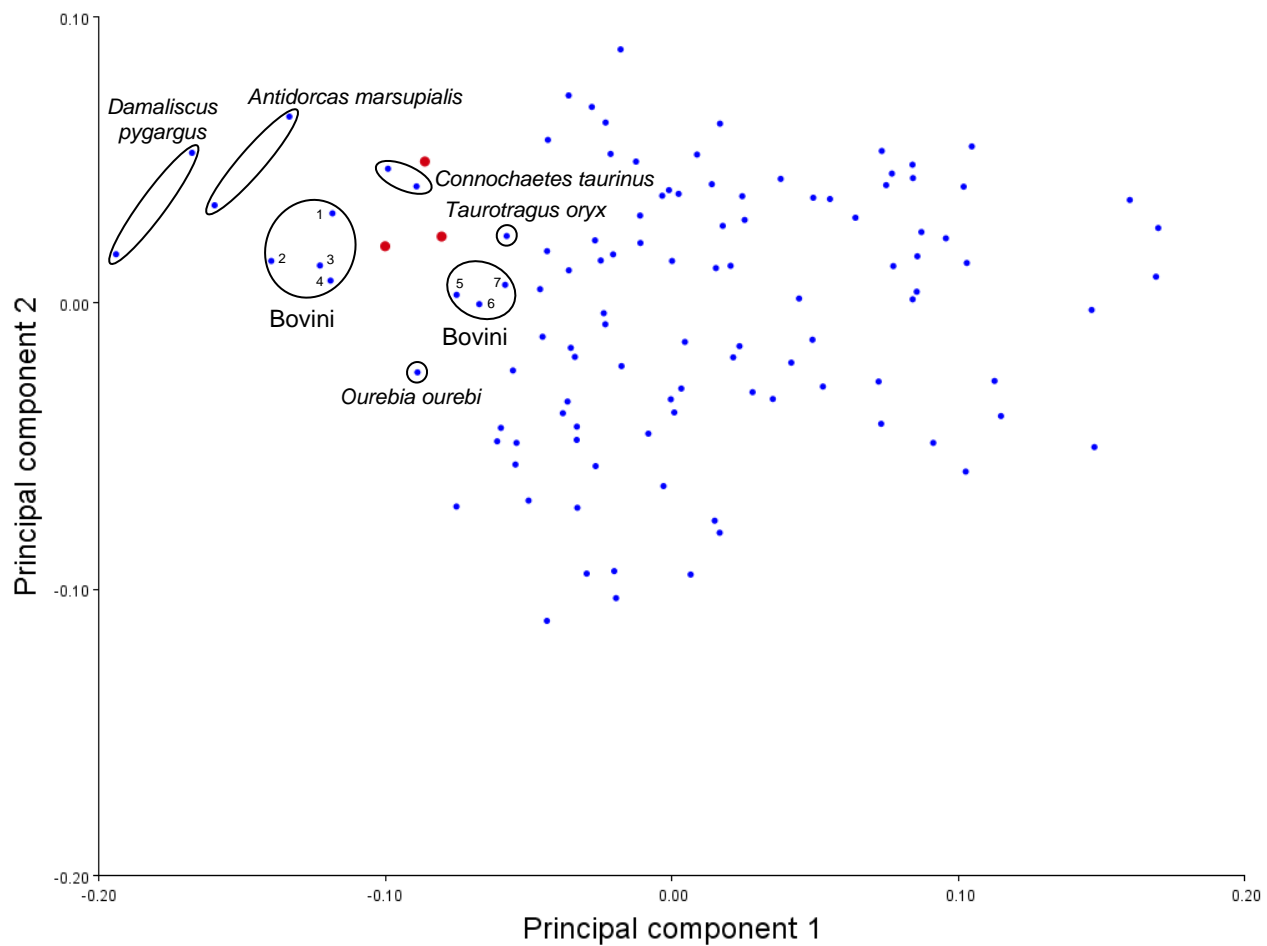


Figure 20: Visualization of Principal Components Analysis (PCA) on 3D Procrustes coordinates, including *Rusingoryx* – PC1 and PC2

Showing PC1 and PC2 with no colour-coding of the extant bovids, and three *Rusingoryx* specimens shown in red. Extant bovids located close to *Rusingoryx* in the morphospace are labelled and details of these animals can be found in Table 16.

N.B. For visual simplicity, the seven individuals which are closest to *Rusingoryx* are numbered rather than named, but the species information is provided in Table 16.

Table 16: Details of bovids closest to *Rusingoryx* in the PC2 vs PC1 morphospace

Species name	Tribe	Habitat preference	Body mass category (kg)	Mean body mass (kg)
<i>Connochaetes taurinus</i>	Alcelaphini	GT	180-360	215
<i>Damaliscus pygargus</i>	Alcelaphini	GT	45-90	71
<i>Taurotragus oryx</i>	Tragelaphini	HWB	360-575	575
<i>Ourebia ourebi</i>	Neotragini	WBG	Oct-45	12.5
<i>Antidorcas marsupialis</i>	Antilopini	WBG	Oct-45	29
Bovini 1 - <i>Bos javanicus</i>	Bovini	F	>575	600
Bovini 2 - <i>Syncerus caffer</i>	Bovini	LWB	>575	625
Bovini 3 - <i>Syncerus caffer</i>	Bovini	LWB	>575	625
Bovini 4 - <i>Syncerus caffer</i>	Bovini	LWB	>575	625
Bovini 5 - <i>Bos grunniens</i>	Bovini	F	360-575	395
Bovini 6 - <i>Bubalus bubalis</i>	Bovini	F	>575	700
Bovini 7 - <i>Bison bison</i>	Bovini	GT	>575	679

Providing tribe and ecology details about the bovids which are located closest to the *Rusingoryx* specimens in the visualization of PC2 vs PC1 (Figure 20).

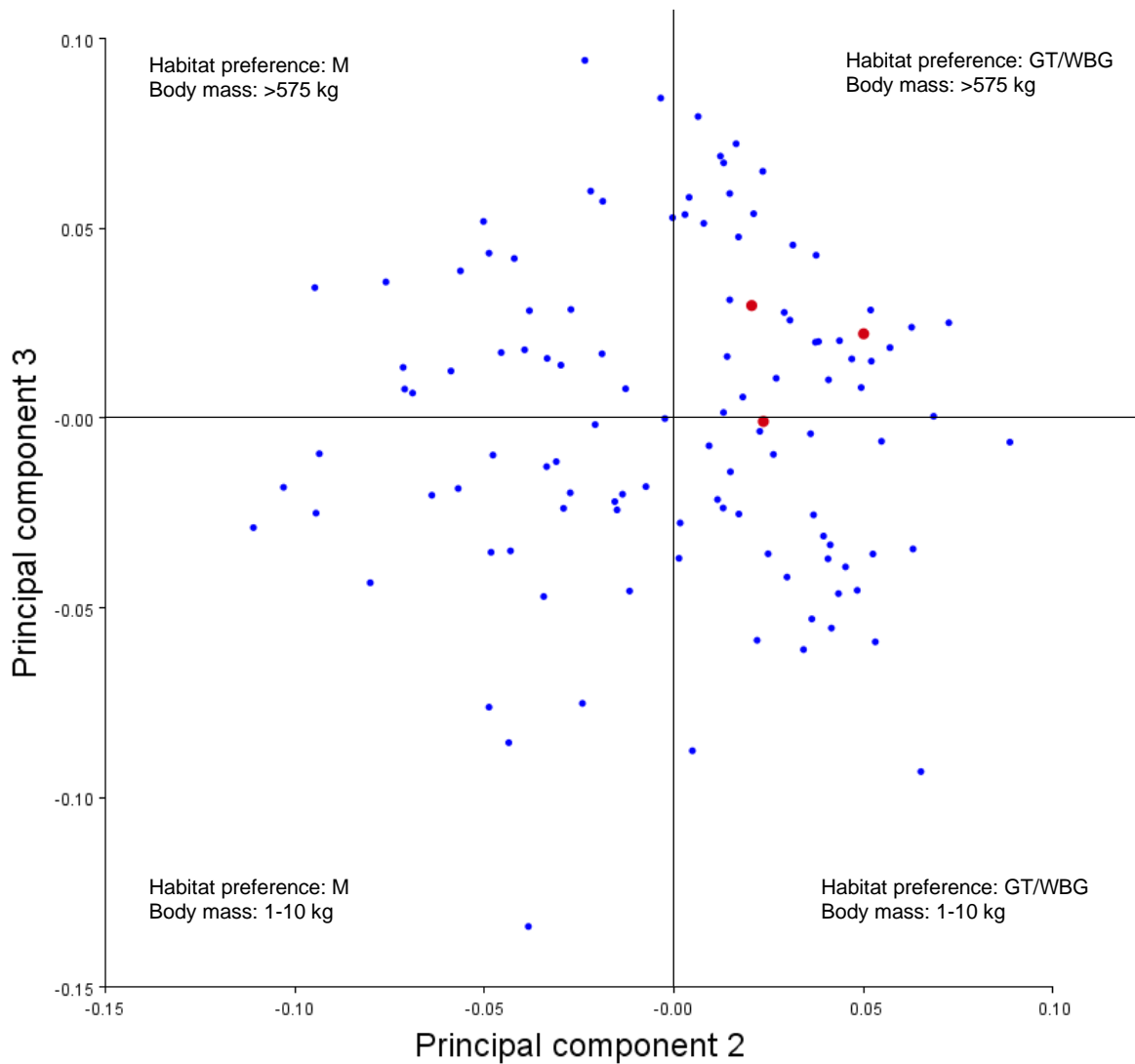


Figure 21: Visualization of Principal Components Analysis (PCA) on 3D Procrustes coordinates, including *Rusingoryx* – PC2 and PC3

Showing PC2 and PC3, and additionally divided into four visual quadrants with the statistically implied characteristics of the extremes of each quadrant given (as Figure 15 in the 3D Analysis section). The three *Rusingoryx* specimens are shown in red.

Summary

- *Rusingoryx atopocranion* is reconstructed in tribe Alcelaphini based on the morphology of its distal humerus, supporting literature assignment (Pickford and Thomas 1984).
- *Rusingoryx atopocranion* is reconstructed as favouring an open grassland/treeless habitat based on the morphology of its distal humerus, supporting previous reconstructions in the literature (Kovarovic et al. 2021).
- *Rusingoryx atopocranion* is unexpectedly reconstructed with the heaviest bovids in the analysis (>575 kg) based on the morphology of its distal humerus, contradicting previous mass estimates (O'Brien et al. 2016).

Chapter 5: Discussion

Extant Bovids

The results obtained in this study reflect the anticipated ecologically-related plasticity of the distal humerus in bovids, demonstrating that aspects of the morphology have evolved convergently across differing tribes when the animals share a habitat preference or approximate body mass. It is also evident that this complex structure is influenced by multiple factors simultaneously – those presented here and, undoubtedly, other factors not considered in this study. The fact that relative Procrustes distances between tribe groups do not reflect phylogenetic relatedness is interesting. It reflects the high level of convergent evolution of distal humerus morphology in bovids observed across these analyses – tribes with a predominant habitat preference or body mass are relatively closely associated in the results with other tribes sharing that characteristic, regardless of their genetic relatedness to that tribe.

It is important to note and discuss similarities and differences between habitat preference groups and body mass categories. Both open-living bovids and those with high body mass experience high levels of strain on their long bones, and morphological similarities in the long bones of these two groups have been previously identified and linked to this strain (Etienne et al. 2020). Notably in Etienne et al.'s study, both were found to have large epiphyses on the long bones, and a cranio-caudally enlarged medial epicondyle of the humerus (among other long bone morphologies not relevant to this study). The results presented here also show evidence of morphological similarities between open-living and heavy bovids. In both groups, the lateral epicondyle is enlarged (cranially and/or distally), and the caudal extremity is laterally directed. Additionally, in both groups, the olecranon fossa is deep and medio-laterally wide, particularly extending laterally. Lastly, the protuberance on the lateral epicondyle is enlarged in both groups. However, there are also several morphological differences between these two groups which distinguish them, which were described above. Interestingly, though there is evidence here of a cranio-caudally enlarged medial epicondyle in the heavier bovids (as Etienne et al. (2020) also observed), this feature was not observed in this sample of open-living bovids.

The montane bovids appear to have the most morphologically distinctive distal humerus of the bovids included in this study. Some of the features are found in other categories (Figure 22) but montane bovids exhibit a unique combination of features. This likely reflects the high level of specialisation necessary for these bovids to move around in montane environments. Intuitively, it is congruent for montane bovids to be morphologically opposed to open-living bovids – open-living bovids specialise to move quickly to avoid predators, while montane bovids specialisation prioritizes manoeuvrability and agility. Bovid living in more covered environments are also specialised for manoeuvrability, so one might expect them to have similar adaptations to those seen in montane bovids. It is true that both appear to have similarly angled capitula, with the proximal edge being more laterally positioned than in other bovids. However, it appears from the results presented here that, in fact, the nature of the movements required for a lifestyle in closed/covered environments differ enough from the requirements of montane living to have resulted in divergent distal humerus morphology. Notably, montane bovids have a more reduced medial epicondyle and more medially positioned olecranon fossa, while covered habitat-preferring bovids have a more reduced lateral epicondyle and highly medially positioned proximo-medial corner of the trochlea.

As can be seen in Figure 22, there are key features which can be used to identify each of the following categories: open-living bovids, bovids preferring more cover, montane bovids, high body mass bovids and low body mass bovids. These five categories can be arranged into two highly distinct groups: a) the open-living and high body mass bovids, and b) the montane, cover-preferring and low body mass bovids. While the former group is united by more than one characteristic, the latter group is united predominantly by the reduced size of the lateral epicondylar protuberance. The size of the lateral epicondylar protuberance which is so prominent in *Rusingoryx* is, in fact, the main morphological distinction between the two categories.

What is most clear is that the distal humerus is a morphologically and evolutionarily plastic region in bovids, highly influenced by both an animal's phylogenetic affinity, and its ecology. The results of this study provide evidence that tribe affinity, habitat preference and approximate body mass (to category level) can be predicted from distal humerus morphology in extant bovids. The assumption leading from this is that distal humerus morphology could be a powerful tool in predicting these characteristics in extinct bovids,

and this is the rationale behind using the extant bovid results to the functional significance of the enlarged lateral epicondylar protuberance in *Rusingoryx*.

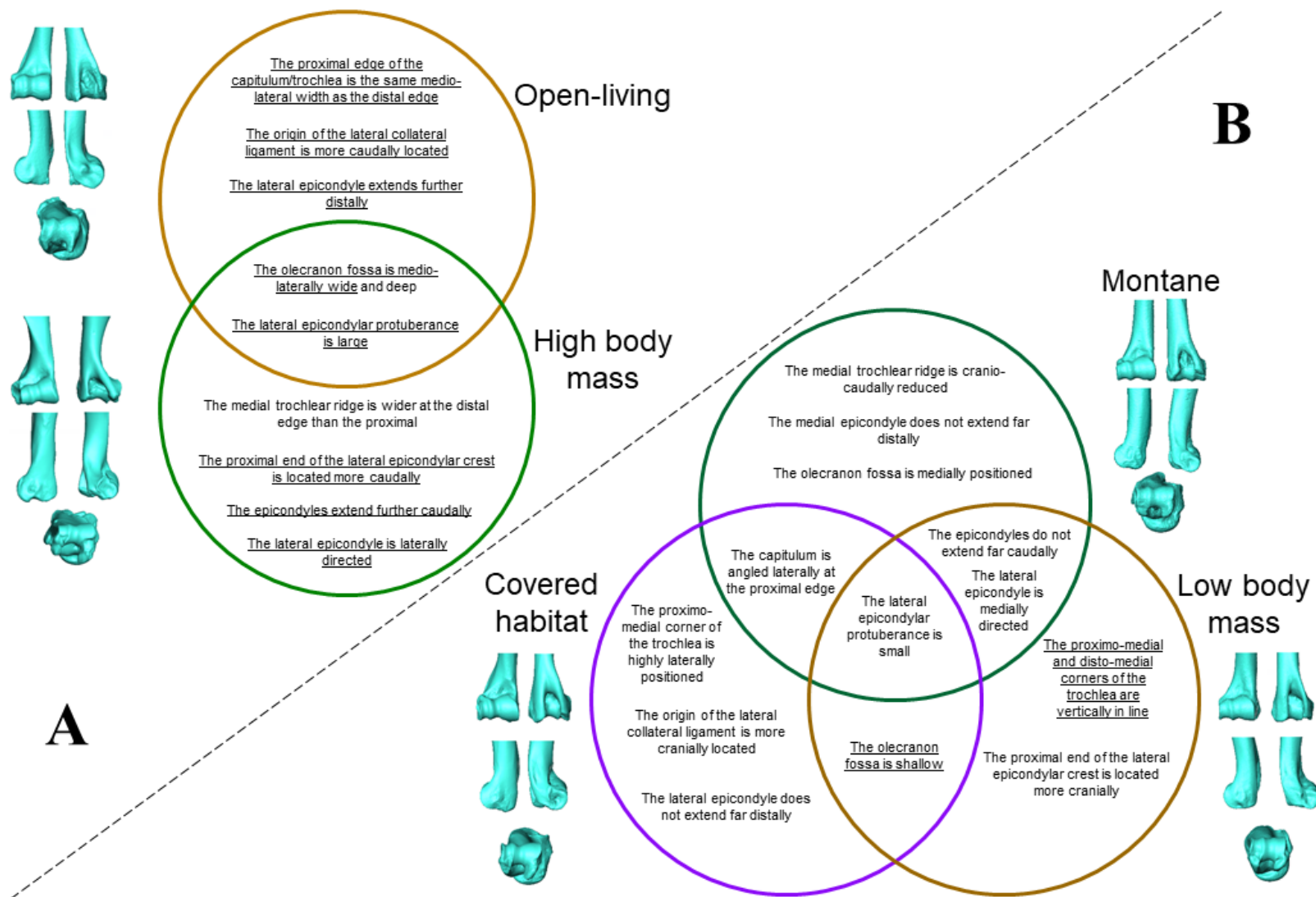


Figure 22: Notable characteristics of categories within the analysis

Showing Venn diagrams representing the overlaps in morphologies between categories in the analysis, and features distinguishing the categories from one another. Characteristics which are underlined are present in *Rusingoryx atopocranion*. A) The relationship between open-living bovids and high body mass bovid morphologies; B) the relationships between covered habitat-preferring bovids, high body mass bovids and montane bovids. N.B. groups A and B are separated because there is no overlap between the two groups in relation to the features specified.

Rusingoryx atopocranion

Rusingoryx's assignment to the tribe Alcelaphini and reconstruction as having a preference for grassland/treeless habitats aligns with and supports previous analyses and ecomorphological studies of the area during the Pleistocene (Pickford and Thomas 1984; Faith et al. 2011; Tryon et al. 2014; Kovarovic et al. 2021). However, though no formally-derived mass estimates have been published for *Rusingoryx*, based on its size it is expected to have had a body mass similar to that of the similarly-sized and closely related *Connochaetes taurinus* (O'Brien et al. 2016), and this is not the result obtained in the analyses presented here. The previous estimate appears appropriate based on the size of the skeletal elements known for *Rusingoryx*, and it is more likely that the true mass of *Rusingoryx* was closer to the roughly 215 kg of *C. taurinus* (Etienne et al. 2020) than the >575 kg bovids it was found to share morphologies with in this analysis. As previously discussed, long bones of open-living bovids have been shown to share characteristics with those of heavy bovids due to the strain-tolerance required in both (Etienne et al. 2020) and, while the analyses here were able to accurately identify open-living species and heavy species regardless of these similarities in extant bovids, it may be this factor which has led to *Rusingoryx* being reconstructed as >575 kg in mass.

It is possible that *Rusingoryx*'s apparent morphological similarity to very heavy bovids is related to another unusual aspect of its morphology – *Rusingoryx* has unexpectedly small feet, specifically short phalanges (Kovarovic et al. 2021). Kovarovic et al. (2021) posit that this is an extreme open habitat adaptation, as short phalanges have previously been associated with open habitats (DeGusta and Vrba 2005). In fact, compared to extant bovids, *Rusingoryx* has the distal phalanges (and, by extension, hoof area) of a much smaller bovid, being most similar in size to *Addax nasomaculatus* with a body mass of approximately 92.5 kg (Etienne et al. 2020) – less than half the predicted body mass of *Rusingoryx*. A fuller analysis of hoof area and pressure in *Rusingoryx* as compared to extant bovids can be found in Appendix II. To facilitate the development of such small hooves on a bovid the size of *Rusingoryx*, the muscles of the forelimb would have needed to become more heavily distributed proximally (this is similar to the redistribution of forelimb musculature during the evolution of unguligrady, and that observed in chiropterans to lighten the distal forelimb and facilitate flight (Amador et al. 2018)). Essentially, in order to have the hooves of a much smaller bovid, *Rusingoryx* may have had the upper limbs of a much larger bovid, thus

explaining the morphological similarity between the distal humerus of *Rusingoryx* and the heaviest bovids.

Rusingoryx shares all of the identifying characteristics of open habitat bovids, and most of the characteristics of the high body mass bovids (though the medial trochlear ridge in *Rusingoryx* is approximately the same width at the proximal and distal edges) (Figure 22 shows all characteristics observed in *Rusingoryx* underlined). *Rusingoryx* also generally exhibits the shared characteristics of open habitat and high body mass bovids, though the olecranon fossa in *Rusingoryx* is relatively shallow. Interestingly, having a relatively shallow olecranon fossa is a characteristic of the covered habitat/low body mass bovids. The notable feature in which *Rusingoryx* differs from high body mass bovids is actually a feature in which it is more similar to low body mass bovids – the proximo-medial and disto-medial corners of the trochlea are vertically in line in cranial view, where the proximo-medial corner is laterally positioned relative to the disto-medial corner in heavy bovids. The most relevant characteristic is, of course, the lateral epicondylar protuberance, and the fact that this is large in *Rusingoryx* aligns it with the open habitat/high body mass bovids and distinguishes it from the covered habitat/low body mass/montane bovids.

Interestingly, an enlarged protuberance on the lateral epicondyle of the distal humerus has previously been identified to be related to strain at the joint in bovids, but as a pathology – specifically a pathology known as ‘penning elbow’ identified by zooarchaeologists (Baker and Brothwell 1981; Upex and Dobney 2012; Bendrey 2014). In this condition, an osteophyte (also referred to as an exostosis) develops on the lateral epicondyle, usually in association with a corresponding osteophyte on the proximal radio-ulna, and it is believed that this may develop in order to stabilise a joint which has become ‘mechanically compromised’ (O’Connor 2008). Penning elbow is considered to be associated with incorrect husbandry practices in the penning and handling of livestock, such that repeated trauma to the elbow joint occurs (e.g. animals kept penned in extremely close proximity will frequently collide with one another and with the enclosure walls – hence the name, penning elbow) (Bendrey 2014; Upex and Dobney 2012). The condition is well-documented in English archaeology, having been identified in material from Northampton, North Elmham Park, Barnsley Park, Aikerness, Winchester (Clark 2009), and Flixborough (Upex and Dobney 2012), but this pathology has also been identified in modern populations of sheep from St Kilda (Clutton-Brock et al. 1990), Herdwick (Upex and Dobney 2012),

North Ronaldsay, and the Welsh mountains (Clark 2009), which are not housed in conditions which would lead to this repeated elbow trauma, but do roam rough and hard terrain. Therefore, it has been suggested that the osteophytes may also form in response to joint trauma associated with repeated jolting while moving across hard, rocky ground – an idea reinforced by an unpublished study comparing sheep from contrasting environments on the island of North Ronaldsay (Clark 2009).

The pathology presents on the humerus as a broad-based osteophyte protruding from the proximo-lateral edge of the capitulum on the cranial side and extending around to the caudal side as it develops (Figure 23). The osteophyte can be distinguished from the healthy bone due to a visible line of vascularisation accompanying the departure from the normal bone topology. The osteophyte arises from the origin site of the lateral collateral ligament on the humerus, and from the attachment of the same ligament on the radius (Clark 2009).

Intriguingly, while the condition is relatively common in sheep, it has never been identified in goats (despite their phylogenetic closeness). The reason for this is unclear, but Clark (2009) proposes that the subtle morphological differences of the humerus between the two species may be enough to explain the phenomenon – goats exhibit a more developed medial epicondyle, and the trochlea is more posteriorly directed.

Unfortunately, the condition is poorly studied. Zooarchaeologists are only able to speculate on the exact causes behind the pathology they are observing, being unable to witness the daily life of the animal. The condition is almost entirely absent from modern veterinary literature, possibly due to improved husbandry practices, but likely due to the condition not affecting the commercial viability of the animal (O'Connor 2008). The animal likely continues to produce milk and/or wool, and meat of the same quality regardless of the injury and, thus it is rarely identified and even more rarely treated. If the osteophyte has grown to become a hinderance to the animal's productivity, slaughter is generally considered.

The same type of osteophyte appears in cattle suffering from osteoarthritis. In fact, the term osteoarthritis has often been used synonymously in the literature to refer to any condition of the joints which results in exostoses. However, in 1981, Baker and Brothwell listed four criteria for the diagnosis of osteoarthritis as distinct from other joint pathologies: eburnation (bone taking on a polished appearance), grooves forming on the articular surfaces,

extension of the articular surfaces by new bone, and exostoses forming around the periphery of the joint. These are osteological characteristics that can be detected even in dry bone specimens, resulting as a side effect of the condition itself, which is an inflammatory condition affecting the cartilage at the joint. Osteoarthritis has been directly related to biomechanical stress at the joints, with repeated stress causing degradation of the cartilage and, thus, exposing the bone to eburnation and grooving. This significantly affects the function of the joint and may lead to realignment, which then leads to irregular formation of perichondral cartilage (found adjacent to developing bone), and finally the formation of the characteristic osteophytes (known as ‘lipping’) (O’Connor 2008).

Unfortunately, from dry bone it can be difficult to distinguish osteophytes arising due to osteoarthritis from those arising from joint trauma, and there is even evidence that ‘lipping’ occurs more frequently in individual cattle with higher body mass (Bartosiewicz et al. 1997). Despite this, and the general lack of literature on the subject, what is clear is that extensions of the bone at the elbow joint (particularly at the lateral epicondyle) are relatively common pathologies in response to trauma and strain at the joint (whether as a direct result or as a consequence of cartilage pathologies).

The protuberance on the lateral epicondyle of *Rusingoryx* does not exhibit the characteristics of an osteophyte/exostosis (there is no evidence of eburnation, grooving, or vascularisation), and coupled with the fact that the protuberance can be seen in all five individual specimens available of the *Rusingoryx* distal humerus, it is unlikely that the morphology of *Rusingoryx* can be explained as a bone pathology. However, it certainly appears that there is some kind of mechanical advantage to the development of a protuberance in this location in response to high levels of stress on the joint, and it is certainly possible that the morphology observed in *Rusingoryx* is directly related to stabilising and mitigating strain on the elbow joint due to the species’ lifestyle. In particular, the morphology could be related to the apparent high level of specialisation that *Rusingoryx* displays for life on very hard, open terrain – the hard terrain being a factor in the development of osteophytes in North Ronaldsay sheep. Additionally, the link between ‘lipping’ (and general joint asymmetry) and high body mass in cattle (Bartosiewicz et al. 1997) may be informative here – *Rusingoryx* being reconstructed in the 3D analyses alongside the largest bovids in the dataset certainly does imply that its morphology has developed in response to stresses similar to those experienced at the elbow joints of heavy

animals. Of course, it is not just the protuberance which associates *Rusingoryx* with the high joint stress bovids (open living and high body mass) – even with the protuberance excluded from analyses, *Rusingoryx* is still significantly similar to these groups, indicating that the distal humerus is generally well-adapted for high stress and loading.

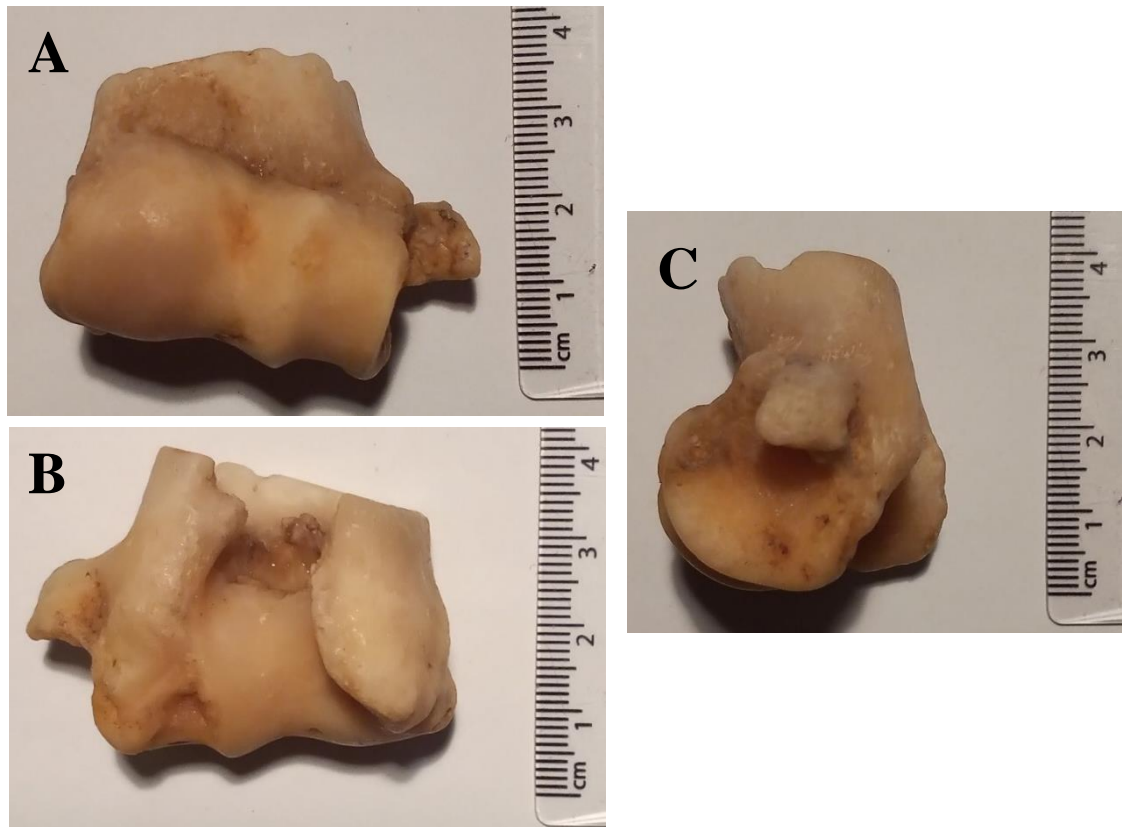


Figure 23: Penning elbow in a possible North Ronaldsay sheep

An example of the penning elbow pathology found in the left distal humerus of a possible North Ronaldsay sheep, found at the Sands of Wright, Orkney, in 2019.

A) Cranial view; B) caudal view; C) lateral view

Critical Assessment of the Study

The scale of this study was limited due to the time constraints of a one-year master's degree, and due to the Covid-19 pandemic. Nevertheless, a sample was obtained which is felt to be representative of the variation in extant bovids. With a longer timescale, much could be gained by introducing semilandmarks (used to better capture curved surfaces) to represent the true morphology at higher resolution. An argument could be made that, given the predictive power shown using the 30 landmarks included in this study, introducing semilandmarks could introduce unnecessary noise into the data, but without running the analyses we cannot discount the possible advantages of semilandmarking. Introducing more landmarks, whether manually or via semilandmarking, increases the complexity of the data interpretation, making it more difficult to differentiate the relative importance of individual feature shape changes. However, by capturing the shape of the object with greater accuracy, multivariate analyses may be more accurately able to associate and differentiate categories.

With regard to phylogenetic analyses, PGLS has been a popular method for phylogenetic correction in functional morphology and GMM since its development (Grafen 1989), offering a relatively simple way of testing for convergent morphological evolution within a sample. However, it is not immune to criticism. There are two main shortcomings of the method: i) it is a regression test, which entails several assumptions about the data (independence, normal distribution, homoscedasticity); ii) it only allows investigations of the relationships between variables and the conditional mean of another variable (the expected value, in this case the phylogenetic placement of an animal, which may reflect reality to varying degrees) (Saulsbury 2020). For the purposes of this study, PGLS provides a satisfactory method for confirming convergent evolution of distal humerus morphology in extant bovids according to ecology, but the drawbacks of the method are worth bearing in mind. Alternative methods to assess the effect of phylogeny in comparative morphology data have been developed, such as Blomberg's K (Blomberg et al. 2003) which tests for a phylogenetic signal, and Moran's I (Gittleman and Kot (1990), based on Moran (1950)) which test for phylogenetic non-independence. These are permutation tests which do not rely on the assumptions of parametric tests, but they require continuous rather than discrete data and, thus would not be applicable to this study in which tribe, habitat preference and body mass are discrete independent variables. Saulsbury has recently developed a

permutation test approach based on Blomberg's K , but as this has not yet been peer-reviewed, it was not considered for this study (Saulsburry 2020). With more time, it would certainly have been beneficial to explore other methods of testing and accounting for phylogenetic signal in the distal humerus data, and this is undoubtedly an area of GMM and comparative morphology still in development which will continue to improve research in the field.

CVAs were used extensively within this study, and there are several important considerations when using analyses such as these (i.e. Discriminant Function Analysis, DFA), specifically pertaining to prediction accuracies. Notably, there is a tendency for the models to over-fit – due to the nature of the analysis being dataset-specific, the resulting predictive power is heavily influenced by the composition of the dataset (the choice of taxa and the sample sizes for each taxon (Klein et al. 2010)), and high accuracy for the sample may not translate into correct predictions for novel incidences subsequently added to the analysis (Kovarovic et al. 2011). Of course, when these analyses are used within ecomorphology and functional morphology, there is an underlying assumption that strong associations between specimens are functionally significant and taxon-free when, in fact, this is not always the case (Barr and Scott 2014). However, this was addressed within the study through the use of PGLS. Lastly, the use of these analyses also requires several statistical assumptions: independence in the observations, multivariate normal distribution, and homoscedasticity in the within-group variance-covariance matrices (Kovarovic et al. 2011). The latter is often violated when the sample size of one or more groups is smaller than the number of variables. Unfortunately, this is the case within this study; however, there are arguments in favour of the analyses being able to hold up against this violation (Tabachnick and Fidell 2007).

Lastly, it is clear from the PCA results that morphological variation of the distal humerus in bovids is related to a complex array of factors, and it is highly likely that there are variables significantly related to this variation which were not considered in this study. For example, though body mass was considered, the relative distribution of the overall body mass to forelimbs versus hindlimbs was not considered. Additionally, given difficulties in obtaining material, sex of the specimen was not considered (and is not known for the majority of specimens), but sexual dimorphism may have a large impact on the results, especially as it relates to body size.

Future Work

In order to further understand the unusual morphology of *Rusingoryx*'s distal humerus, it would be advantageous to perform Finite Elements Analysis (FEA), a method which can be used to assess strain distribution on a skeletal element. Comparing *Rusingoryx* to extant bovids may provide more information about the hypothesised relationship between the enlarged lateral epicondylar protuberance and joint strain mitigation.

Though specimen numbers are limited and poorly documented, a GMM analysis including sheep exhibiting penning elbow and cows exhibiting 'lipping' osteoarthritis may be informative. Specifically, if *Rusingoryx* is reconstructed within or near the morphospace of these pathological specimens, it would strongly indicate that an enlarged protuberance on the lateral epicondyle, whether arising evolutionarily or pathologically, has an adaptive function. Of course, further research into the biomechanical implications of these joint pathologies would also greatly illuminate the current idea that it is related to increasing joint stability due to trauma/illness.

Chapter 6: Conclusions

The distal humerus region in extant bovids is morphologically plastic, varying in response to the complex interactions of phylogeny, habitat preference and body mass found within the family. It is possible to accurately predict tribe affinity, habitat preference and body mass from the morphology of the distal humerus in extant bovids due to convergent evolution in response to environmental pressures.

Based on these results, the distal humerus of *Rusingoryx atopocranion* was assessed and found to be most similar to other alcelaphine bovids, the most open-living species, and the heaviest animals in the dataset. The latter point is unexpected given *Rusingoryx*'s estimated body size, and it is likely that this result reflects effects of strain at the elbow joint being high, rather than indicating a larger body mass for *Rusingoryx* overall. This supports the idea that *Rusingoryx* was highly specialised for cursorial locomotion on the vast, hard and flat terrain in which it lived on the eastern edge of Lake Victoria in the late Pleistocene.

References

- Amador LI, Giannini NP, Simmons NB, Abdala V. 2018. Morphology and Evolution of Sesamoid Elements in Bats (Mammalia: Chiroptera). *Am Museum Novit.* **3905**(3905):1–40.
- Andrews P, Lord JM, Evans EMN. 1979. Patterns of ecological diversity in fossil and modern mammalian faunas. *Biol J Linn Soc.* **11**(2):177–205. x.
- Anyonge W. 1993. Body mass in large extant and extinct carnivores. *J Zool.* **231**:339–350.
- Baker J, Brothwell D. 1981. *Animal Diseases in Archaeology*. London: Academic Press.
- Barr WA. 2014. Functional morphology of the bovid astragalus in relation to habitat: Controlling phylogenetic signal in ecomorphology. *J Morphol.* **275**(11):1201–1216.
- Barr WA. 2020. The Morphology of the Bovid Calcaneus: Function, Phylogenetic Signal, and Allometric Scaling. *J Mamm Evol.* **27**(1):111–121.
- Barr WA, Scott RS. 2014. Phylogenetic comparative methods complement discriminant function analysis in ecomorphology. *Am J Phys Anthropol.* **153**(4):663–674.
- Bartosiewicz L, Van Neer W, Lentacker A. 1997. Draught cattle: their osteological identification and history. *Ann Zool Wet.* **281**:1–147.
- Bendrey R. 2014. Animal Paleopathology. In: Smith C (Ed.). *Encycopaedia of Global Archaeology*. New York: Springer Science.
- Bibi F. 2013. A multi-calibrated mitochondrial phylogeny of extant Bovidae (Artiodactyla, Ruminantia) and the importance of the fossil record to systematics. *BMC Evolutionary Biology.* **13**:1-15
- Blomberg SP, Garland TJ, Ives AR. 2003. Testing for phylogenetic signal in comparative data: behavioural traits are more labile. *Evolution (NY).* **57**(4):717–745.
- Bookstein FL. 1991. *Morphometric Tools for Landmark Data Geometric and Biology*. Cambridge: Cambridge University Press.
- Brink JS. 2005. The evolution of the black wildebeest, *Connochaetes gnou*, and modern large mammal faunas in Central Southern Africa. PhD thesis, University of Stellenbosch.

- Campione NE, Evans DC. 2012. A universal scaling relationship between body mass and proximal limb bone dimensions in quadrupedal terrestrial tetrapods. *BMC Biol.* **10**:1-21.
- Clark K. 2009. Pathologies of the sheep. In: Serjeantson D, Rees H (Ed.). *Food Craft, and Status in Medieval Winchester*. p. 158–165.
- Clifford AB. 2010. Evolution and Mechanics of Unguligrady in Artiodactyls. Biomechanics. PhD thesis, Brown University.
- Clutton-Brock J, Dennis-Bryan K, Armitage P., Jewell P. 1990. Osteology of the Soay sheep. *Bull Br Museum, Nat Hist Zool.* **56**(1):1–56.
- Cumming DHM, Cumming GS. 2003. Ungulate community structure and ecological processes: Body size, hoof area and trampling in African savannas. *Oecologia.* **134**(4):560–568.
- DeGusta D, Vrba E. 2005. Methods for inferring paleohabitats from the functional morphology of bovid phalanges. *J Archaeol Sci.* **32**(7):1099–1113.
- Etienne C, Filippo A, Cornette R, Houssaye A. 2020. Effect of mass and habitat on the shape of limb long bones: A morpho-functional investigation on Bovidae (Mammalia: Cetartiodactyla). *J Anat.* **2020**;00:1–19.
- Faith JT, Choiniere JN, Tryon CA, Peppe DJ, Fox DL. 2011. Taxonomic status and paleoecology of *Rusingoryx atopocranion* (Mammalia, Artiodactyla), an extinct Pleistocene bovid from Rusinga Island, Kenya. *Quat Res.* **75**(3):697–707.
- Figueirido B, Pérez-Claros JA, Hunt RM, Palmqvist P. 2011. Body mass estimation in amphicyonid carnivoran mammals: A multiple regression approach from the skull and skeleton. *Acta Palaeontol Pol.* **56**(2):225–246.
- Fisher R. 1921. On the “probable error” of a coefficient of correlation deduced from a small sample. *Metron.* **1**:1–32.
- Flower WH. 1876. The Arm and Forearm. In: *An Introduction to the Osteology of the Mammalia*. p. 250–251.
- Fox J, Weisberg S, Price B, Adler D, Vates D, Baud-Bovy G, Bolker B, Ellison S, Firth D, Friendly M, et al. 2021. *car* package.
- Gálvez-López E, Kilbourne B, Cox PG. 2021. Cranial shape variation in mink: Separating

two highly similar species. *J Anat.* **2021**;**00**:1-16

Galvez Lopez E. 2014. Limb Morphometrics in Carnivora: Locomotion, Phylogeny and Size. PhD thesis, Universitat de Barcelona.

Garland T, Janis CM. 1993. Does metatarsal/femur ratio predict maximal running speed in cursorial mammals? *J Zool.* **229**(1):133–151.

Gentry AW, Gentry A, Mayr H. 1995. Rediscovery of fossil antelope holotypes (Mammalia, Bovidae) collected from Olduvai Gorge, Tanzania, in 1913. *Mitt. Bayer. Staatsslg. Paläont. hist. Geol.* **35**:125–135.

Geraads D, Alemseged Z, Reed D, Wynn J, Roman DC. 2004. The Pleistocene fauna (other than Primates) from Asbole, lower Awash Valley, Ethiopia, and its environmental and biochronological implications. *Geobios.* **37**:697–718.

Gill T. 1872. Arrangement of the families of mammals. With analytical tables. Washington DC: Smithsonian Institution

Gittleman JL, Kot M. 1990. Adaptaion: statistics and a null model for estimating phylogenetic effects. **39**(3):227–241.

Gower JC. 1975. Generalized procrustes analysis. *Psychometrika.* **40**(1):33–51.

Grafen A. 1989. The Phylogenetic Regression. *Philos Trans R Soc B Biol Sci.* **326**(1233):119–157.

Gray JE. 1821. On the natural arrangement of vertebrose animals. *London Med Repos.* **5**(1):296–310.

Grzimek B. 2004. Grzimek’s Animal Life Encyclopedia Volume 1: Mammals V. McDade MC (Ed.). Farmington Hills, MI: Gale Group Inc.

Hallström BM, Janke A. 2008. Resolution among major placental mammal interordinal relationships with genome data imply that speciation influenced their earliest radiations. **13**:1–13.

Hallström BM, Janke A. 2010. Mammalian evolution may not be strictly bifurcating. *Mol. Biol. Evol.* **27**(12):2804–2816.

Harris JM. 1991. Koobi Fora Research Project Volume 3: The Fossil Ungulates: Geology, Fossil Artiodactyls, and Palaeoenvironments. Oxford: Claredon Press

- Heesy CP. 2005. Function of the mammalian postorbital bar. *J Morphol.* **264**(3):363–380.
- Hernández Fernández M, Vrba ES. 2005. A complete estimate of the phylogenetic relationships in Ruminantia: A dated species-level supertree of the extant ruminants. *Biol Rev Camb Philos Soc.* **80**(2):269–302.
- Herries AIR. 2011. A Chronological Perspective on the Acheulian and Its Transition to the Middle Stone Age in Southern Africa: The Question of the Fauresmith. *Int J Evol Biol.* **2011**:1–25.
- Holmes T. 1980. Locomotor adaptation in the limb skeletons of North American mustelids. PhD thesis, Humboldt State University
- Hotelling H. 1933. Analysis of a complex of statistical variables into principal components. *J Educ Psychol.* **24**:417–441.
- Hotelling H. 1936. Relations Between Two Sets of Variates. *Biometrika.* **28**(3/4):321–377.
- Huffman B. 2020. Ultimate Ungulate. <http://www.ultimateungulate.com/>. Accessed June 2021
- Huiskes R. 2000. If bone is the answer , then what is the question? *J Anat.* **197**:145–156.
- Jenkins KE, Nightingale S, Faith JT, Peppe DJ, Michel LA, Driese SG, McNulty KP, Tryon CA. 2017. Evaluating the potential for tactical hunting in the Middle Stone Age: Insights from a bonebed of the extinct bovid, *Rusingoryx atopocranion*. *J Hum Evol.* **108**:72–91.
- Kingdon J. 2013. *The Kingdon Field Guide to African Mammals*. 2nd ed. London: Bloomsbury.
- Klein RG, Franciscus RG, Steele TE. 2010. Morphometric identification of bovid metapodials to genus and implications for taxon-free habitat reconstruction. *J Archaeol Sci.* **37**(2):389–401.
- Klingenberg CP. 2011. MorphoJ: an integrated software package for geometric morphometrics. *Mol Ecol Resour.* **11**:353–357.
- Konrad-Zuse-Zentrum Berlin Z. 2012. Avizo.
- Kovarovic K, Aiello LC, Cardini A, Lockwood CA. 2011. Discriminant function analyses

in archaeology: Are classification rates too good to be true? *J Archaeol Sci.* **38**(11):3006–3018.

Kovarovic K, Andrews P. 2007. Bovid postcranial ecomorphological survey of the Laetoli paleoenvironment. *J Hum Evol.* **52**(6):663–680.

Kovarovic K, Andrews P, Aiello L. 2002. The palaeoecology of the Upper Ndolanya Beds at Laetoli, Tanzania. *J Hum Evol.* **43**(3):395–418.

Kovarovic K, Faith JT, Jenkins KE, Tryon CA, Peppe DJ. 2021. Ecomorphology and ecology of the grassland specialist, *Rusingoryx atopocranion* (Artiodactyla: Bovidae), from the late Pleistocene of western Kenya. *Quat Res.* **101**:187-204.

Kriegs JO, Churakov G, Kieffmann M, Jordan U. 2006. Retroposed Elements as Archives for the Evolutionary History of Placental Mammals. *PLoS Biol.* **4**(4):e91.

Lele SR, Richtsmeier JT. 2001. *An Invariant Approach to Statistical Analysis of Shapes*. 1st ed. London: Chapman & Hall.

Linnaeus C. 1758. *Systema naturæ per regna tria naturæ, secundum classes, ordines, genera, species, cum characteribus, differentiis, synonymis, locis*. Tomus I. Editio decima, reformata.

Mcbrearty S, Brooks AS. 2000. The revolution that wasn't: A new interpretation of the origin of modern human behavior. *J Hum Evol.* **39**(5):453–563.

Monteiro LR, Abe AS. 1999. Functional and historical determinants of shape in the scapula of Xenarthran mammals: Evolution of a complex morphological structure. *J Morphol.* **241**(3):251–263.

Morgan LE, Renne PR. 2008. Diachronous Dawn of Africa's Middle Stone Age: New 40 Ar/39 Ar ages from the Ethiopian Rift. *Geology.* **36**(12):967–970.

Nery MF, González DJ, Hoffmann FG, Opazo JC. 2012. Resolution of the laurasiatherian phylogeny: Evidence from genomic data. *Mol Phylogenet Evol.* **64**(3):685–689.

Nicholson SE. (1998) Historical fluctuations of Lake Victoria and other Lakes in the Northern Rift valley of East Africa, In: Lehman, JT. (Ed.), *Environmental Change and Response in East African Lakes*. Dordrecht: Kluwer Academic Publishers.

Nishihara H, Maruyama S, Okada N. 2009. Retroposon analysis and recent geological

data suggest near-simultaneous divergence of the three superorders of mammals. PNAS. **1**(23):5235-5240.

Novak RM. 1991. Walkers Mammals of the World 5th Ed Volume 1. Baltimore: Johns Hopkins University Press.

O'Brien HD, Faith JT, Jenkins E, Price G, Tryon CA, Brien HDO, Faith JT, Jenkins KE, Peppe DJ, Plummer TW, et al. 2016. Unexpected Convergent Evolution of Nasal Domes between Pleistocene Bovids and Cretaceous Hadrosaur Dinosaurs Report Unexpected Convergent Evolution of Nasal Domes between Pleistocene Bovids and Cretaceous Hadrosaur Dinosaurs. **26**:503–508.

O'Connor T. 2008. On the differential diagnosis of anthropany in bovinds. Doc Archaeobiologiae. p165–186.

Orme D, Freckleton R, Thomas G, Petzoldt T, Fritz S, Isaac N, Pearse W. 2018. *caper* package.

Owen R. 1848. Description of Teeth and portions of jaws of two extinct Anthracotheroid quadrupeds (*Hyopotamus vectianus* and *Hyopbovinus*) discovered by the Marchioness of Hastings in the Eocene Deposits on the N. W. coast of the Isle of Wight: with an attempt to develop Cuvier's idea of the classification of pachyderms by the number of their toes. Q J Geol Soc London. **IV**(November):103–143.

Pares-Casanova PM, Oosterlinck M. 2012. Relation between Hoof Area and Body Mass in Ungulates Reared under Semi-Extensive Conditions in the Spanish Relation between Hoof Area and Body Mass in Ungulates Reared under Semi-Extensive Conditions in the Spanish Pyrenees. **2**(4):374–379.

Pearson K. 1901. LIII. On lines and planes of closest fit to systems of points in space. London, Edinburgh, Dublin Philos Mag J Sci. **2**(11):559–572.

Pickford M, Thomas H. 1984. An aberrant new bovid (Mammalia) in subrecent deposits from Rusinga Island, Kenya. Proc Koninklke Ned Akad van Wet Ser B Palaeontol Geol Phys Chem. **87**(4):441–452.

Pilgrim GE. 1939. The fossil Bovidae of India. In: Calcutta: Geological Survey of India.

Prasad AB, Allard MW, Comparative N, Program S, Green ED. 2008. Confirming the Phylogeny of Mammals by Use of Large Comparative Sequence Data Sets. Mol. Biol.

Evol. **25**(9):1795-1808

Profico A, Buzi C, Castiglione, Silvia Melchionna M, Piras P, Raia P, Veneziano A. 2021. *Arothron* package.

Raup DM, Stanley SM. 1978. Chapter 8: Adaptation and Functional Morphology. In: Principles of Paleontology. 2nd ed. San Francisco: W. H. Freeman and Company. p. 165–196.

Reilly SM, McElroy EJ, Biknevicus AR. 2007. Posture, gait and the ecological relevance of locomotor costs and energy-saving mechanisms in tetrapods. **110**:271–289.

Revell LJ. 2021. *phytools* package.

Ripley B, Venables B, Bates DM, Hornik K, Gebhardt A, Firth D. 2021. *MASS* package.

Rohlf FJ. 2017. tpsDig232.

Rohlf FJ. 2019. tpsUtil232.

Saulsbury JG. 2020. Permutation tests for comparative data. bioRxiv. p1–25.

Schlager S, Jefferis G, Ian D. 2021. *Morpho* package.

Simpson GG. 1945. The principles of classification and a classification of mammals. Bull Am Museum Nat Hist. **85**:1–350.

Tabachnick BG, Fidell LS. 2007. Using Multivariate Statistics. 5th ed. Boston, MA: Allyn & Bacon.

The R Foundation for Statistical Computing. 2020. R.

Tryon CA, Faith JT, Peppe DJ, Beverly EJ, Blegen N, Blumenthal SA, Chritz KL, Driese SG, Patterson D, Sharp WD. 2016. The Pleistocene prehistory of the Lake Victoria basin. Quat Int. **404**:100–114.

Tryon CA, Faith JT, Peppe DJ, Keegan WF, Keegan KN, Jenkins KH, Nightingale S, Patterson D, Plantinga A Van, Driese S, et al. 2014. Sites on the landscape : Paleoenvironmental context of late Pleistocene archaeological sites from the Lake Victoria basin, equatorial East Africa Inset. Quat Int. **331**:20–30.

Tryon CA, McBrearty S. 2006. Tephrostratigraphy of the Bedded Tuff Member (Kapthurin Formation, Kenya) and the nature of archaeological change in the later middle

Pleistocene. *Quat Res.* **65**(3):492–507.

Tryon CA, Peppe DJ, Tyler Faith J, Van Plantinga A, Nightingale S, Ogondo J, Fox DL. 2012. Late Pleistocene artefacts and fauna from Rusinga and Mfangano islands, Lake Victoria, Kenya. *Azania.* **47**(1):14–38.

Tryon CA, Tyler Faith J, Peppe DJ, Fox DL, McNulty KP, Jenkins K, Dunsworth H, Harcourt-Smith Will W. 2010. The Pleistocene archaeology and environments of the Wasiriya Beds, Rusinga Island, Kenya. *J Hum Evol.* **59**(6):657–671.

Upex B, Dobney K. 2012. More Than Just Mad Cows: Exploring Human-Animal Relationships through Animal Paleopathology. In: Grauer AL (Ed.). *A Companion to Paleopathology*. Hoboken, NJ: Blackwell's Publishing. p191–213.

Wallace AR. 1876. *The geographical distribution of animals*. New York: Harper & Brothers

Wentworth Thompson D. 1961. Chapter VIII: On Form and Mechanical Efficiency. In: Bonner J, editor. *On Growth and Form*. 1961st ed. Cambridge: Cambridge University Press. p. 221–267.

Wickham H, Chang W, Henry L, Line Pedersen T, Takahashi K, Wilke C, Woo K, Hiraoki Y, Dunnington D. 2021. *ggplot2* package.

Zelditch ML, Swiderski DL, Sheets HD, Fink WL. 2004. *Geometric Morphometrics for Biologists: A Primer*. 2nd ed. Elsevier Inc.

Zurano JP, Magalhães FM, Mesquita DO, Costa GC, Asato AE, Silva G, Bidau CJ. 2019. Cetartiodactyla: Updating a time-calibrated molecular phylogeny. *Mol Phylogenet Evol.* **133**(May 2018):256–262.

Appendix I: Preliminary 2D Analyses

Although the aim of this project was to conduct a 3D analysis of distal humerus morphology in bovids, a preliminary 2D study was carried out prior to the full study. This preliminary study provided the opportunity to ‘road-test’ the classification system for the categorical variables, habitat preference and body mass, but also importantly provided training and practice in the basics of landmarking and data analysis in MorphoJ ver. 1.07a (Klingenberg 2011).

A screenshot was taken of each 3D scan available as of January 2021, with the humerus oriented in cranial view. The image files were combined into a .tps file using tpsUtil32 ver. 1.78 (Rohlf 2019), then the resulting .tps file was brought into tpsDig232 ver. 2.31 (Rohlf 2017) for landmarking of the images. The landmarking schema for this analysis (Figure I) was primarily devised to capture the outline shape of the distal humerus in cranial view. The landmark data were imported into MorphoJ for analysis. It should be noted that the set of specimens used in the preliminary 2D landmarking study is smaller than the final data set used in the 3D analysis. This is due to the 2D analysis being undertaken early in the project as training and proof of concept, when many scans had not yet been acquired. Conversely, some specimens are included in the 2D analysis but excluded from the 3D analysis due to not being file types readable by Avizo for 3D landmarking (N.B. all those excluded represent duplicates of species which are still represented in the 3D dataset by other specimens). The full list of 119 specimens included in the 2D analysis can be found in the main text Table II.

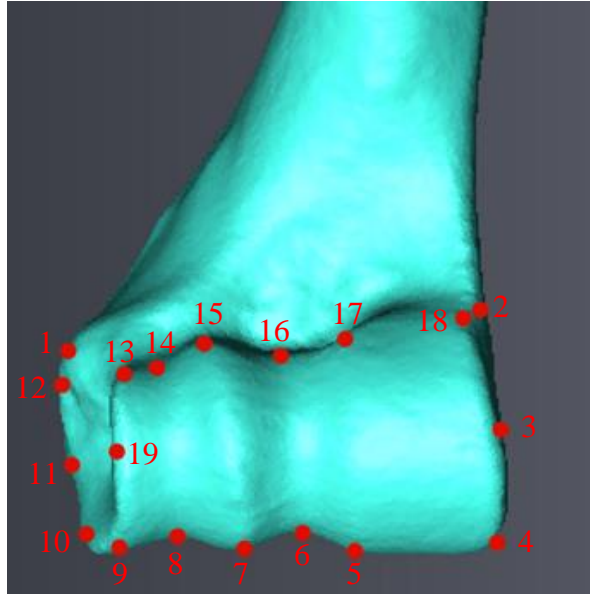


Figure I: 19 landmark schema used for 2D landmarking

Screenshots of *Connochaetes gnou* (MNHN 1976-344) distal humerus in cranial view, landmarked in tpsDig232 following a 19 landmark schema. Landmarks are numbered in red according to the order in which the locus was landmarked. Full descriptions of the landmark locus are given in Table I.

Table I: 19 landmark schema used for 2D landmarking

Landmark number	Landmark type	Description
1	3	Most lateral extent of the lateral epicondyle protuberance
2	Other	Medial edge of the bone horizontally in line with landmark 1
3	Other	Medial edge of trochlea at 50% distance between landmarks 2 and 4
4	1	Disto-medial corner of trochlea
5	2	Disto-lateral corner of medial trochlear ridge
6	2	Distal edge of trochlear groove
7	2	Distal edge of lateral trochlear ridge
8	2	Distal edge of capitular groove
9	1	Disto-lateral corner of capitulum
10	1	Disto-lateral corner of bone
11	Other	Lateral edge of bone at 50% distance between landmarks 10 and 12
12	Other	Lateral edge of bone horizontally in line with proximo-lateral corner of capitulum (landmark 13)
13	1	Proximo-lateral corner of capitulum
14	2	Proximal edge of capitular groove
15	2	Proximal edge of lateral trochlear ridge
16	2	Proximal edge of trochlear groove
17	2	Proximo-lateral corner of medial trochlear ridge
18	1	Proximo-medial corner of medial trochlear ridge
19	Other	Lateral edge of capitulum at 50% distance between landmarks 9 and 13

Providing anatomical placement and type for each landmark used in the 2D preliminary analysis.

Tribe classification follows ultimateungulate.com (Huffman 2020) and references therein. A 6-level classification system was used to classify habitat preference: Open, Light cover, Heavy cover, Forest, Mountain, Swamp. These classification data were compiled from Kingdon (2013), Barr (2014), and Etienne et al. (2020). Body mass estimates were taken from Kingdon (2013) with additional data from Etienne et al. (2020), and categories were established mathematically, such that each category contained approximately the same number of individual specimens. The resulting categories used are 0-50 kg, 50-100 kg, 100-250 kg, 250-350 kg and >350 kg.

Results

In a Principal Components Analysis (PCA) of the 2D Procrustes coordinates from extant bovids, there is no visual separation on any of the first four PCs of any tribe/habitat preference/body mass categories (Figure II shows a visualisation of PC1 and PC2). However, despite this lack of visual clustering, all of the first four PCs have a significant relationship with tribe (Table II), notably with Antilopini lying high on PC1, and Bovini and Caprini lying low on PC1. PC1 and PC2 are also significantly related to habitat preference, but PC2 and PC4 are not. Lastly, all of the first four PCs are significantly related to body mass category. Broadly speaking, mass decreases from the top left (low on PC1, high on PC2) to the bottom right (high on PC1, low on PC2). While there are significant relationships between shape variation and the categorical ecological variables, the PCA is difficult to interpret with reference to only one of the variables. Instead, it appears that the shape variation detected by the analysis is related to the mosaic interactions of phylogenetic affinity, habitat preference and body mass. For this reason, this PCA is not highly informative in understanding *Rusingoryx*, especially as the five *Rusingoryx* specimens are scattered surprisingly widely, especially on the PC2 axis.

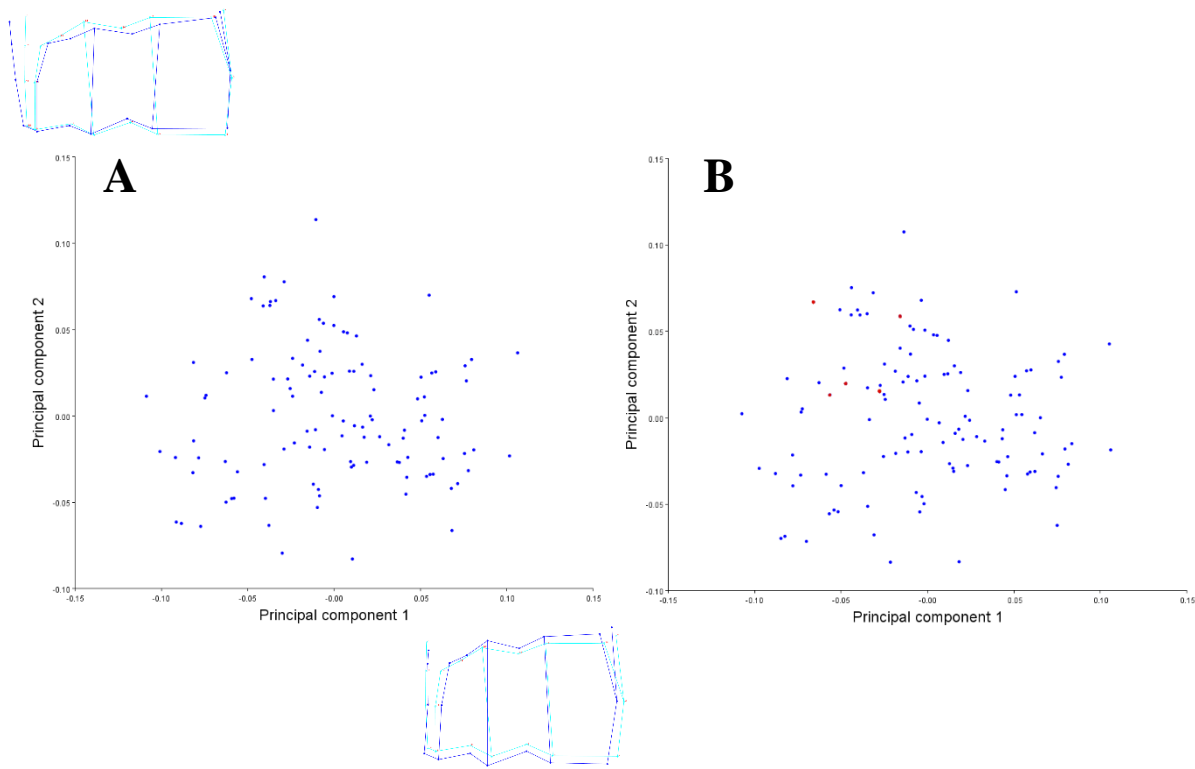


Figure II: Visualization of Principal Components Analysis (PCA) on 2D Procrustes coordinates

Showing the first two principal component axes. A) Extant bovids only, including wireframe visualization of shape change along each axis (light blue representing mean shape and dark blue representing shape transformation); B) Extant bovids and including *Rusingoryx atopocranion* represented by red points. n = 114 extant bovids + 5 *Rusingoryx*.

Table II: Significance of relationships between PCA axes and categorical variables in the extant bovid analysis

	Tribe affinity	Habitat preference	Body mass category
PC1	<2.2E-16	2.18E-06	2.15E-09
PC2	0.00017	0.09415	0.00054
PC3	0.0001	0.0339	0.02971
PC4	0.00033	0.1465	0.00085

Showing p-values for the regression relationship between the PC scores of each of the first four PCs and the three categorical variables (tribe affinity, habitat preference, and body mass category). n = 114 extant bovids.

Canonical Variate Analysis: Tribe

A Canonical Variate Analysis (CVA) of the 2D Procrustes coordinates by Tribe for extant bovids is 94.7% accurate (Figure IIIA). However, there is a lack of visual separation between categories in the first four CVs (the first two are shown in Figure IIIA). For this reason, it is difficult to ascertain associations between the shape changes along each axis and the tribe affinity of the specimen.

Shape variation along the CV1 axis results in a distal humerus which is elongated medio-laterally and compressed proximo-distally, with the trochlear ridges more laterally directed at the proximal edge (the lateral trochlear ridge lying at a more extreme angle than the medial). Variation on the CV2 axis also leads to compression proximo-distally, but not elongation medio-laterally. Additionally, the disto-medial corner of the trochlea protrudes further disto-medially, and the lateral epycondylar protrusion (prominent in *Rusingoryx*), extends out further laterally.

In Figure IIIB, it can be seen that *Rusingoryx* lies closest to the morphospaces of Alcelaphini and Bovini, but according to the Procrustes distances (not shown here), *Rusingoryx* is actually closest to the Bovini in multidimensional space, followed by the Hippotragini and then the Alcelaphini. As *Rusingoryx* has been assigned to the tribe Alcelaphini (Pickford and Thomas 1984), this lack of clear affinity for the tribe is unexpected.

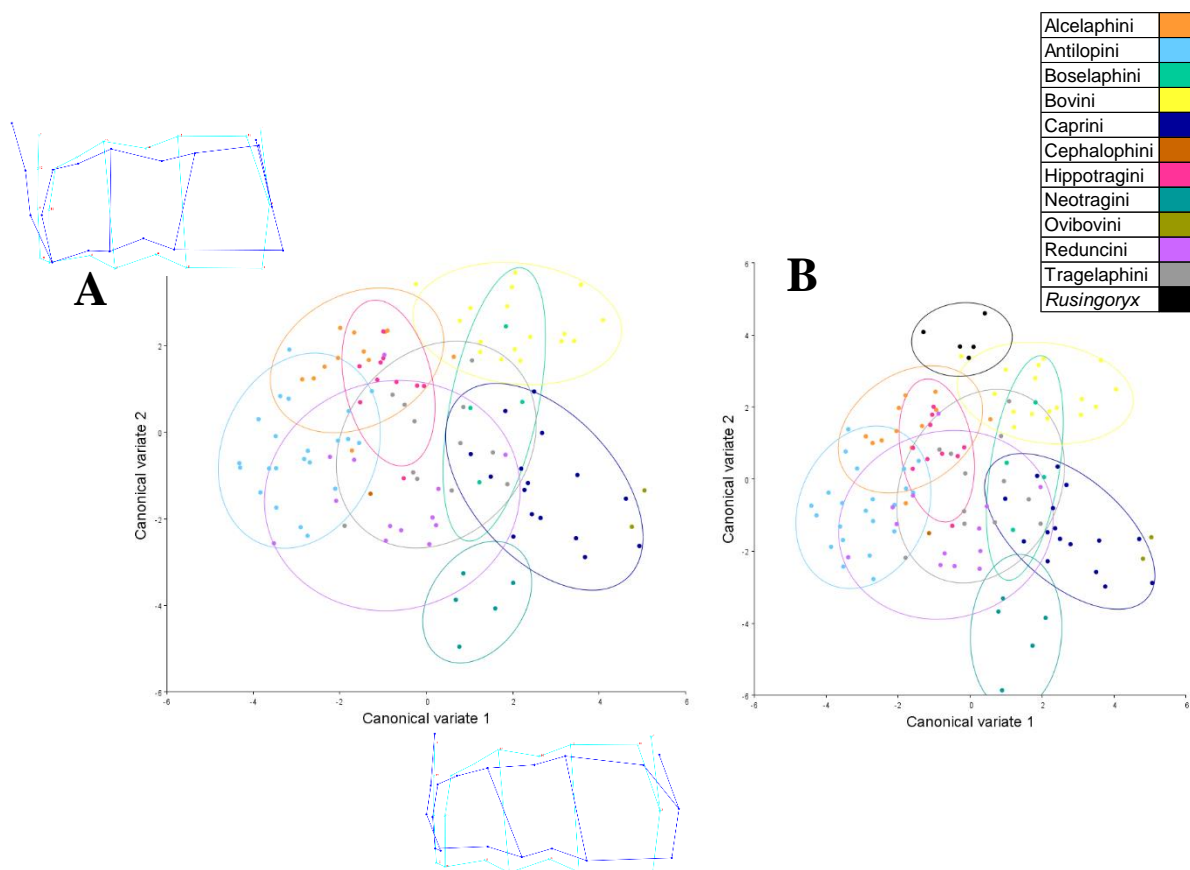


Figure III: Visualization of Canonical Variate Analysis (CVA) on 2D Procrustes coordinates by tribe affinity

Showing the first two canonical variate axes. A) Extant bovids only, including wireframe visualization of shape change along each axis (light blue representing mean shape and dark blue representing shape transformation); B) Extant bovids plus *Rusingoryx atopocranion*. $n = 114$ extant bovids + 5 *Rusingoryx*. Ellipses represent 90% confidence interval.

Canonical Variate Analysis: Habitat Preference

A CVA of the 2D Procrustes coordinates by habitat preference for extant bovids is 85.1% accurate. In a visualisation of the first two CVs (Figure IVA), it can be seen that in the central area of the morphospace all habitat preference category morphospaces overlap and, as such, the location of a point in this space is not informative of its habitat preference group affinity. Moving outwards to the extremes of the CVs, however, there is greater visual separation of the morphospaces, in particular the Mountain category is high on CV1 and low on CV2, and the Open category low on CV1. Shape variation along the CV1 axis results in a distal humerus that is elongated medio-laterally and compressed proximo-distally, with the trochlear ridges more laterally directed at the proximal edge. Along the CV2 axis, however, the shape of the trochlea and capitulum change little, but the lateral epicondylar protrusion (prominent in *Rusingoryx*) extends laterally to a greater extent, and the proximo-medial corner of the trochlea is more laterally positioned.

Visually in Figure IVB, *Rusingoryx* overlaps with the morphospaces of all habitat preference categories except Mountain. According to Procrustes distances, *Rusingoryx* is closest to Heavy cover, followed by Forest. Since *Rusingoryx* has previously been reconstructed as an open habitat-dwelling species (Kovarovic et al. 2021), this is highly unexpected.

It was decided that the Swamp category is uninformative as it contains only two individuals which both represent *Bubalus bubalis*, and there is clear overlap between this category and the Mountain category. For the 3D analysis, a different six-level habitat classification system based on a seven-level system developed for Kovarovic et al. (2021) and based on Kovarovic and Andrews (2007) was used. Kovarovic et al. (2021) utilise multiple habitat classification systems (three-level, four-level and five-level) in their paper, but these systems all exclude a montane category. The seven-level system provides two separate montane categories which differ according to vegetation cover, but for the purposes of this project, the two montane categories were combined.

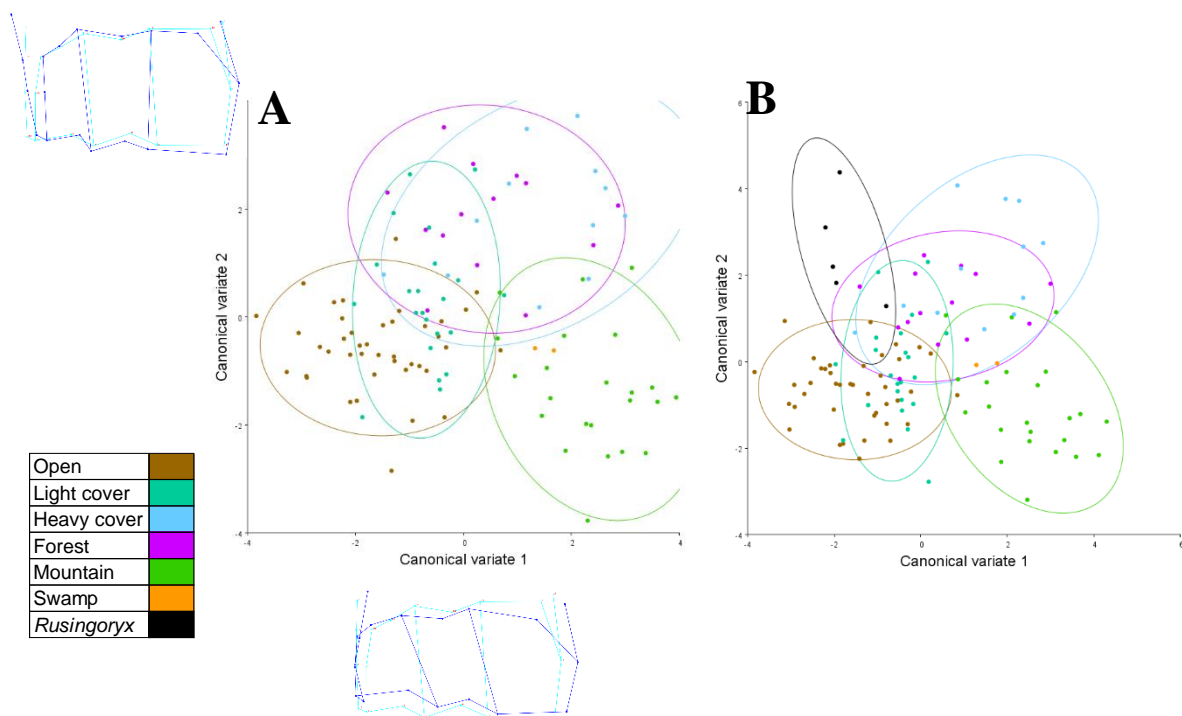


Figure IV: Visualization of Canonical Variate Analysis (CVA) on 2D Procrustes coordinates by habitat preference

Showing the first two canonical variate axes. A) Extant bovids only, including wireframe visualization of shape change along each axis (light blue representing mean shape and dark blue representing shape transformation); B) Extant bovids plus *Rusingoryx atopocranion*. $n = 114$ extant bovids + 5 *Rusingoryx*. Ellipses represent 90% confidence interval.

Canonical Variate Analysis: Body Mass

A CVA of the 2D Procrustes coordinates by body mass category in extant bovids is 86.0% accurate. This is visualised in Figure VA, and it can be seen that the largest mass category (>350 kg) lies at the lowest end of the CV1 axis, and the smallest category lies at the highest end (the opposite arrangement is true for Figure VB including *Rusingoryx*). However, beyond this clear separation, the three other intermediate categories are poorly separated and are not arranged from largest to smallest size along the CV1 axis. On the CV2 axis, there is very poor visual separation of the categories, and this is also the case in CV3 and CV4.

Shape variation along CV1 results in a distal humerus that is proximo-distally elongated and medio-laterally compressed. Variation on the CV2 axis, however, results in proximo-distal ‘pinching’ of the trochlear groove, and lateral protrusion of the proximo-lateral corner of the capitulum.

In the visualisation in Figure VB, *Rusingoryx* overlaps the morphospaces of the highest body mass categories, 250-350 kg and >350 kg. According to Procrustes distances, *Rusingoryx* is closest to the >350 kg, then by the 100-250 kg category, followed closely by the 250-350 kg category. Given that *Rusingoryx* is expected to have a similar body mass to *Connochaetes taurinus* (O’Brien et al. 2016), it would be expected to be most like the 200-250 kg category, so these results are unexpected – though *Rusingoryx* is close to the 100-250 kg category, it is not confidently reconstructed there.

While the majority of the lower mass categories are informative, the largest category, >350 kg, actually contains a large body mass range, with the largest animal in the dataset being *Bubalus bubalis* at 700 kg. Due to this, the fact that *Rusingoryx* appears to lie closest to the >350 kg category animals does not, in fact, provide a great deal of insight into *Rusingoryx*’s actual body mass. As a result, it appears that a mathematically-derived system for body mass classification is ineffective and a biologically-derived system will be used for the 3D analysis. This is based on the allometric scaling of body size and follows Kovarovic et al. (2002) and Andrews et al. (1979). The result is a seven-level system of the following categories: 1-10 kg, 10-45 kg, 45-90 kg, 90-180 kg, 180-360 kg, 360-575 kg, >575 kg.

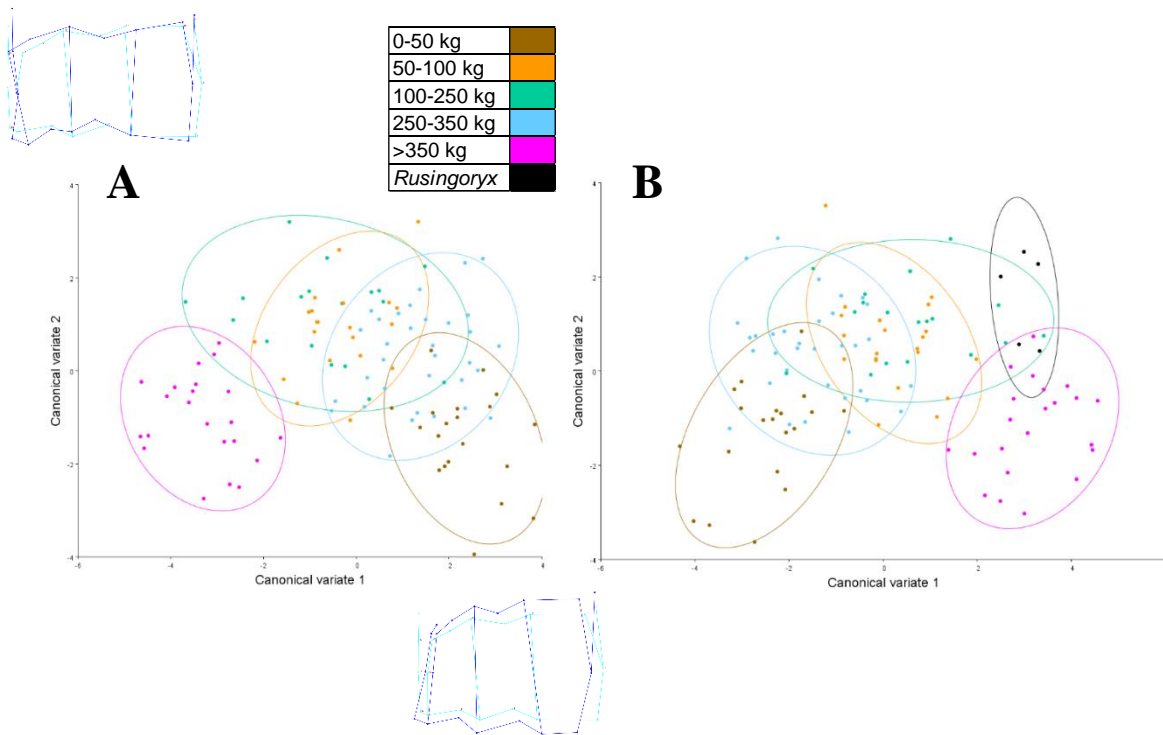


Figure V: Visualization of Canonical Variate Analysis (CVA) on 2D Procrustes coordinates by body mass category

Showing the first two canonical variate axes. A) Extant bovids only, including wireframe visualization of shape change along each axis (light blue representing mean shape and dark blue representing shape transformation); B) Extant bovids plus *Rusingoryx atopocranion*. n = 114 extant bovids + 5 *Rusingoryx*. Ellipses represent 90% confidence interval.

Conclusions & Discussion

Overall, this 2D pilot study was informative in refining categorical variable classifications. It became clear that, in only two dimensions, separation of categories within CVA and PCA morphospaces is poor. Even if this were not the case, a great deal of morphological information is lost in the 2D analysis, as it accounts for only the cranial view of the distal humerus. Notably, variation at the olecranon fossa and in the caudal protrusion of the epicondyles is not represented; nor is the relative angle between the medio-lateral axis of the articular surfaces and the proximo-distal axis of the diaphysis. These results do suggest an association between distal humerus morphology and ecology in bovids, but with unsatisfactory resolution, and *Rusingoryx atopocranion* is not confidently reconstructed into any of the groups it would be expected to have an affinity for. While this could reflect biological actuality, it is not possible to have enough confidence in the affinities suggested by these analyses to conclude that previous assumptions were incorrect. This all supports the necessity of a full 3D analysis in order to adequately capture shape variation and relate it to ecology.

Appendix II – Hoof Area and Pressure Analysis

Inherently, by the physical definition of pressure (pressure = mass/area), hoof area contacting the ground and body mass of the bovid define pressure exerted at the hoof. Hoof area (that is, the keratinous area of the hoof contacting the ground, in cm²) has been found to be related to body mass in a log-log regression for African ungulate species (Cumming and Cumming 2003), and thus, body mass can be used to predict hoof area in these animals via the following equation:

Equation 1: $\log(\text{hoof area in cm}^2) = 0.9888 \times \log(\text{body mass in kg}) - 0.574$

It is also possible to estimate hoof area based on palmar area of the two distal phalanges of a limb in bovids, using the equation:

Equation 2: $\text{Hoof area} = 2.9556 \times \text{phalanx area in cm}^2 - 5.2539$

Hoof area estimates produced via these two equations are not significantly different ($p = 0.499971$), so they can both be considered valid methods of hoof area estimation – one independent of body mass and the other independent of distal phalanx area. This is of great utility in the context of extinct bovids, because it makes it possible to estimate hoof area from material remains (distal phalanx bones), without relying on mass estimates for the animal which, in themselves, rely on estimation and assumption. Using Equation 2, the hoof area of *Rusingoryx* may be estimated from the area of the distal phalanges (mean of 5 individuals = 13.18 cm²):

$$\begin{aligned}\text{Hoof area} &= 2.9556 \times 13.18 - 5.2539 \\ &= \mathbf{33.7 \text{ cm}^2}\end{aligned}$$

Based on other aspects of the skeleton, *Rusingoryx* has been estimated to have had a body mass of 215 kg, equal to that of *Connochaetes taurinus* (its extant relative) (O'Brien et al. 2016). The hoof area of *C. taurinus*, as estimated using Equation 2, is 56.49 cm², approximately 1.7 times larger than that of *Rusingoryx*. It can therefore be expected that pressure exerted at the hooves is approximately 1.7 times higher in *Rusingoryx* than in *C.*

taurinus. To quantify this, hoof pressure is calculated using Equation 3 (Parés-Casanova and Oosterlinck 2012):

Equation 3: Hoof pressure in $\text{kg}/\text{cm}^2 = \text{Body mass per hoof}/\text{Hoof area}$

$$\Rightarrow \text{Hoof pressure in } C. \text{ taurinus} = \mathbf{0.952 \text{ kg}/\text{cm}^2}$$

$$\Rightarrow \text{Hoof pressure in } Rusingoryx = \mathbf{1.595 \text{ kg}/\text{cm}^2}$$

Unfortunately, Parés-Casanova and Oosterlinck's equation relies on acquiring an estimate of body mass per hoof by dividing the overall body mass by four when, in reality, body mass is not necessarily distributed equally across the four hooves in ungulates. As a result, the estimates of hoof area obtained via this method may not reflect true values of pressure at the hoof, but are, nevertheless, useful for interspecies comparison. Not only is the estimate of hoof pressure for *Rusingoryx* high in comparison to *C. taurinus*, it is far higher than the values obtained for any bovid in this dataset (for which estimates of distal phalanx area were possible in order to estimate hoof area using Equation 2). Across all the extant animals, hoof pressure does not exceed $1 \text{ kg}/\text{cm}^2$.

Rusingoryx has the distal phalanges (and by extension, the hoof area) of a much smaller bovid (being most similar to the 92.5 kg *Addax nasomaculatus*), while having a body size implying a mass closer to *C. taurinus* at 215 kg. This may explain *Rusingoryx* association with the largest two body mass categories in 3D GMM analyses – with the distal end of the limb decreased in size, muscle mass must concentrate more proximal to the body. In essence, in order to have the hooves of a much smaller animal, *Rusingoryx* must have the upper forelimbs of a much larger animal, and its distal humerus morphology reflects this muscular adaptation.

Appendix III - 3D Landmarking Repeatability Testing

In order to establish the repeatability of each proposed landmark (the clarity of the definition, the ability to accurately select the same locus successively by eye, etc.), as well as the effect of human error, a series of repeatability tests were carried out. The null hypothesis of all trials is that all landmarks have 100% repeatability accuracy.

Trial 1

A proposed 36 landmark schema was used (Figure VI). A single specimen of *Damaliscus lunatus* (NMNH 163170) was landmarked in Avizo ten times successively in a single sitting. *D. lunatus* was selected because the schema was designed on a specimen of *Connochaetes gnou*, and *D. lunatus* is in the same tribe, Alcelaphini, as *C. gnou*, but is not its closest relative. The rationale is that if there are significant issues with the proposed landmarks when applied even to closely related animals, an overhaul may be necessary.

Landmarking and Generalized Procrustes Analysis methods are as in the Materials & Methods section of the main text.

The Procrustes coordinates of each successive landmarking attempt were extracted from MorphoJ. For each landmark, the coefficient of variation was calculated: that is, for the x, y and z, components the mean and standard deviation across all ten attempts was calculated, then coefficient of variation was calculated as standard deviation/mean x 100, and a mean coefficient of variation across the three components of each landmark was then calculated. The majority of landmarks did not have a coefficient of variation exceeding 2%, but those which did are considered for exclusion (Table III). Thus, seven landmarks were considered for exclusion – 28, 29, 30, 31, 32, 33 and 36. Landmark 3 had the highest coefficient of variation at 6.62%.

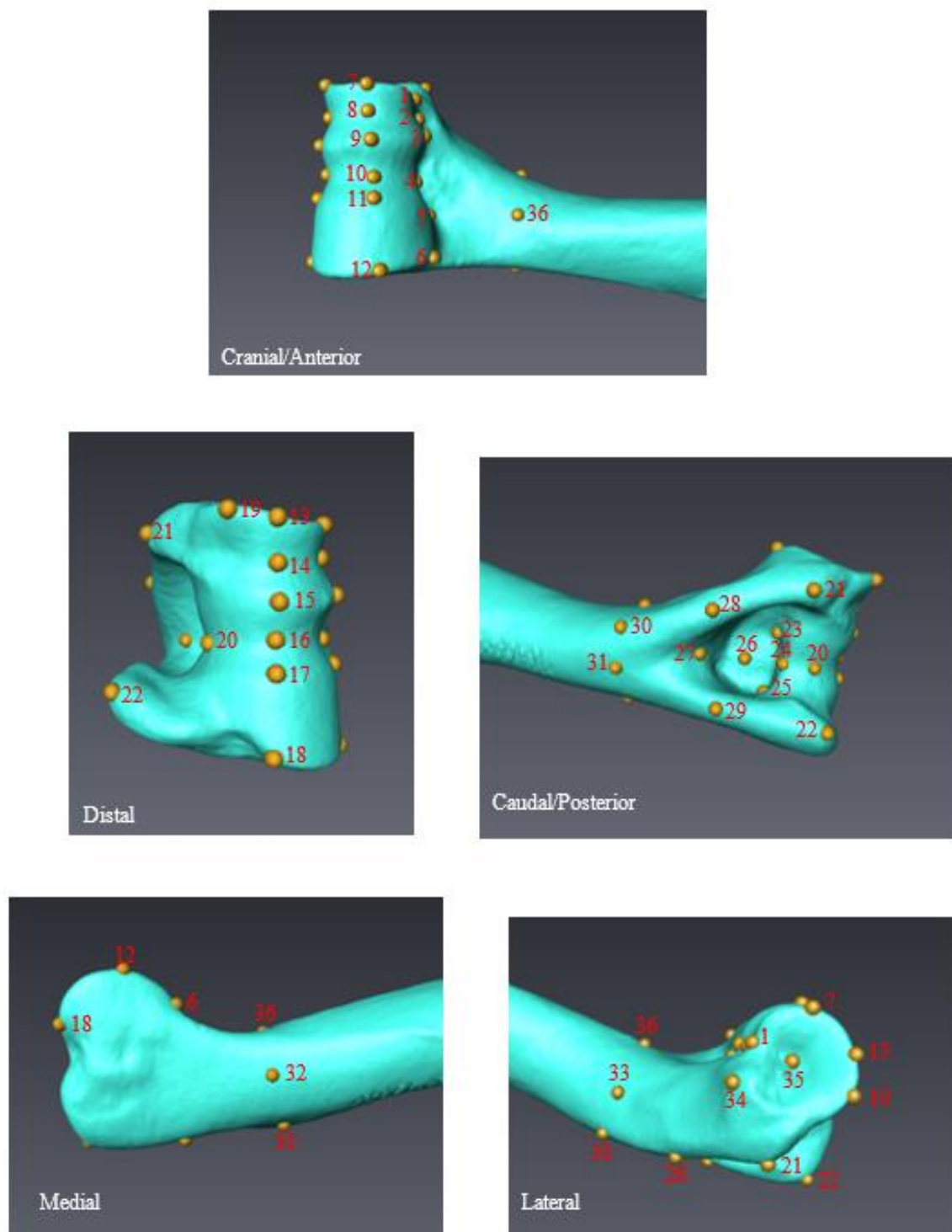


Figure VI: 36 landmark schema used in Trial 1 and Trial 3

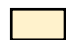
Screenshots of *Connochaetes gnou* (MNHN 1976-344) landmarked in Avizo following a 36 landmark schema. Landmarks are numbered in red according to the order in which the locus was landmarked.


Landmark	Coefficient of variation
1	0.35
2	0.39
3	0.51
4	1.05
5	0.99
6	1.55
7	0.35
8	0.53
9	0.46
10	0.67
11	0.68
12	1.39
13	0.40
14	0.66
15	0.51
16	0.68
17	0.70
18	1.07
19	0.27
20	0.49
21	0.54
22	0.54
23	0.72
24	0.78
25	0.56
26	1.35
27	0.58
28	3.21
29	4.29
30	2.26
31	5.44
32	5.92
33	2.66
34	0.62
35	0.52
36	6.62

Table III: Coefficients of variation of landmarks in Trial 1

Coefficient of variation = (standard deviation/mean) x 100

The coefficient of variation listed here represents the mean coefficient of variation calculated across the three coordinates of each landmark.

 Coefficient of variation = 1-2%

 Coefficient of variation >2%

In addition, a Principal Components Analysis (PCA) was carried out on the Procrustes coordinates. A visualization of the result can be seen in Figure VII. It can be seen that the greatest variation between attempts is represented on PC1 (this axis accounts for 53.52% of variation in the data). PC1 is dominated by landmarks 28, 29 and 32. PC2 accounts for 14.69% of variation in the data, and is dominated by landmarks 20, 22, 26 and 33. As a result, landmarks 20, 22, 26, 28, 29, 32 and 33 were considered for exclusion.

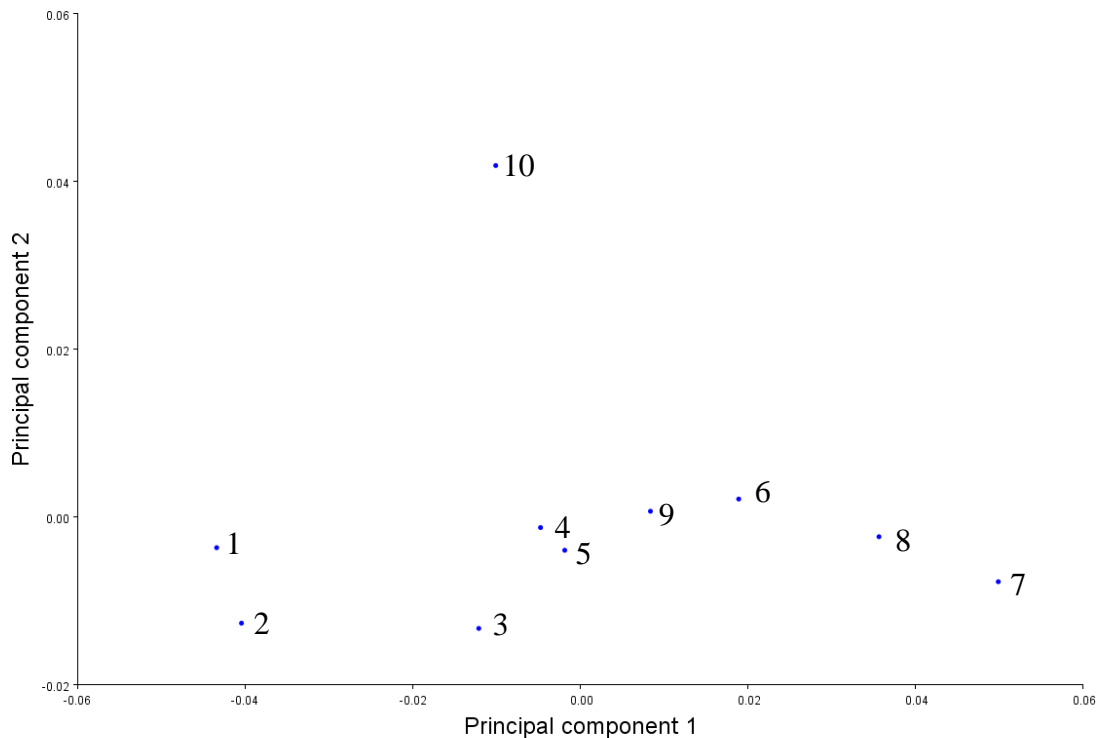


Figure VII: Principal Components Analysis (PCA) visualization of Trial 1 data
Showing results of 10 successive landmarking attempts on *Damaliscus lunatus* specimen (NMNH 163170) using the 36 landmark schema. Attempts are numbered 1-10 in the order they were carried out.

Based on these results, two exclusion variations were trialed – one based on landmark coefficients of variation and one based on PCA loadings. Firstly, based on coefficients of variation, landmarks 28, 29, 30, 31, 32, 33 and 36 were excluded, and the resulting PCA can be seen in Figure VIIIA. What can be seen is that the data show overall less variation, with the range of both PC axes being halved in comparison to the PCA in Figure VII with no exclusions. Secondly, based on the loadings of that first PCA, landmarks 20, 22, 26, 28,

29, 32 and 33 were excluded, and the same reduction in axis range can be seen in a PCA of these data as compared to the PCA with no exclusions (Figure VIIIB).

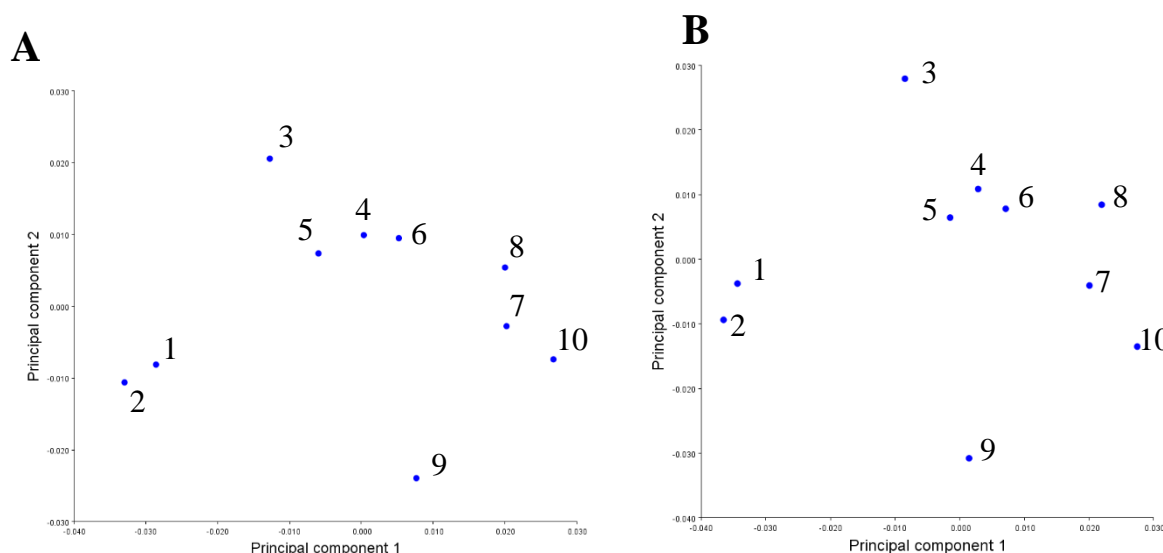


Figure VIII: Principal Components Analysis (PCA) visualization of Trial 1 data following adjustment

A) Results when landmark set is adjusted according to coefficient of variation results – removal of landmarks 28, 29, 30, 31, 32, 33 and 36; B) results when landmark set is adjusted according to Figure VII PCA results – removal of landmarks 20, 22, 26, 28, 29, 32 and 33.

Time taken to landmark each successive attempt (in minutes) generally decreased over time (Figure IXA), but not significantly ($p = 0.07096$), and peaked again at attempt 10. On average, it took 3.6 mins to landmark the specimen, with attempt 9 being fastest (1 min) and attempt 6 taking the longest (6 mins). Coefficient of variation does not appear to be significantly related to time take for the attempt (Figure IXB, $p = 0.30076$), as the coefficient of variation is not significantly related to increasing attempt number (Figure IXC, $p = 0.34659$).

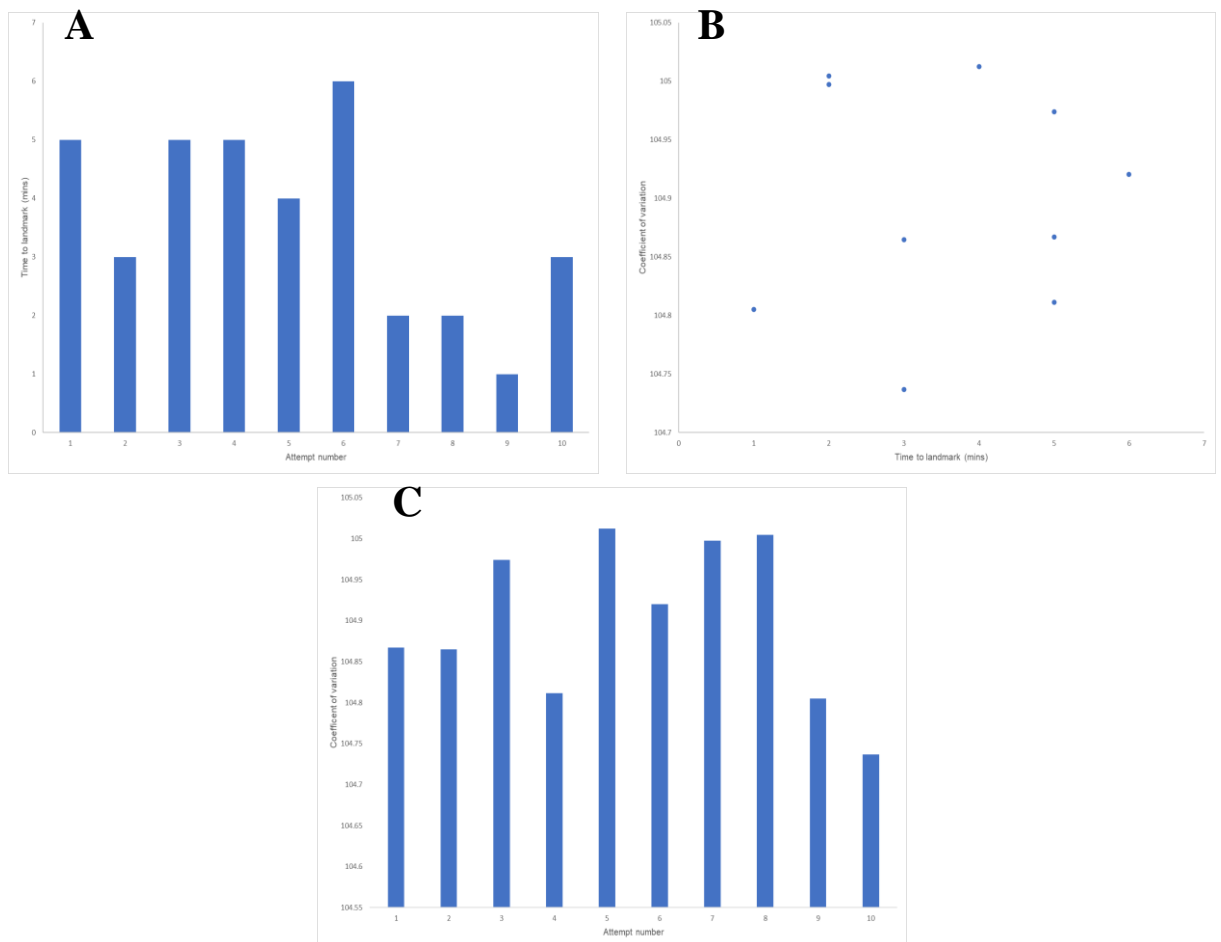


Figure IX: Results relating to human error in landmarking

A) Bar chart of time taken (in minutes) to landmark the specimen across successive attempts; B) scatter plot of mean coefficient of variation of the attempt against time taken to landmark the specimen (mins); C) bar chart of coefficient of variation across successive landmarking attempts.

When successive attempts are directly compared for variation (e.g. comparing the mean coordinated value of attempts 1 and 2), it would be expected under the null hypothesis that there is no difference. However, it can be seen in Figure X that the difference between successive attempts begins high with a difference of 0.989775 between attempts 1 and 2, and generally decreases across successive attempts to the lowest difference being between attempts 7 and 8 at 0.44921. The variation between successive attempts then increases again for attempts 8-10. This suggests that no more than 8 specimens should be landmarked in one sitting as, beyond this, fatigue begins to set in and affect the accuracy of the landmarking. This number may be increased with increased landmarking experience.

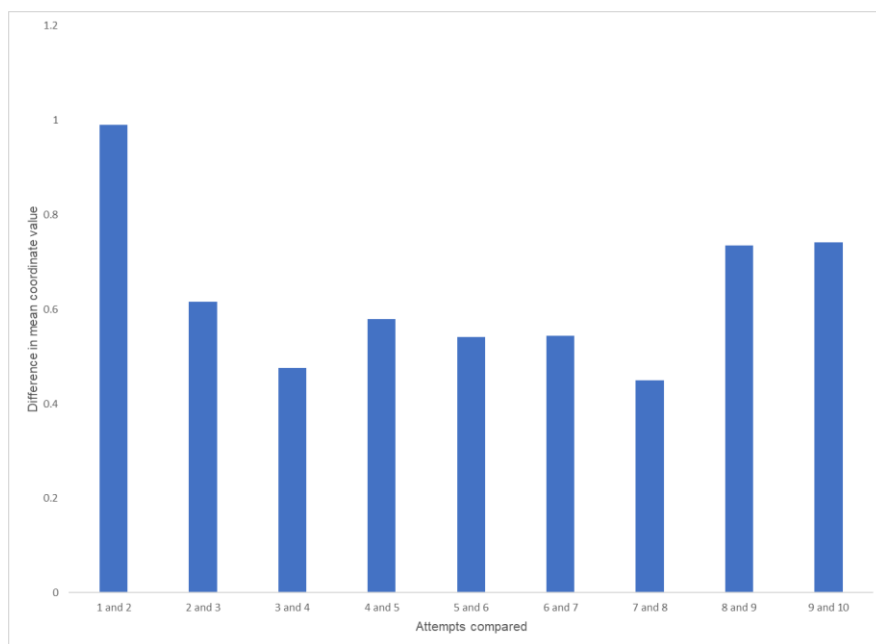


Figure X: Variation between successive landmarking attempts
Bar chart showing the difference in mean coordinate value between successive landmarking attempts.

Trial 2

Based on the results of Trial 1 (and to test removing diaphysis landmarks entirely), the trial was repeated on the same specimen of *Damaliscus lunatus*, excluding landmarks 20, 28, 29, 30, 31, 32, 33 and 36, resulting in the 28 landmark schema shown in Figure XI.

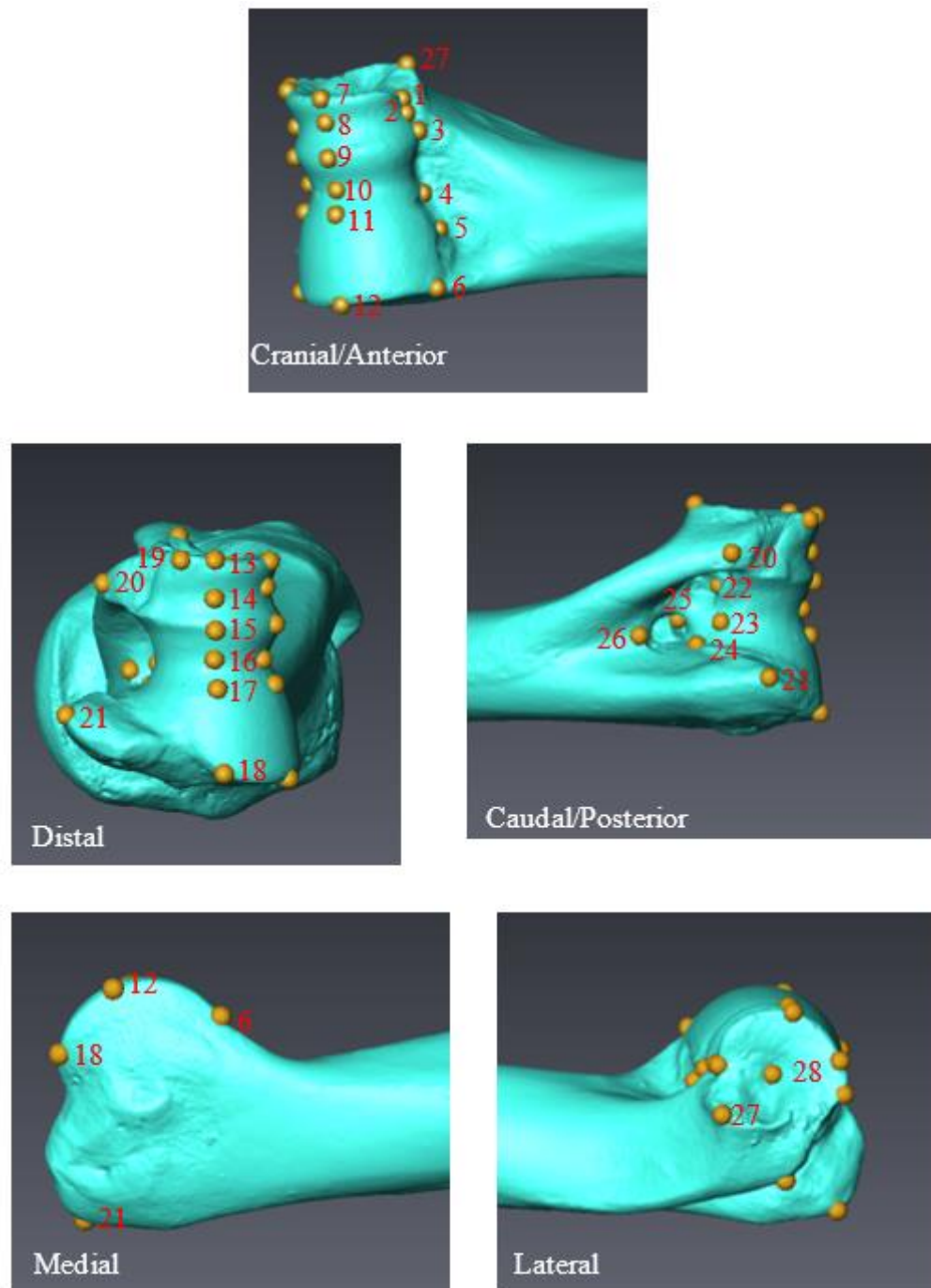


Figure XI: 28 landmark schema used in Trial 2

Screenshots of *Damaliscus lunatus* (NMNH 163170) landmarked in Avizo following a 28 landmark schema. Landmarks are numbered in red according to the order in which the locus was landmarked.

As can be seen in Table IV, in this new landmark schema there are no landmarks with a coefficient of variation exceeding 1.15%.

Landmark	Coefficient of variation
1	0.344873
2	0.375027
3	0.494795
4	1.149401
5	0.979508
6	0.468073
7	0.52723
8	0.690877
9	0.651177
10	0.679912
11	0.968684
12	1.072495
13	0.209927
14	0.297835
15	0.334128
16	0.350445
17	0.474656
18	0.272648
19	0.297264
20	0.550349
21	0.402738
22	0.491818
23	0.876243
24	0.586867
25	0.692801
26	0.502535
27	0.472657
28	0.331202

Table IV: Coefficients of variation of landmarks in Trial 2

Coefficient of variation = (standard deviation/mean) x 100.

The coefficient of variation listed here represents the mean coefficient of variation calculated across the three coordinates of each landmark.



Coefficient of variation = 1-2%

A PCA of these data (Figure XII) shows relatively low variability overall, as evidenced by the scales of the x and y axes. The landmarks most responsible for this variation are 4, 11 and 12.

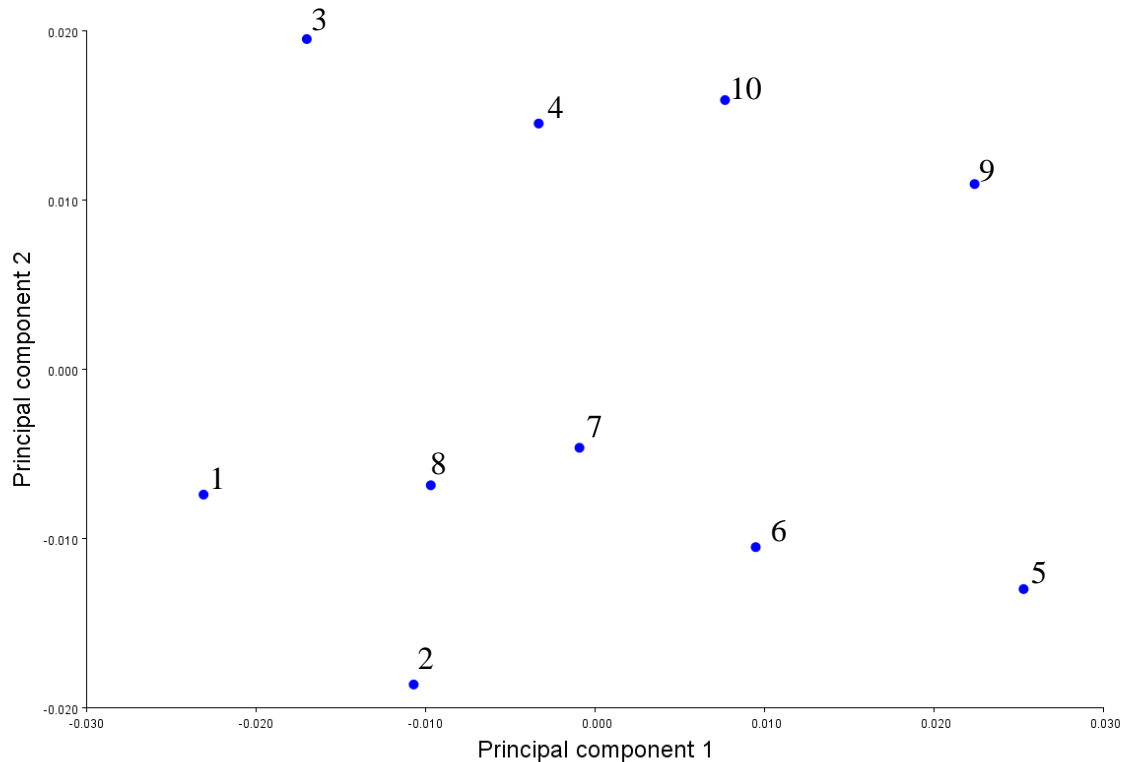


Figure XII: Principal Components Analysis (PCA) visualization of Trial 2 data
Showing results of 10 successive landmarking attempts on *Damaliscus lunatus* specimen (NMNH 163170) using the 28 landmark schema. Attempts are numbered 1-10 in the order they were carried out.

The mean time taken to landmark the specimen in this trail was 2 mins, a significant decrease from Trial 1 ($p = 0.005336$), and time taken to landmark the specimen generally decreased over successive attempts, though not significantly ($p = 0.06357$) (Figure XIII A). The difference between successive attempts decreases from the first attempt to reach its lowest between attempt 5 and 6, before increasing with subsequent attempts (Figure XIII B). This reinforces the previously suggested notion that ten is too many attempts to undertake successively, and shows that this is the case regardless of time taken to complete the attempt. Additionally, the coefficient of variation is lowest for attempt 5, and then increases steadily with subsequent attempts (Figure XIII C). Overall, the coefficient of variation is not significantly related to time taken to landmark the specimen ($p = 0.35129$).

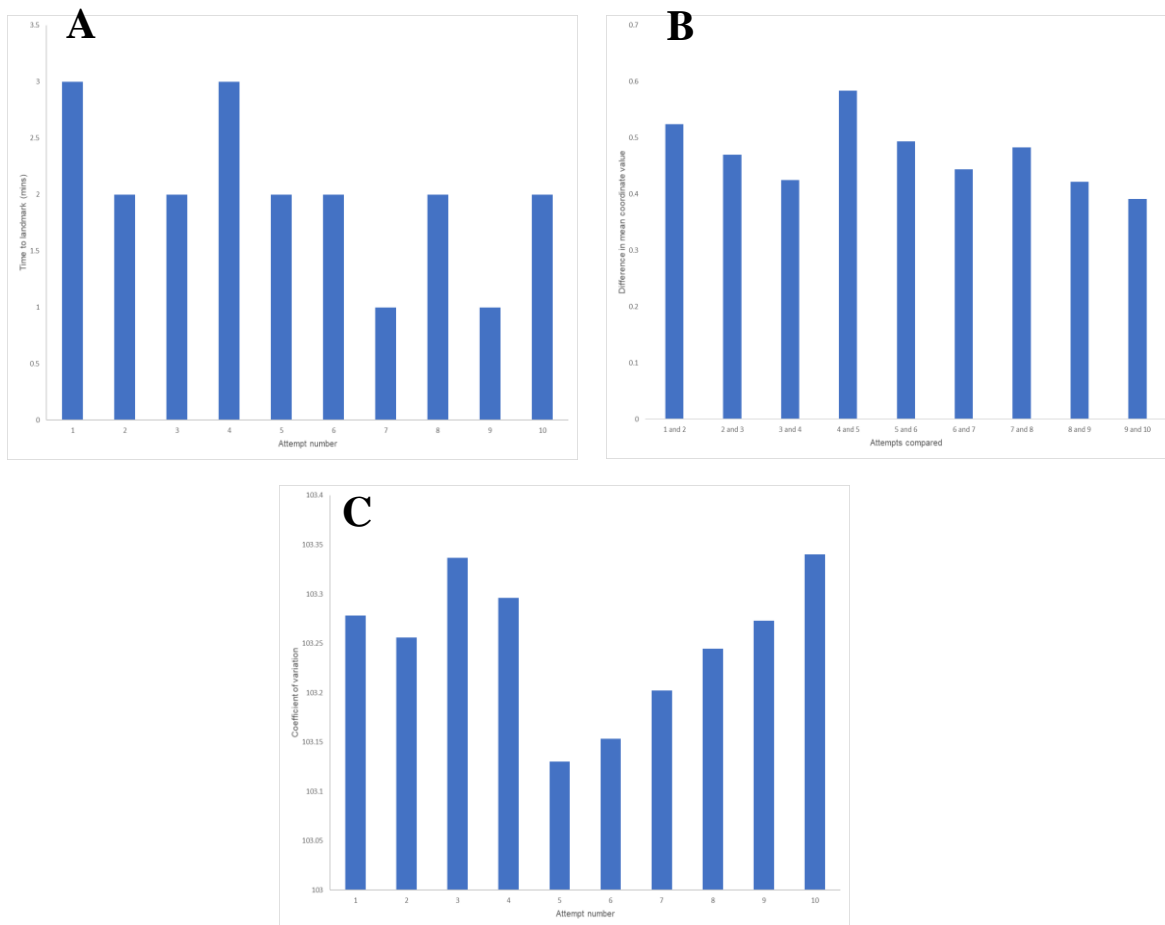


Figure XIII: Results relating to human error in landmarking

A) Bar chart of time taken (in minutes) to landmark the specimen across successive attempts; B) bar chart showing the difference in mean coordinate value between successive landmarking attempts; C) bar chart of coefficient of variation across successive landmarking attempts.

Trial 3

Using the 36 landmark schema in Figure VI, three different specimens were landmarked three times each - *Hippotragus equinus* (MNHN 1969-167 and MNHN 1995-147), and *Hippotragus niger* (BERLIN SSN). Hippotragini were selected for this trial due to both their relative phylogenetic closeness and overall distal humerus morphological similarity to the schema specimen (*C. gnou*).

In a PCA visualisation (Figure XIV), there is overlap between the two *H. equinus* specimens. Given that they are the same species and, therefore, expected to be highly similar, but it can be seen that the overlap is actually due to extensive variation within the three attempts of each specimen. This is problematic as it means error in the landmarking process may lead to specimens being indistinguishable when they would otherwise form distinct morphospaces. Following from Trial 1, two variations of correction were tested – the removal of landmarks with coefficients of variation >2% in Trial 1 (28, 29, 31, 32, 33 and 36), and the removal of 5 landmarks most responsible for variation in Trial 1 PCA (20, 22, 28, 29 and 32).

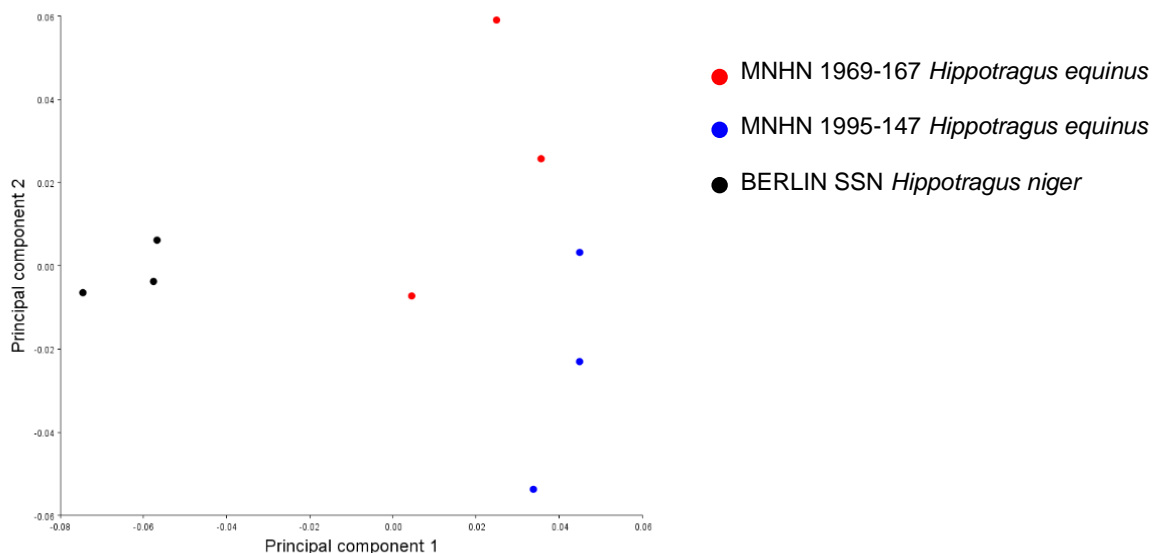


Figure XIV: Principal Components Analysis (PCA) visualization of Trial 3 data
Showing results of three successive landmarking attempts on each of three specimens - *Hippotragus equinus* (MNHN 1969-167 and MNHN 1995-147), and *Hippotragus niger* (BERLIN SSN).

The result of both of these methods is full separation of the three specimens in a visualization of PC2 against PC1 (Figure XV). The minimum number of landmarks that can be excluded based on these results to produce successful and representative separation between specimens is five, these being landmarks 20, 22, 28, 29 and 32. The majority of these can be excluded with little functional loss – they capture some aspects of the object outline but are poorly defined and not related to a specific anatomical marker – however, landmark 22 captures the most postero-distal projection of the medial epicondyle and is anatomically relevant. Excluding the other landmarks while retaining landmark 22 results in poor morphospace separation (not shown). Rather than excluding it or retaining it as is, this landmark needed to be better defined.

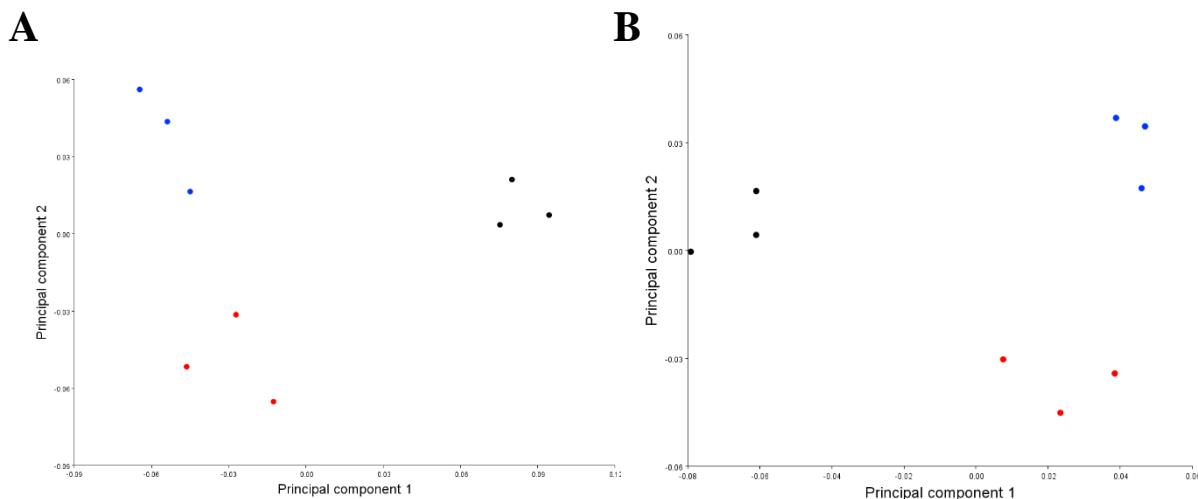


Figure XV: Principal Components Analysis (PCA) visualization of Trial 3 data following adjustment

A) Results when landmark set is adjusted according to coefficient of variation results from Trial 1 – removal of landmarks 28, 29, 31, 32, 33 and 36; B) results when landmark set is adjusted according to Trial 1 PCA results – removal of landmarks 20, 22, 28, 29 and 32. Red = *Hippotragus equinus* MNHN 1969-167; Blue = *Hippotragus equinus* MNHN 1995-147; Black = *Hippotragus niger* BERLIN SSN.

Landmark 32 cannot be excluded without losing information on the diaphysis, so either all diaphysis landmarks should be included or all excluded. Based on Trial 1 coefficient of variation results, they should be excluded, but this would risk losing potentially highly informative information about the angle of the diaphysis relative to the medio-lateral axis of the distal articulation.

Trial 4

The 28 landmark schema from Trial 2 was used, with the addition of better-defined landmarks to represent the diaphysis. The resulting 31 landmark schema is shown in Figure XVI.

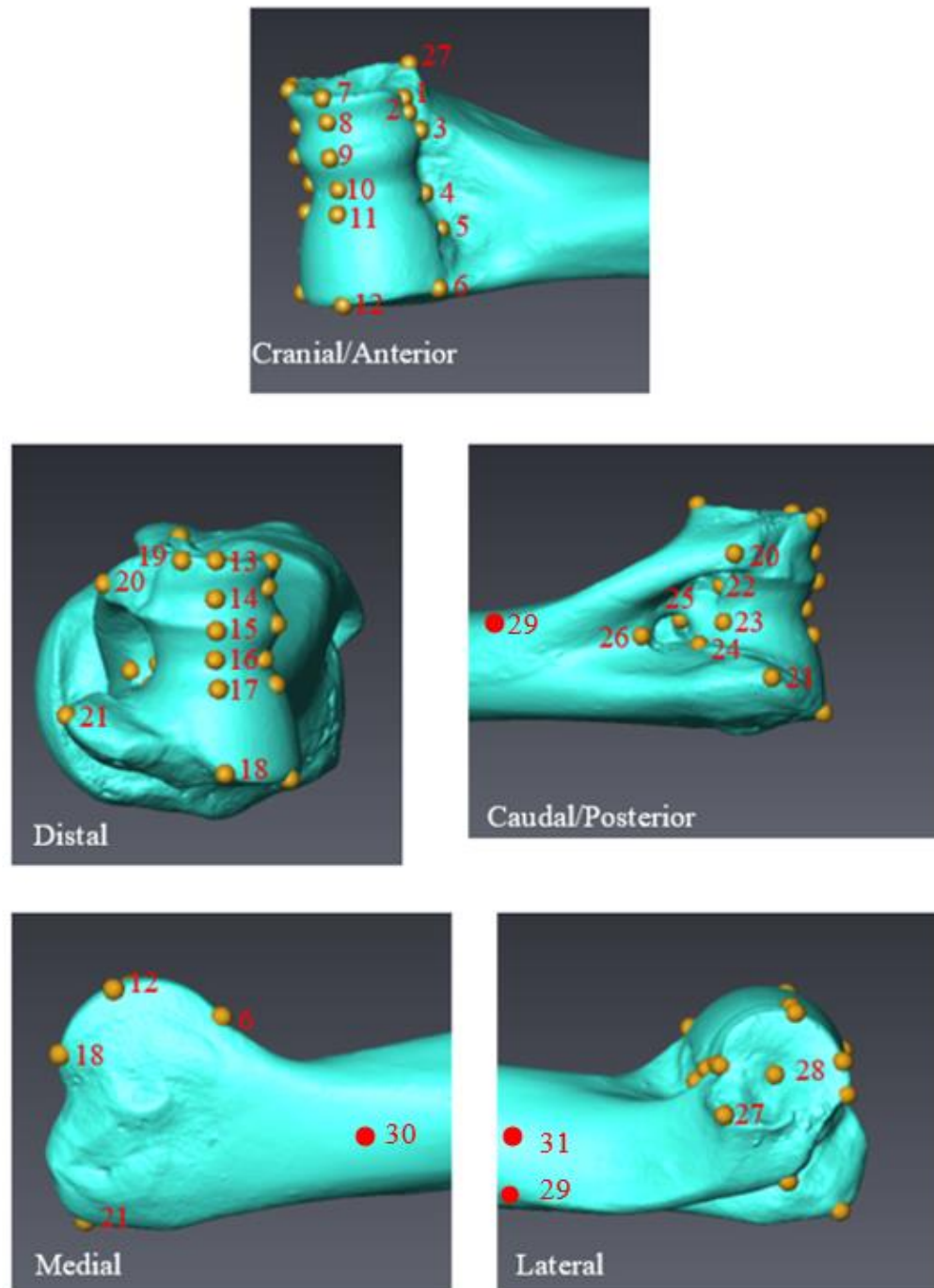


Figure XVI: 31 landmark schema used in Trial 4

Screenshots of *Damaliscus lunatus* (NMNH 163170) landmarked in Avizo following a 31 landmark schema – as the 28 landmark schema used in Trial 2 with the addition of 3 landmarks shown in red. Landmarks are numbered in red according to the order in which the locus was landmarked.


While landmarks 29 and 31 have coefficients of variation below 2%, landmark 30 has a coefficient of variation of 6.66% and, therefore, must be excluded (Table V). The removal of this landmark is not overly problematic as landmarks 29 and 31 alone can adequately represent the relative angle of the distal articulation and diaphysis, while also capturing information about the height of the lateral epicondylar crest.


Landmark	Coefficient of variation
1	0.38245
2	0.368243
3	0.308951
4	0.645995
5	1.901337
6	0.552902
7	0.659638
8	0.664112
9	0.662636
10	0.642377
11	0.776854
12	0.996835
13	0.738686
14	0.520344
15	0.503559
16	0.455945
17	0.492211
18	0.604717
19	0.093346
20	0.419525
21	0.215199
22	0.748108
23	0.419704
24	0.545812
25	0.542948
26	0.370594
27	0.423118
28	0.379776
29	1.369209
30	6.66092
31	1.999237

Table V: Coefficients of variation of landmarks in Trial 4

Coefficient of variation = (standard deviation/mean) x 100.

The coefficient of variation listed here represents the mean coefficient of variation calculated across the three coordinates of each landmark.

 Coefficient of variation = 1-2%

 Coefficient of variation >2%

Trial 5

Based on the previous four trials, a 30 landmark schema (Figure XVII) was established which was shown to be adequately accurate and repeatable for a subset of specimens that were phylogenetically and morphologically similar. The final trial seeks to test its effectiveness across more diverse species. Five different specimens, varying in phylogenetic affinity, habitat preference and body mass (*Damaliscus lunatus* NMNH 163170, *Bubalus bubalis* MNHN 1857-19, *Oreotragus oreotragus* MNHN 2007-1388, *Taurotragus derbianus* NMNH 164646, and *Hemitragus jemlahicus* MNHN 1972-133) were landmarked ten times successively each, using the new 30 landmark schema.

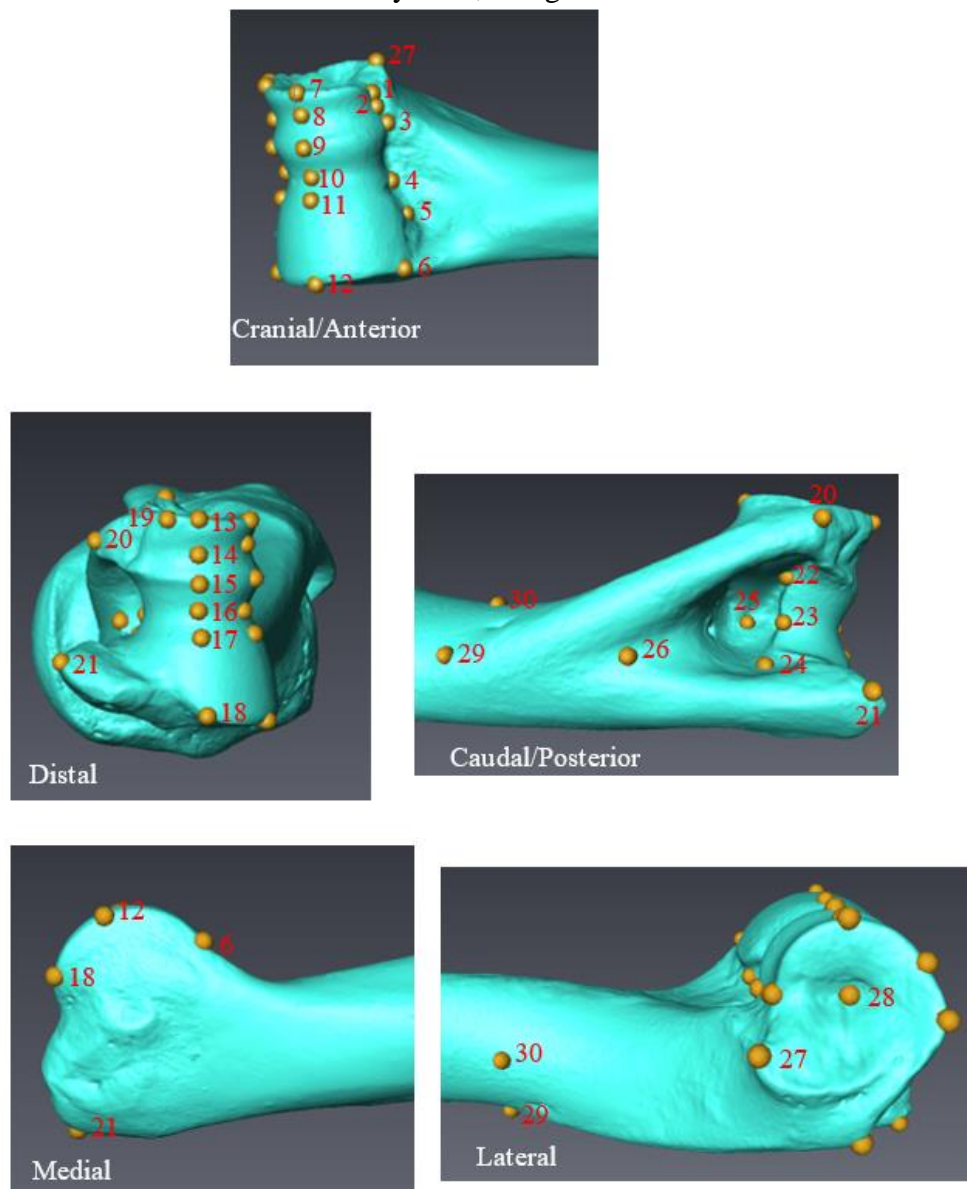


Figure XVII: 30 landmark schema used in Trial 5

Screenshots of *Damaliscus lunatus* (NMNH 163170) landmarked in Avizo following a 30 landmark schema. Landmarks are numbered in red according to the order in which the locus was landmarked.

The coefficients of variation do frequently exceed 2%, reaching as high as 24.19% for landmark 6 in *Hemitragus jemlahicus* (Table VI), but the coefficient of variation for a given landmark is very inconsistent across the species. What can be seen in Figure XVIII, is that this appears to be related to centroid size of the scan, with larger scans having a lower coefficient of variation (this is not necessarily directly related to size of the physical specimen, but reflects differences in equipment used to produce the scans). This reflects the difficulty of accurately identifying a locus with a mouse click on smaller scans.

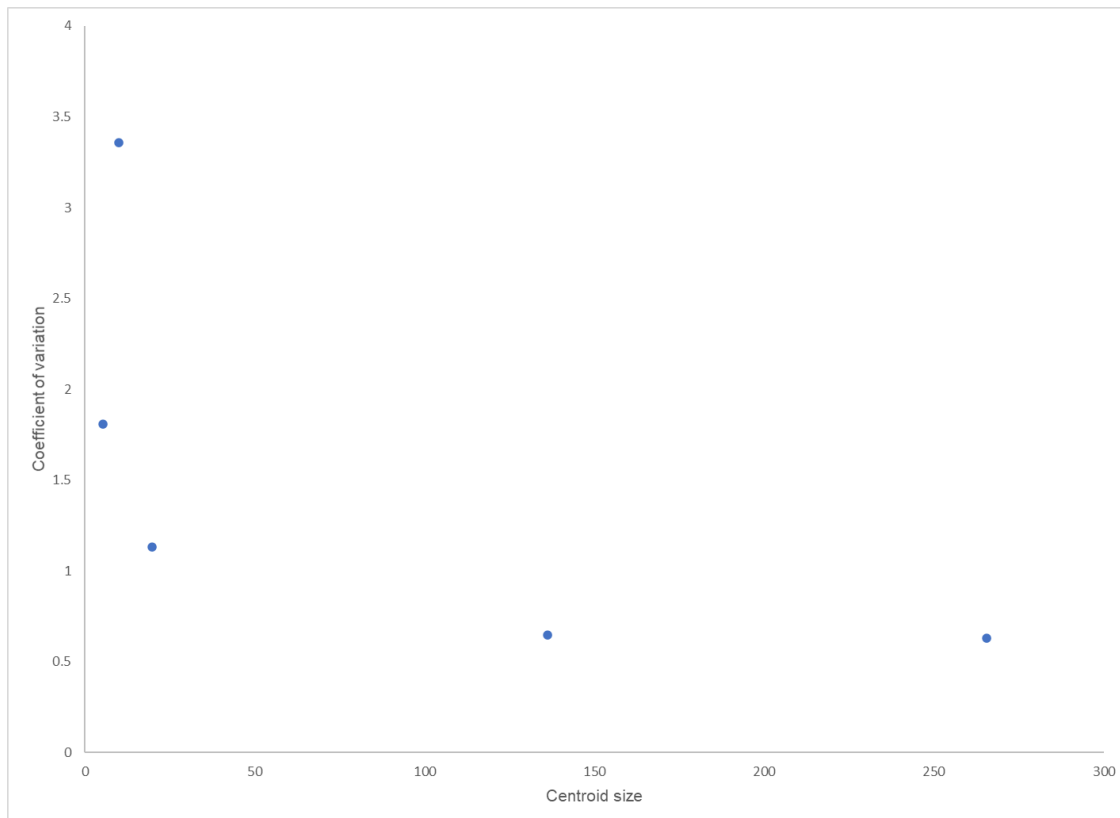


Figure XVIII: Relationship between coefficient of variation and scan centroid size


Scatter plot showing mean coefficient of variation of a specimen against the centroid size of that specimen's scan (as determined by MorphoJ).


Table VI: Coefficients of variation of landmarks in Trial 5


Coefficient of variation = (standard deviation/mean) x 100.

The coefficient of variation listed here represents the mean coefficient of variation calculated across the three coordinates of each landmark.

Landmark	Mean coefficient of variation					Mean
	<i>Bubalus</i>	<i>Damaliscus</i>	<i>Hemitragus</i>	<i>Oreotragus</i>	<i>Taurotragus</i>	
1	0.261597082	0.382450089	0.829261456	0.653447601	0.309699714	0.487291
2	0.25295009	0.368243168	0.668875337	0.904204073	0.136475006	0.46615
3	0.390123789	0.308951277	1.106180573	1.591140403	0.156375623	0.710554
4	1.287975108	0.645995074	1.625314474	0.684287998	0.596148716	0.967944
5	0.526878495	1.90133717	3.913902281	1.799140224	0.958872393	1.820026
6	0.057090313	0.552902481	24.19220801	0.909031157	0.190713631	5.180389
7	0.168576841	0.659638413	0.455694919	0.557842955	0.558553668	0.480061
8	0.338596005	0.664112453	0.607427688	0.731159932	0.616613509	0.591582
9	0.228369328	0.662636065	0.614801426	0.827016243	0.756085682	0.617782
10	0.187972203	0.642376833	1.219587118	0.845033906	0.70626263	0.720247
11	0.534028941	0.776854071	3.910715143	1.035001497	0.887755804	1.428871
12	0.290259488	0.996834521	1.50804398	1.078390055	0.99315668	0.973337
13	0.46827976	0.738686458	0.819985343	1.176828318	0.283955922	0.697547
14	0.72922736	0.520343887	1.071461886	1.201186171	0.299997381	0.764443
15	0.631971284	0.503559292	1.156156386	1.336886571	0.318048843	0.789324
16	0.852947826	0.455944596	3.4392576	1.04397511	0.326893831	1.223804
17	1.09542073	0.492211367	5.00958725	1.445344452	0.344271122	1.677367

 Coefficient of variation = 1-2%

 Coefficient of variation >2%

 Coefficient of variation >10%

18	1.372051803	0.60471747	0.101084637	1.236290896	0.283912444	0.719611
19	2.144819726	0.09334572	1.230067165	1.341571985	0.113257769	0.984612
20	5.232004081	0.419524674	21.17457019	5.867780947	0.108055293	6.560387
21	6.144608715	0.215198794	0.979631884	7.155752498	0.232420052	2.945522
22	2.125597758	0.748108338	2.981726533	3.583797202	0.709051785	2.029656
23	0.523731225	0.419703834	3.030867099	1.027156866	0.484871395	1.097266
24	0.688991324	0.545811523	11.40000245	4.942436286	0.415176027	3.598484
25	0.099865887	0.542947596	1.586617002	0.958301849	0.46733696	0.731014
26	1.495692312	0.370594072	2.010272467	2.048169747	0.707068806	1.326359
27	0.558970664	0.423118099	1.377897934	1.773390755	0.232431039	0.873162
28	0.692579675	0.379776002	1.119920661	1.630488931	0.263401875	0.817233
29	4.16440763	1.369208975	0.694352	2.998306802	0.891228702	2.023501
30	0.404399965	1.999236883	0.879353471	1.88286545	5.5626827	2.145708
Mean	1.13166618	0.646812306	3.357160812	1.808874229	0.630359167	

However, despite this issue, both PCA and Linear Discriminant Analysis (LDA) of the data (Figure XIX) reveal complete separation of species morphospaces.

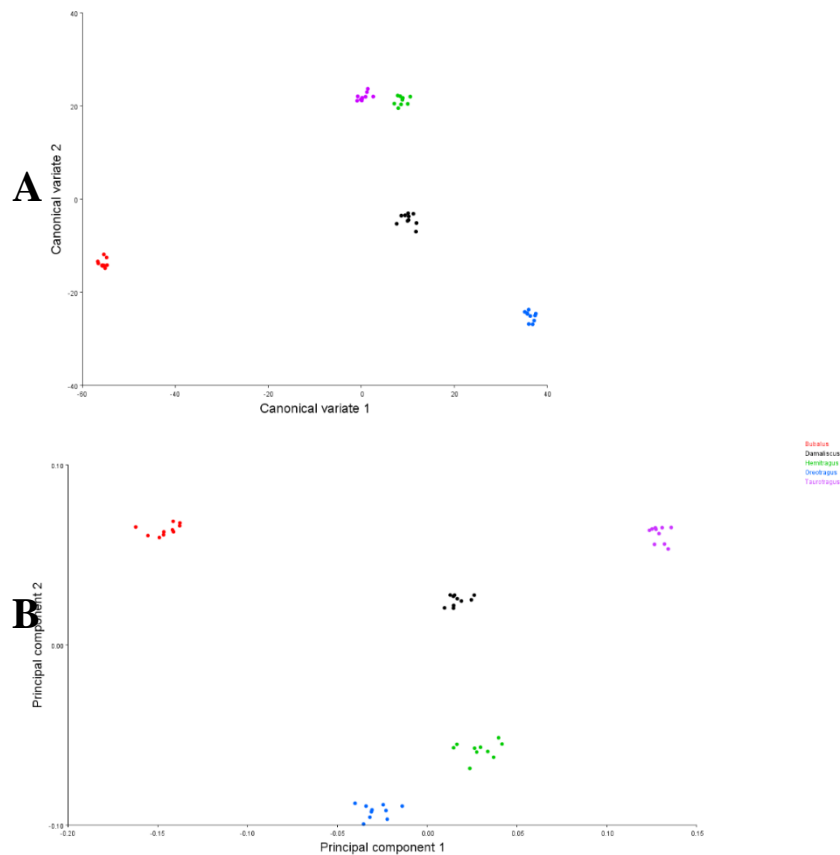


Figure XIX: Linear Discriminant Analysis (LDA) and Principal Components Analysis (PCA) visualization of Trial 5 results

A) Results of LDA on Trial 5 dataset (10 successive landmarking attempts on 5 different specimens); B) results of PCA on Trial 5 dataset

Overall, this suggests that it may not be possible to optimize the landmarks such that the coefficient of variation is $<2\%$ for all landmarks for all specimens, especially given effects of differing centroid sizes. Nevertheless, it appears that the 30 landmark schema is sufficiently repeatable across a range of bovids that it can be used for the full 3D GMM analysis.

Appendix IV: R Code

Formatting 3D landmarks data from Avizo

```
Library(Arothron)
LMs<-read.amira.dir("C:/Users/Sophia/Desktop/LM data/", "auto")
LMs
#### Export the whole thing to MorphoJ
library(Morpho)
r2morphoj(LMs,"LM data.txt")
```

Canonical Variate Analysis (CVA)

```
LDAdat <- read.table("C:/Users/Sophia/Desktop/Procrustes coordinates.csv", header=T,
sep=",")
LDAdat
library(MASS)
my.lda <- lda(Tribe ~
ProcCoord1+ProcCoord2+ProcCoord3+ProcCoord4+ProcCoord5+ProcCoord6+ProcCoord7+ProcCoord8+ProcCoord9+ProcCoord10+ProcCoord11+ProcCoord12+ProcCoord13+ProcCoord14+ProcCoord15+ProcCoord16+ProcCoord17+ProcCoord18+ProcCoord19+ProcCoord20+ProcCoord21+ProcCoord22+ProcCoord23+ProcCoord24+ProcCoord25+ProcCoord26+ProcCoord27+ProcCoord28+ProcCoord29+ProcCoord30+ProcCoord31+ProcCoord32+ProcCoord33+ProcCoord34+ProcCoord35+ProcCoord36+ProcCoord37+ProcCoord38+ProcCoord39+ProcCoord40+ProcCoord41+ProcCoord42+ProcCoord43+ProcCoord44+ProcCoord45+ProcCoord46+ProcCoord47+ProcCoord48+ProcCoord49+ProcCoord50+ProcCoord51+ProcCoord52+ProcCoord53+ProcCoord54+ProcCoord55+ProcCoord56+ProcCoord57+ProcCoord58+ProcCoord59+ProcCoord60+ProcCoord61+ProcCoord62+ProcCoord63+ProcCoord64+ProcCoord65+ProcCoord66+ProcCoord67+ProcCoord68+ProcCoord69+ProcCoord70+ProcCoord71+ProcCoord72+ProcCoord73+ProcCoord74+ProcCoord75+ProcCoord76+ProcCoord77+ProcCoord78+ProcCoord79+ProcCoord80+ProcCoord81+ProcCoord82+ProcCoord83+ProcCoord84+ProcCoord85+ProcCoord86+ProcCoord87+ProcCoord88+ProcCoord89+ProcCoord90, data = LDAdat)
my.lda
my.lda$scaling
library(dplyr)
```

```

data.sub <-
  LDAdat %>%
  dplyr::select(ProcCoord1:ProcCoord90) %>%
  as.matrix # cast to matrix for calculations
data.sub
CVA.scores <- data.sub %*% my.lda$scaling
my.CV <- data.frame(CVA.scores)
my.CV$Tribe <- LDAdat$Tribe

#### Visualize CVA
library(ggplot2)
my.cva.plot <-
  ggplot(my.CV, aes(x = LD1, y = LD2)) +
  geom_point(aes(color=Tribe, shape=FALSE), alpha=0.5) +
  labs(x = "LD1", y = "LD2") +
  coord_fixed(ratio=1) my.cva.plot

#### Prediction information
predictions <- my.lda %>% predict(LDAdat)
predictions
names(predictions)
mean(predictions$class==LDAdat$Tribe)

```

Principal Components Analysis (PCA)

```

PCAdat <- read.table("C:/Users/Sophia/Desktop/Procrustes coordinates.csv", header=T,
  sep=",")
PCAdat
depvar <- subset(test, select=ProcCoord1:ProcCoord90)
summary(depvar)
str(depvar)
prco <- prcomp(depvar, scale=T)
summary(prco)
prco

```

```
head(prco$x)
```

```
#### Visualize PCA
```

```
library(ggfortify)
```

```
autoplot(prco, data=test, label=TRUE, shape=TRUE, colour='Tribe')
```

Phylogenetic Generalized Least Squares (PGLS)

```
theTree <- read.tree("C:/Users/Sophia/Desktop/Final tree.phy")
```

```
plot(theTree, cex = 0.2)
```

```
#### PGLS on PCA output
```

```
X <- read.table("C:/Users/Sophia/Desktop/ PC scores final.csv", header=T, sep="," )
```

```
X
```

```
model.pgls1<-pgls(PC1 ~ Habitat, data = forAnalysis, lambda  
="ML")
```

```
summary(model.pgls1)
```

```
model.pgls2<-pgls(PC2 ~ Habitat, data = forAnalysis, lambda  
="ML")
```

```
summary(model.pgls2)
```

```
model.pgls3<-pgls(PC3 ~ Habitat, data = forAnalysis, lambda  
="ML")
```

```
summary(model.pgls3)
```

```
model.pgls4<-pgls(PC4 ~ Habitat, data = forAnalysis, lambda  
="ML")
```

```
summary(model.pgls4)
```

```
model.pgls1<-pgls(PC1 ~ Mass, data = forAnalysis, lambda  
="ML")
```

```
summary(model.pgls1)
```

```
model.pgls2<-pgls(PC2 ~ Mass, data = forAnalysis, lambda  
="ML")
```

```
summary(model.pgls2)
```

```
model.pgls3<-pgls(PC3 ~ Mass, data = forAnalysis, lambda
```

```

="ML")
summary(model.pgls3)
model.pgls4<-pgls(PC4 ~ Mass, data = forAnalysis, lambda
="ML")
summary(model.pgls4)

#### PGLS on CVA habitat output
X <- read.table("C:/Users/Sophia/Desktop/CV habitat.csv", header=T, sep="," )
X
forAnalysis <- comparative.data(phy = theTree, data = X, names.col="Taxa")
plot(forAnalysis$phy, cex=0.5)
forAnalysis$phy
model.pgls1<-pgls(CV1 ~ Habitat, data = forAnalysis, lambda
="ML")
summary(model.pgls1)
model.pgls2<-pgls(CV2 ~ Habitat, data = forAnalysis, lambda
="ML")
summary(model.pgls2)
model.pgls3<-pgls(CV3 ~ Habitat, data = forAnalysis, lambda
="ML")
summary(model.pgls3)
model.pgls4<-pgls(CV4 ~ Habitat, data = forAnalysis, lambda
="ML")
summary(model.pgls4)

#### PGLS on CVA mass output
X <- read.table("C:/Users/Sophia/Desktop/CV mass.csv", header=T, sep="," )
X
forAnalysis <- comparative.data(phy = theTree, data = X, names.col="Taxa")
plot(forAnalysis$phy, cex=0.5)
forAnalysis$phy
model.pgls1<-pgls(CV1 ~ Mass, data = forAnalysis, lambda
="ML")
summary(model.pgls1)

```



```

model.pgls2<-pgls(CV2 ~ Mass, data = forAnalysis, lambda
="ML")
summary(model.pgls2)
model.pgls3<-pgls(CV3 ~ Mass, data = forAnalysis, lambda
="ML")
summary(model.pgls3)
model.pgls4<-pgls(CV4 ~ Mass, data = forAnalysis, lambda
="ML")
summary(model.pgls4)

```

Linear regression

```

#####Allometry
X <- read.table("C:/Users/Sophia/Desktop/corrected shape vs centroid", header=T,
sep=",")

model1 <- LM(Shape.variation ~ Centroid.size, data = X)
summary(model1)

plot(Shape.variation ~ Centroid.size, pch=16, data=X)
abline(model1, col="black")

#####Body mass vs. habitat
X <- read.table("C:/Users/Sophia/Desktop/Mass vs habitat.csv", header=T, sep=",")

par(cex=0.7)
boxplot(Mean.body.mass ~ Habitat.preference.category, data=X)

model <- lm(Mean.body.mass ~ Habitat.preference.category, data=X)
summary(model)

```

ANOVA

```

X <- read.table("C:/Users/Sophia/Desktop/CV habitat.csv", header=T, sep=",")

model1<-lm(CV4 ~ Habitat + Raw.mass + Habitat*Raw.mass, data=X)
summary(model1)

library(car)
Anova(model1,type="II")

```

Appendix V: Phylogenetic Tree

Modified from Hernández Fernández and Vrba (2005) and Bibi (2013)

(((((Tragulus_javanicus:28.4,Tragulus_napu:28.4):0,Moschiola_meminna:28.4):6.8,Hyemoschus_aquaticus:35.2):14.8,(((Giraffa_camelopardalis:17.8,Okapia_johnstoni:17.8):10.3,Antilocapra_americana:28.1):5.1,(((Moschus_berezovskii:3.4,(Moschus_chrysogaster:1.8,((Moschus_cupreus:0.8,Moschus_leucogaster:0.8):0.4,Moschus_fuscus:1.2):0.6):1.6):2.7,Moschus_moschiferus:6.1):23.4,(Hydropotes_inermis:19.7,((((Axis_axis:0.9,(Hyelaphus_calamianensis:0.4,Hyelaphus_kuhlii:0.4):0.3,Hyelaphus_porcinus:0.7):0.2):6.1,(Dama_dama:0.8,Dama_mesopotamica:0.8):6.2):2.9,((Rusa_alfredi:3.9,(Rusa_mariannus:3.5,Rusa_timorensis:3.5,Rusa_unicolor:3.5):0.4):1.7,(Rucervus_duvaucelii:2.7,Rucervus_eldi:2.7,Rucervus_schomburgki:2.7):2.9,(Przewalskium_albirostris:4.2,(Cervus_elaphus:4.2,Cervus_nippon:4.2):0):1.4):2.8,Elaphurus_davidianus:8.4):1.5):4.8,(Elaphodus_cephalopus:14.7,(((Muntiacus_crinifrons:1.4,Muntiacus_gongshanensis:1.4):2.7,Muntiacus_faei:4.1,Muntiacus_muntjak:4.1):0.7,Muntiacus_atherodes:4.8,Muntiacus_reevesi:4.8,Muntiacus_rooseveltorum:4.8,Muntiacus_truongsonensis:4.8,Muntiacus_putaoensis:4.8,Megamuntiacus_vuquangensis:4.8):9.9):0):4.7,((Alces_alces:11,(Capreolus_capreolus:3.4,Capreolus_pygargus:3.4):7.6):3.6,(((Blastoceros_dichotomus:2,Ozotoceros_bezoarticus:2):7,(Odocoileus_hemionus:4.7,Odocoileus_virginianus:4.7):4.3,(Mazama_americana:6.1,Mazama_gouazoupira:6.1,(Mazama_chunyi:4.7,((Mazama_bricenii:2.3,Mazama_rufina:2.3):1.4,Mazama_nana:3.7):1):1.4):2.9,(Pudu_mephistophiles:2.4,Pudu_puda:2.4):6.6,(Hippocamelus_antisensis:2.4,Hippocamelus_bisulcus:2.4):6.6):1.8,Rangifer_tarandus:10.8):3.8):4.8):0.3):9.8):2.5,(((Boselaphus_tragocamelus:10.4,Tetracerus_quadricornis:10.4):10.1,((Pseudoryx_nghetinhensis:16.9,((((Bison_bison:1.1,Bison_bonassus:1.1):2.3,Bos_grunniens:3.4):2.4,(Bos_sauveli:0.6,Bos_taurus:0.6):5.2):1.2,(Bos_frontalis:2.5,Bos_javanicus:2.5):4.5):9.9,(((Bubalus_bubalis:3.2,Bubalus_mindorensis:3.2):0.7,(Bubalus_depressicornis:3.9,Bubalus_quarlesi:3.9):0):7.9,Syncerus_caffer:11.8):5.1):0):1.4,(((Taurotragus_derbianus:1.6,Taurotragus_oryx:1.6):3.8,(Tragelaphus_strepsiceros:2.6,Tragelaphus_buxtoni:2.6):2.8):1.5,(Tragelaphus_eurycerus:6,Tragelaphus_scriptus:6,Tragelaphus_spekii:6):0.9):3.6,(Tragelaphus_angasii:2.8,Tragelaphus_imberbis:2.8):7.7):7.8):2.2):4.9,(Oreotragus_oreotragus:23.2,((Neotragus_batesi:3.4,Neotragus_moschatus:3.4):2,Neotragus_pygmaeus:5.4):17.8,((Saiga_tatarica:18,(Litocranius_walleri:18,(Ammodorcas_clarkei:4.2,Antidorcas_marsupialis:4.2):13.8,(Antelope_cervicapra:18,(((Eudorcas_rufina:4.8,(Eudorcas_rufifrons:1.9,Eudorcas_thomsonii:1.9):2.9):5.8,((Nanger_dama:3.1,Nanger_soemmerringii:3.1):1.3

,Nanger_granti:4.4):6.2):0,((((Gazella_arabica:0,Gazella_gazella:0):1.4,Gazella_bilkis:1.4):0.9,(Gazella_saudiya:0.8,Gazella_dorcas:0.8):1.5,Gazella_spekei:2.3):0.2,Gazella_bennettii:2.5):3.2,(Gazella_cuvieri:1.5,Gazella_subgutturosa:1.5,Gazella_leptoceros:1.5):4.2):4.9):7.4):0):1.7,(Procapra_gutturosa:6.2,(Procapra_picticaudata:3.9,Procapra_przewalskii:3.9):2.3):13.5,((Madoqua_guentheri:1.4,Madoqua_kirkii:1.4):3.9,(Madoqua_piacentini:2.7,Madoqua_saltiana:2.7):2.6):14.4,Ourebia_ourebi:19.7,(Dorcatragus_megalotis:8.9,(Raphicerus_campestris:7.9,Raphicerus_melanotis:7.9,Raphicerus_sharpei:7.9):1):10.8):3.5,((((Cephalophus_adersi:10.2,(((Cephalophus_callipygus:3.2,Cephalophus_weynsi:3.2):1.5,Cephalophus_rubidus:4.7):5.1,Cephalophus_niger:9.8,(((Cephalophus_harveyi:0.8,Cephalophus_natalensis:0.8):3.1,(Cephalophus_rufilatus:1.6,Cephalophus_nigrifrons:1.6):2.3):3.8,Cephalophus_leucogaster:7.7):2.1):0.4):0.6,(((Cephalophus_dorsalis:7.5,(Cephalophus_silvicultor:4.5,Cephalophus_spadix:4.5):3):1,Cephalophus_jentinki:8.5):1.5,(Cephalophus_ogilbyi:4.6,Cephalophus_zebra:4.6):5.4):0.8):2.7,(Philantomba_maxwellii:5.1,Cephalophus_monticola:5.1):8.4):0,Sylvicapra_grimmia:13.5):6.3,(Pelea_capreolus:13.5,(((Redunca_arundinum:3,Redunca_redunca:3):3.7,Redunca_fulvorufula:6.7):6,((Kobus_kob:1.2,Kobus_vardonii:1.2):2.3,((Kobus_leche:1.6,Kobus_megaceros:1.6):1.9,Kobus_ellipsiprymnus:3.5):0):9.2):0.8):6.3):3.4,(Aepyceros_melampus:22.3,((((Alcelaphus_buselaphus:3.1,Sigmoceros_lichtensteinii:3.1):7.7,(Connochaetes_gnou:2.5,Connochaetes_taurinus:2.5):8.3,(Beatragus_hunteri:7.7,(Damaliscus_lunatus:6.2,Damaliscus_pygargus:6.2):1.5):3.1):7.1,((Addax_nasomaculatus:5,(Oryx_dammah:2.5,Oryx_gazella:2.5,Oryx_leucoryx:2.5):2.5):6,((Hippotragus_equinus:2.5,Hippotragus_leucophaeus:2.5):6.3,Hippotragus_niger:8.8):2.2):6.9):2.3,(Pantholops_hodgsonii:17.8,(((Ammotragus_lervia:11.1,(((Capra_falconeri:5.1,Capra_hircus:5.1,Capra_caucasica:5.1,Capra_cylindricornis:5.1,Capra_pyrenaica:5.1,Capra_ibex:5.1,Capra_nubiana:5.1,Capra_sibirica:5.1,Capra_walievskii:5.1):2.9,((Hemitragus_hylocrius:1.8,Hemitragus_jayakari:1.8):1,Hemitragus_jemlahicus:2.8):5.2):3.1,(Pseudois_nayaur:2.4,Pseudois_schaeferi:2.4):8.7):0):0.2,((Ovis_ammon:2.7,(Ovis_aries:0.8,Ovis_vignei:0.8):1.9):4.1,((Ovis_canadensis:0.2,Ovis_dalli:0.2):0.3,Ovis_nivicola:0.5):6.3):4.5):3.2,(Oreamnos_americanus:8.8,(Rupicapra_pyrenaica:3.8,Rupicapra_rupicapra:3.8):5):5.7,Budorcas_taxicolor:14.5,Ovibos_moschatus:14.5,((Naemorhedus_baileyi:3.3,(Naemorhedus_caudatus:0.1,Naemorhedus_goral:0.1):3.2):7,(Capricornis_sumatraensis:4.3,(Capricornis_crispus:2.7,(Capricornis_swinhoei:1.661,Capricornis_milneedwardsii:1.661):1.039):1.6):6):4.2):3.3):2.4):2.1):0.9):2.2):6.6):1.2):16.8);